GROWTH OF METAL-NITRIDE THIN FILMS BY PULSED LASER DEPOSITION

A thesis submitted in partial fulfilment of the

requirements for the Degree

of Doctor of Philosophy in Physics

in the University of Canterbury

by Ian Laurence Farrell

University of Canterbury

2010

"A noble spirit embiggens the smallest man"

Jebediah Springfield

ABSTRACT

The growth of thin-film metal nitride materials from elemental metal targets by plasma-assisted pulsed laser deposition (PLD) has been explored and analysed.

A new UHV PLD growth system has been installed and assembled and its system elements were calibrated. A series of GaN thin films have been grown to calibrate the system. *In-situ* RHEED indicated that the films were single crystal and that growth proceeded in a three-dimensional fashion. SEM images showed heavy particulation of film surfaces that was not in evidence for later refractory metal nitride films. This may be connected to the fact that Ga targets were liquid while refractory metals were solid. Most GaN films were not continuous due to insufficient laser fluence. Continuous films did not exhibit photoluminescence.

HfN films have been grown by PLD for the first time. Films grown have been shown to have high reflectivity in the visible region and low resistivity. These factors, along with their crystal structure, make them suitable candidates to be used as back-contacts in GaN LEDs and could also serve as buffer layers to enable the integration of GaN and Si technologies. Growth factors affecting the films' final properties have been investigated. Nitrogen pressure, within the operating range of the plasma source, has been shown to have little effect on HfN films. Substrate temperature has been demonstrated to have more influence on the films' properties, with 500 °C being established as optimum. ZrN films have also been grown by PLD. Early results indicated that they exhibit reflectivities 50 % ± 5 % lower than those of HfN. However, further growth and characterisation would be required in order to establish this as a fundamental property of ZrN as nitride targets were mostly used in ZrN production.

Single-crystal epitaxial GdN and SmN films have been produced by PLD. This represents an improvement in the existing quality of GdN films reported in the literature, which are mostly polycrystalline. In the case of SmN, these are the first epitaxial films of this material to be grown. Film quality has been monitored *in-situ* by RHEED which has allowed growth to be tailored to produce ever-higher crystal quality. Post-growth analyses by collaborators was also of assistance in improving film growth. Substrate temperatures and nitrogen plasma parameters have been adjusted to find optimum values

for each. In addition, laser fluence has been altered to minimise the presence of metal particulates in the films, which interfere with magnetic measurements carried out in analyses. Capping layers of Cr, YSZ or AlN have been deposited on the GdN and SmN prior to removal from vacuum to prevent their degradation upon exposure to atmospheric water vapour. The caps have been steadily improved over the course of this work, extending the lifetime of the nitride films in ambient. However, they remain volatile and this may persist since water vapour can enter the film at the edge regardless of capping quality. Optical transmission has shown an onset of absorption at 1.3 eV for GdN and 1.0 eV for SmN.

ACKNOWLEDGEMENTS

First and foremost I would like to thank my supervisors Prof. Roger Reeves and Assoc. Prof. Steve Durbin for their guidance, support, enthusiasm, advice and patience during this research. I am also very grateful to Dr. Rueben Mendelsberg for discussions on the minutiae of PLD and Dr. Chito Kendrick for sharing his wealth of vacuum system experience. Many thanks also to Dr. Phil Anderson and Dr. Robert Kinsey for their assistance with chamber assembly and characterising nitrogen sources.

I also thank my collaborators at Victoria University, Wellington, Dr. Ben Ruck, Bart Ludbrook and Dr. Andrew Preston for their drive and commitment in keeping up the momentum of research and their helpful input at all times.

For tolerating my bellicose ramblings, the noise of my espresso machine and occasional useful discussions of physics, I sincerely thank the other members of the Solid State Physics group; Dr. Paul Miller, Dr. Scott Choi, Dr. Martin Henseler, Young-Wook Song and Masaed Almotari.

Particular thanks to Wayne Smith in the Physics workshop for translating my ill-conceived designs into working objects. Thanks also to Graeme Kershaw, Bob Flygenring and Stephen Hemmingway for similar assistance and for lending me dangerous tools without asking any questions. I also extend my gratitude to Nick, Danny and Oliver in the Chemistry workshop for their help, and I apologise for randomly interchanging your names.

Thank you to all members of the Physics Department, past and present, who have accepted me into their midst, even those who do so begrudgingly.

Finally, I would like to acknowledge the support of the MacDiarmid Institute and the Department of Physics and Astronomy in conducting this research.

CONTENTS

PUBLICATIONS

The following peer reviewed conference proceedings and journal articles have been published, which in part have related to study towards this thesis

I. L. Farrell, R. J. Reeves, A. R. H. Preston, B. M. Ludbrook, J. E. Downes, B. J. Ruck and S. M. Durbin, "Tunable electrical and optical properties of hafnium nitride thin films", Applied Physics Letters 96, 071914 (2010)
This paper discusses the structural and electronic properties of epitaxial hafnium nitride films grown on magnesium oxide substrates by pulsed laser deposition. The study is described in chapter 5.

B. M. Ludbrook, I. L. Farrell, M. Kuebel, B. J. Ruck, A. R. H. Preston, H. J. Trodahl, L. Ranno, R. J. Reeves and S. M. Durbin, "Growth and properties of epitaxial GdN", Journal of Applied Physics, 106, 063910 (2009)
This paper describes the epitaxial growth and measured properties of gadolinium nitride thin films on yttrium stabilised zirconia substrates and the oxide layer that forms at its interface. The study is described in chapter 4.

P. A. Anderson, R. J. Kinsey, C. E. Kendrick, I. Farrell, D. Carder, R. J. Reeves and S. M. Durbin, "Influence of Nitrogen Species on InN Grown by PAMBE", Materials Research Society Symposium Proceedings: GaN, AIN, InN and Related Materials, 892, 89 (2006)
This proceedings describes the characterisation of a nitrogen plasma source and the role active nitrogen species can play in determining the properties of InN film growth. The characterisation procedure is described in section 2.4

Chapter 1 INTRODUCTION TO METAL NITRIDES

1.1 Introduction

This is a thesis on the growth of metal nitride thin films by Pulsed Laser Deposition (PLD). The reasons for choosing PLD as a growth method will be outlined in Chapter 2, in which the principles and processes of PLD will be described more fully. This chapter will justify the choice and explain the motivations for growing thin films using elemental metal targets in the presence of an active nitrogen plasma.

PLD was first used to deposit thin films by Smith and Turner [1] in 1965, shortly after the invention of the first high-power ruby laser. The real breakthrough of the technique, however, did not come until the successful growth of high-T_C superconducting films in 1987 by Dijkkamp *et al* [2]. A Y-Ba-Cu-O bulk target was irradiated with 30ns pulses from a 248nm KrF laser and it was found that the film retained the same stoichiometric ratios of the target material, thereby making the technique of immediate interest in the growth of complex multi-elemental material systems. The consistency in stoichiometry is a result of the highly non-equilibrium nature of short-pulse laser ablation. Heating and cooling rates occur on timescales shorter than those required for phase separation to occur in the bulk material. The resulting films then have a higher level of crystallographic and chemical purity that allow for a more accurate analysis of the material's properties. PLD is therefore an excellent method for investigation of new complex materials that simply could not be prepared by existing methods like chemical vapour deposition (CVD).

PLD has a wider array of process variables than most other thin film growth techniques. In plasma-assisted PLD, laser fluence, substrate temperature, gas pressure, plasma power, target-to-substrate distance and laser repetition rate can all be varied. Laser fluence itself can be varied by spot size or beam energy, each having a different effect on the target. This creates a large parameter space in which one can work, which makes tailoring growth a complex task. However, this also opens up avenues of investigation for materials processing where one would normally run out of options for growth improvement. By way of examples, some transition metals have very low vapour

pressures and excess metal will not desorb from the growing surface in the practical temperature range allowed by the substrate heater (<1000°C). In this case, the arrival rate of metal precursors at the substrate can be reduced to a minimum by reducing the laser fluence while simultaneously increasing nitrogen pressure to ensure that both the metal flux and nitrogen flux are occurring at a rate that allows congruent reaction at the substrate to grow a stoichiometric film.

1.2 Materials grown by PLD

PLD is now routinely used to grow every type of thin film, from simple elemental and binary films such as Cr [3] and GaN[4] to complex lasing garnets such as Nd and Cr-doped $Gd_6Sc_2Ga_6O_{12}$ [5]. This latter material contains 6 elements and has over 160 atoms per unit cell and as such it is highly unlikely that it could be grown by thermal methods. Indeed, in 1992 Saenger complied a list [6] of almost 200 compounds grown by PLD, a mere 5 years after the pioneering work of Dijkkamp *et al*., such was the flood of research inspired by this emerging research tool. The aforementioned stoichiometry transfer was the key driving factor and this is evidenced by the dominance of multi-elemental films in the list.

1.3 Growth of nitrides from elemental metal targets

A less-studied branch of PLD is the growth of films that use a single-element ablation target and its combination with a process gas to form a thin film. At first glance it would seem that this area of research should be well-covered by thermal growth methods like CVD and MBE. However, many transition metals and in particular refractory metals have high melting points, often in excess of 2000°C [7], which rules out thermal processes as a viable means of creating an atomic beam. The intense radiation present in a focused laser beam creates a local energy density sufficient to ablate a small volume of the metal. Short wavelength excimer lasers in particular can accomplish this task as metals have lower reflectivity at UV wavelengths (248nm for KrF, 193nm for ArF) than other available high-power lasers like pulsed Nd:YAG (1.06μm) or CW CO_2

(10.6μm). Since the more common demand made of PLD-grown materials has been in stoichiometric transfer from a multi-elemental target, binary growth combining an ablation plume and a process gas has received less attention. The dynamics of this growth regime is not yet well understood and in the present work some observations in this area will be formulated.

The issue of loosely bound ceramic targets emitting particulates is not a problem in this work as, for the most part, ceramic targets are not used. Instead, metallic droplets are the prevalent particulates in films. Studies [8,9] have shown that the laser causes gradual formation of cone-like structures pointing in the direction of the beam. The structures build up as ablation of the target metal continues and as they melt and break off, droplet density on the growing film increases. Droplet density has been found to vary between metals. A study on this [10] viewed the ablated droplets from Al, Y, Fe, Cu and Au and found that the range of droplet sizes is broader for Al and Y, while particle density is higher for Fe, Cu and Au. These differences were not found to have a simple correlation to metal properties such as thermal conductivity, heat capacity, melting or boiling points, etc., making predictions about droplet formation difficult prior to actually carrying out an ablation experiment. The study did conclude, however, that the most likely mechanism for particle formation at $10^7 – 10^9$ W cm^{-2} power densities (comparable to those used in the present research) was rapid surface evaporation and consequent recoil pressure producing a shock wave in the molten material, which leads to the ejection of particles.

Particulate formation is also a function of laser parameters such as fluence, spot size, beam profile and laser wavelength, which are more controllable parameters in PLD. For example, metals typically have a high reflectivity in the IR, which makes Nd:YAG lasers unsuitable for metal ablation. Even if they are frequency doubled to 532nm or tripled to 366nm, the resulting reduction in energy per pulse from hundreds to tens of millijoules reduces growth rates to impractically low levels. In our present set-up, there is no means for eliminating droplets from the plume, such as a rotating shutter or the employment of a shadowmask. In fact, the chamber pressures achievable during growth are limited by the nitrogen plasma source to a maximum of 1×10^{-4} mbar. At this pressure, there would be insufficient scattering of the ablation plume for film growth to

occur; shadowmask growth typically requires pressures of 100 mTorr to achieve a reasonable growth rate [11]. Attempts to reduce particulates have been made by decreasing laser fluence, either by broadening the laser spot size, reducing the pulse energy, or both. Generally, decreasing the laser fluence will reduce the size and density of particulates emitted from the target [6]. This also means reducing the growth rate as less material is ablated and a trade-off must be reached which yields an acceptable growth rate while minimising particulates in the film. As this work progressed, fluence reduction was enacted more often by reducing beam energy since changing the spot size results in a different shape emission plume, which introduces yet another parameter into the growth process. Broader plumes create a wider distribution of ablated material, resulting in films that are more sharply graded in terms of thickness and this can be undesirable in subsequent analysis where sample homogeneity can be an issue. The cumulative target damage mentioned above and in references [8] and [9] was minimised by moving the laser spot to ablate different tracks in the rotating target and by flipping the target after many ablation tracks are formed. Sanding targets flat with fine-grit SiC sandpaper followed by diamond paste polishing and degreasing before re-use is also an option for metal targets. This procedure would be more difficult with brittle ceramic targets. Finally, it is worth noting that such reduced growth rates and substrate coverage area would be a major drawback in commercial growth processes like CVD and MBE but are acceptable in PLD, where substrates are typically 1 × 1 cm and materials are generally grown for analysis of their fundamental physical properties rather than as mass-produced devices.

1.4 Materials investigated

1.4.1 Gallium Nitride

Gallium Nitride (GaN) was first grown epitaxially in 1969 by Maruska and Tietjen [12] using a chemical vapour deposition technique to deposit a large area layer on a sapphire substrate. The material they produced was of sufficient quality to determine that it had a direct bandgap of 3.39 eV and an electron concentration of 10^{19} cm^{-3}. The potential of this material to be a candidate for optoelectronic application created a flurry

of research and zinc-doping led to the first blue LED being fabricated in 1971 [13]. After further intense research and having overcome the obstacle of p-doping (pure GaN is intrinsically n-doped), the first blue laser diode was developed by Shuji Nakamura at Nichia Chemical Industries in 1996 [14]. The blue laser emitted light from 390 – 440 nm at room temperature using InGaN multiquantum wells as an active medium. By integrating blue, green and red LEDs, white light solid-state sources have flourished and exploited the highly efficient nature of light generation by electroluminescence. The small size and low power consumption of white LEDs have made them the technology of choice in hand-held and display devices. They have yet to expand into the market of domestic and workspace lighting and it should be noted that other materials such as zinc oxide and organic LEDs are also suitable candidates for this role. The blue laser diode has increased storage density in optical disks fourfold and is now emerging as market leader in the next generation of "Blu-Ray" DVDs.

GaN also has mechanical advantages of being thermally and chemically stable and physically hard. Electrically, it and its alloys demonstrate high-power and low-noise performance on a par with the more mature GaAs technology and, significantly, without the latter's toxic precursor constituents. When doped with 5% Mn it has a Curie temperature exceeding room temperature, making it a suitable candidate for spintronic applications[15]. However, for the present work, it is the optoelectronic properties that are of most interest. A large body of work in the literature on the growth of GaN by PLD ([34-46]) has been studied to serve as a guide in conducting GaN growth in the newly installed UHV PLD system. Once the system has been calibrated by a series of GaN growths, more novel materials which are not as well understood will be investigated. GaN will ultimately form the top light-emitting layer of a heterostructure designed to test the suitability of refractory metal nitrides as back contacts for improved GaN LEDs.

1.4.2 Refractory Metal Nitrides

The early refractory metal nitrides in their cubic phase are well known for their high hardness, mechanical strength, high melting points (ca. 3000 °C) [16] and chemical resistance (e.g. to organic solvents and inorganic acids). Because of these properties they

have been used as wear-resistant coatings for machine tools [17,18]. In addition, their gold colour also gives them value as decorative coatings [19-21] and as wavelength-selective optical films [22].

The refractory metal nitrides also possess metallic conductivity [23,24] and reflectivity [23,25] and it is these aspects of their properties that make them interesting in this research. Hafnium nitride and zirconium nitride have lattice constants between those of GaN and Si. Hence, a thin layer of either nitride material deposited on a Si substrate would allow an epitaxial GaN top layer to be grown. The interstitial nitride material, being lattice-matched, should result in good quality GaN with lower defects than that of a film on a non lattice-matched metal and would exhibit improved electroluminescent efficiency. The low resistivity of HfN and ZrN would provide a good ohmic back contact, in much the same way as current metal contacts do, but the reflective nature of the nitride would decrease the amount of light lost to the substrate. The potential for this heterostructure to improve the efficiency of GaN-based LEDs is already known [26,27], but the area needs more research to realise working devices. There is also the potential to integrate GaN and Si technology to develop new optoelectronic components. In particular, the nitride layers themselves warrant further investigation to establish their fundamental properties. The difficulties encountered in growing materials where hard refractory metals are a constituent makes PLD an ideal tool for metal nitride growth.

1.4.3 Rare Earth Nitrides

The rare earth nitrides (RENs) have attracted renewed attention in recent times owing to their potential for use in spintronic devices [28,29]. Their 4*f* orbitals are unfilled and highly localised, giving rise to interesting magnetic properties, and there is evidence for spin-splitting of the bandgap for GdN [30]. Although our understanding of these materials has improved substantially in recent years through theoretical studies [31] as well as experimental measurements, the vast majority of reported samples are polycrystalline. Detailed studies of high-quality single crystal epilayers would lead to better understanding of fundamental properties, particularly the role of defects in determining electrical characteristics.

RENs were the last set of materials grown in this research as they were the most difficult to grow in single crystal form. The experience developed from previous growths in this research was drawn upon to try to maximise the quality of the epilayers. GdN and SmN were the focus of this work; GdN owing to its properties mentioned above and SmN because it has two fewer 4*f* electrons than Gd and is reported to be anti-ferromagnetic [32,33]. To date, SmN has not been epitaxially grown and as such it is of particular interest in this work. This chapter focuses primarily on the growth of these materials and their *in-situ* analysis by reflection high energy electron diffraction. Post-growth analysis of electrical and magnetic properties was carried out at other research facilities and subsequent results partially dictated the parameters for further growth attempts, e.g. particulate reduction, improving crystallinity and developing better protective caps for these easily degradable materials.

1.5 Crystal Structure of Metal and Rare Earth Nitrides

The transition metal nitrides, HfN and ZrN, studied in this work crystallise in the face centered cubic (fcc) rocksalt structure [47], as do the rare earth nitrides, SmN [29] and GdN [48]. The unit cell is the simplest basis of atoms into which a crystal can be subdivided to show the atomic arrangement which is repeated periodically throughout the entire crystal. In the case of the fcc structure, this consists of a simple cubic arrangement of one type of atom, say the metal or rare earth, at the cube vertices as well as in the centre of each face, as shown in Figure 1.1. Situated midway along the axes are the other type of atom, nitrogen in this example. This is also the structure of sodium chloride, hence why it is known as rocksalt. The lattice constant, *a*, is defined as the distance between two neighbouring vertex atoms (metal or rare earth), which in this case is the same distance along the x-, y- or z-directions due to the symmetry of the crystal. In the case of the refractory metal nitrides the high binding energies give rise to high melting points and extreme hardness, generally typical of covalently bonded materials [49]. The unusual hardness enhancement in these materials has been theoretically shown to originate from a particular σ-band of bonding states between the nonmetal *p*-orbitals and the metal *d*-orbitals that strongly resists shearing strains [50].

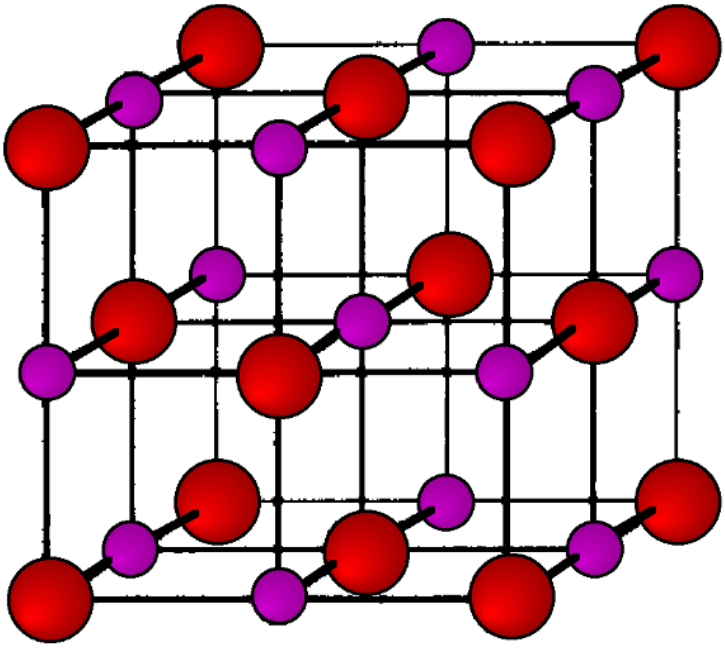

Figure 1.1 A unit cell of the face centred cubic (fcc) rocksalt crystal structure. Metal or rare earth atoms are shown in red and occupy sites at the vertices and cube face centres while nitrogen atoms are shown in purple and are situated midway along a crystal axis between the larger metal/rare earths.

GaN has a different crystal structure that can take one of two forms. The less common form for GaN is the cubic (zincblende) structure, shown in Figure 1.2. The name zincblende is taken from a common mineral form of zinc sulfide (ZnS). The structure consists of the two interpenetrating fcc lattices. However, in zincblende one lattice consists of one of the atoms (Ga in GaN) and the other lattice is composed of the second atom (N in GaN). It may also be described as face centered cubic lattice of N atoms in which half of the tetrahedral sites are filled with Ga atoms.

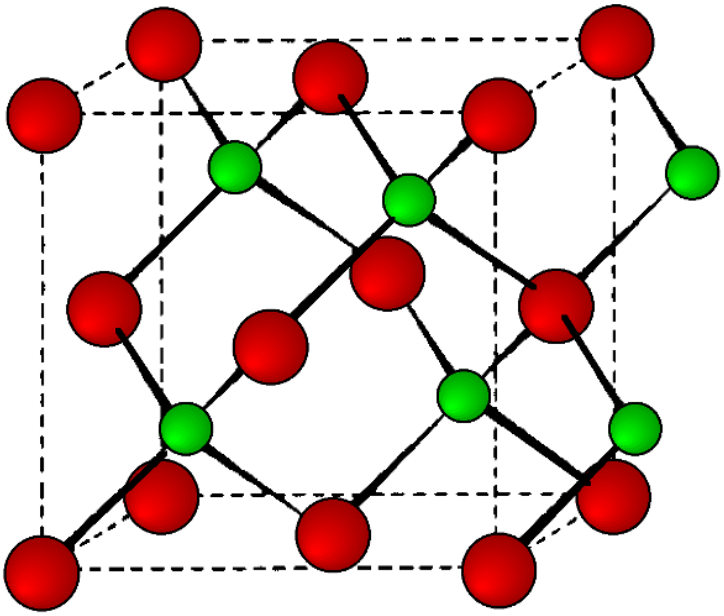

Figure 1.2 A unit cell of cubic (zincblende) GaN. Ga atoms are shown in green and N atoms are shown in red. The dashed lines show the unit cell.

While GaN can be grown in cubic form by controlling growth temperature and using a cubic substrate such as SiC, the more common crystal structure of GaN is the hexagonal or wurtzite form (Figure 1.3). This differs from the zincblende structure only by the rotation of a bond [53]. Hexagonal GaN is grown on sapphire, also a hexagonal crystal. The main difference between the zincblende and wurtzite structures are the stacking sequence of the closest packed diatomic planes, although there is also a difference in bandgap that is of interest in gallium nitride's major application as a light emitter; at room temperature E_g of wurtzite is 3.39 eV while for zincblende it is 3.2 – 3.3 eV [53].

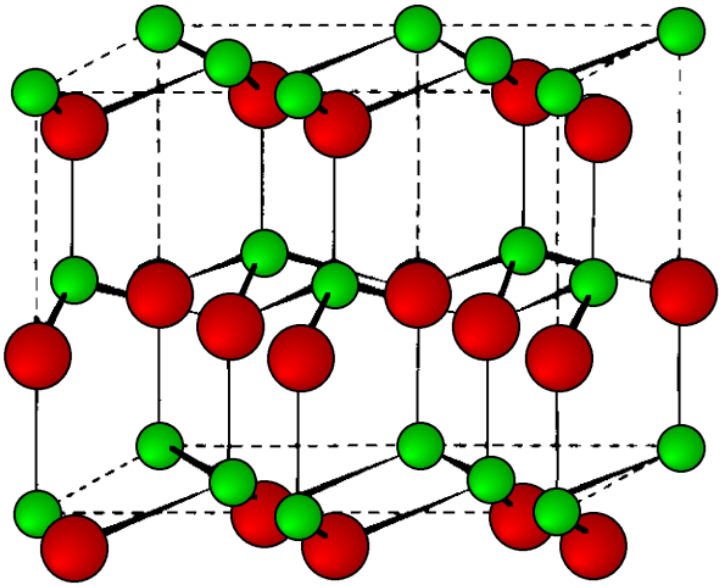

Figure 1.3 A unit cell of hexagonal (wurtzite) GaN. Ga atoms are shown in green and N atoms are shown in red. The dashed lines show the unit cell. As the hexagonal crystal no longer has cubic symmetry, two lattice constants, denoted *a* and *c*, are now required to define the unit cell. In the figure, *a* is the horizontal Ga-Ga atomic distance and *c* is the vertical Ga-Ga distance and they are related by a factor of 5/8.

material	lattice constant / Å
HfN	4.524 [51]
ZrN	4.584 [52]
SmN	5.04 [31]
GdN	4.98 [31]
GaN – cubic	4.52 [53]
GaN - hexagonal	a =3.189, c = 5.185 [53]

Table 1.1 Experimentally obtained lattice constants of nitride materials grown in this research.

References

[1] H. M. Smith and A. F. Turner, Applied Optics 4, 147 – 148

[2] D. Dijkkamp, T. Venkatesan, X. D. Wu, S. A. Shaheen, N. Jisrawi, Y. H. Min-Lee, L. McLean, M. Croft, Applied Physics Letters 51, 619 (1987)

[3] I. L. Farrell and B.M. Ludbrook, "Growth of single crystal SmN by pulsed laser deposition", paper in progress

[4] M. Cazzanelli, D. Cole, J. Verluijs, J. F. Donegan, J. G. Lunney, Materials Science and Engineering B 59, 98 (1999)

[5] P. R. Willmott, P. Manoravi, K. Holliday, Applied Physics A 70, 425 (2000)

[6] D. B. Chrisey and G. K. Hubler, "Pulsed Laser Deposition of Thin Films", Wiley-Interscience, p.581 (1994)

[7] CRC Handbook of Chemistry and Physics 89th Edition, Chemical Rubber Company (2009)

[8] E. van de Riet, J. C. S. Kools and J. Dieleman, Journal of Applied Physics 73, 829 (1993)

[9] E. van de Riet, C. J. C. Nillesen and J. Dieleman, Journal of Applied Physics 74, 2008 (1993)

[10] H. Dupendant, J. P. Gavigan, D. Givord, A. Lienard, J. P. Rebouillat and Y. Souche, "Velocity distribution of micron-size particles in thin film laser ablation deposition (LAD) of metals and oxide superconductors" Applied Surface Science 43, 369 (1989)

[11] R. J. Mendelsberg, M. Kerler, S. M. Durbin and R. J. Reeves, "Photoluminescence behavior of ZnO nanorods produced by eclipse PLD from a Zn metal target", Superlattices and Microstructures 43, 594 (2008)

[12] H.P. Maruska and J.J. Tietjen, "Preparation and properties of vapour-deposited single-crystalline GaN", Applied Physics Letters 15, 367 (1969)

[13] J. I. Pankove, E. A. Miller and J. E. Berkeyheiser, "GaN electroluminescent diodes", RCA Review 32, 383 (1971)

[14] S. Nakamura, "III-V nitride based light-emitting devices", Solid State Communications 102, 237 (1997)

[15] T. Dietl, “Ferromagnetic semiconductors”, Semiconductor Science and Technology 17, 377 (2002)

[16] R.Fix, R.G. Gordon and D.M. Hoffman, “Chemical vapour deposition of titanium, zirconium and hafnium nitride thin films”, Chemical Materials 3, 1138 (1991)

[17] H.E. Hintermann, “Tribological and protective coatings by chemical vapour deposition”,Thin Solid Films 84, 215 (1981)

[18] B.O. Johansson, J. E. Sundren, H. Helmersson and M.K. Hibbs, “Structure of reactively magnetron sputtered Hf-N films”,Applied Physics Letters 44,670 (1984)

[19] R. Buhl, H. K. Pulker, E. Moll, “TiN coatings on steel” Thin Solid Films 80, 265 (1981)

[20] W. Ensinger, K. Volz and M. Kiuchi, “Ion beam-assisted deposition of nitrides of the 4th group of transition metals”, Surface & Coatings Technology 128, 81 (2000)

[21] S. Niyomsoan, W. Grant, D. L. Olson and B.Mishra, “Variation of color in titanium and zirconium nitride decorative thin films”, Thin Solid Films 415, 187 (2002)

[22] S.R. Kurtz and R.G. Gordon, “Chemical vapor deposition of titanium nitride at low temperatures”, Thin Solid Films 140, 277 (1986)

[23] H.S. Seo, T.Y. Lee, I. Petrov, J.E. Greene and D. Gall, “Epitaxial and polycrystalline HfN_x ($0.8 \leq x \leq 1.5$) layers on MgO(100)”, Journal of Applied Physics 97, 083521 (2005)

[24] S Shinkai and K Sasaki, “Influence of Sputtering Parameters on the Formation Process of High-Quality and Low-Resistivity HfN Thin Films”, Japanese Journal of Applied Physics 38, 2097 (1999)

[25] H.M. Benia, A. Guemmaz, G. Schmerber, A. Mosser and J.C. Parlebas, “Optical and electrical properties of sputtered ZrN compounds”, Catalysis Today 89, 307 (2004)

[26] X. Xu, R. Armitage, S. Shinkai, K.Sasaki, C. Kisielowski and E. R. Weber, "Epitaxial condition and polarity in GaN grown on a HfN-buffered Si(111) wafer", Applied Physics Letters 86, 182104 (2005)

[27] R. Armitage, Qing Yang, H. Feick, J. Gebauer, E. R. Weber, S. Shinkai and K. Sasaki, "Lattice-matched HfN buffer layers for epitaxy of GaN on Si", Applied Physics Letters 81, 1450 (2002)

[28] C. M. Aerts, P. Strange, M. Horne, W. M. Temmerman, Z. Szotek and A. Svane, "Half-metallic to insulating behavior of rare-earth nitrides", Physical Review B 69, 045115 (2004).

[29] A. R. H. Preston, S. Granville, D. H. Housden, B. Ludbrook, B. J. Ruck, H. J. Trodahl, A. Bittar, G. V. M. Williams, J. E. Downes, A. DeMasi, Y. Zhang, K. E. Smith and W. R. L. Lambrecht, "Comparison between experiment and calculated band structures for DyN and SmN", Physical Review B 76, 245120 (2007)

[30] F. Leuenberger, A. Parge, W. Felsch, K. Fauth and M. Hessler, "GdN thin films: Bulk and local electronic and magnetic properties", Physical Review B 72, 014427 (2005)

[31] P. Larson, W. R. L. Lambrecht, A. Chantis and M. van Schilfgaarde, "Electronic structure of rare-earth nitrides using the LSDA+*U* approach: Importance of allowing 4*f* orbitals to break the cubic crystal symmetry", Physical Review B 75, 045114 (2007)

[32] F. Hulliger, in *Handbook on the Physics and Chemistry of Rare Earths*, edited by Karl A. Gschneider, Jr. and LeRoy Eyring (North-Holland, New York, 1979), Vol. 4, pp. 153–236.

[33] O. Vogt and K. Mattenberger, in *Handbook on the Physics and Chemistry of Rare Earths*, edited by K. A. Gschneider, Jr., L. Eyring, G. H. Lander, and G. R. Choppin (Elsevier Science, New York, 1993), Vol. 17, pp. 301–407.

[34] M. Cazzanelli, D. Cole, J. F. Donegan, J. G. Lunney, P. G. Middleton, K. P. O'Donnell, C. Vinegoni and L. Pavesi, "Photoluminescence of localized excitons in pulsed-laser-deposited GaN", Applied Physics Letters 73, 3390 (1998)

[35] R.F.Xiao, H. B. Liao, and N. CueX. W. Sun and H. S. Kwok, "Growth of c-axis oriented gallium nitride thin films on an amorphous substrate by the liquid-target pulsed laser deposition technique" Journal of Applied Physics 80, 4226 (1996)

[36] M. Dinescu, P. Verardi , C. Boulmer-Leborgne, C. Gerardi, L. Mirenghi and V. Sandu, "GaN thin films deposition by laser ablation of liquid Ga target in nitrogen reactive atmosphere", Applied Surface Science 127–129, 559 (1998)

[37] R.F. Xiao, X.W. Sun, H.S. Kwok. "Liquid-target pulsed laser deposition of gallium nitride thin films", Applied Surface Science 127-129, 425 (1998)

[38] P.R. Willmott, F. Antoni and M. Döbeli, "Kinetic, crystallographic, and optical studies of GaN and $Al_xGa_{1-x}N$ thin films grown on Si(111) by pulsed reactive crossed-beam laser ablation using liquid alloys and N_2 or NH_3", Journal of Applied Physics 88, 188 (2000)

[39] K.W. Mah, J.-P. Mosnier, E. McGlynn, M. O. Henry, D. O'Mahony and J. G. Lunney, "Study of photoluminescence at 3.310 and 3.368 eV in GaN/sapphire(0001) and GaN/GaAs(001) grown by liquid-target pulsed-laser deposition", Applied Physics Letters 80, 3301 (2002)

[40] J.L.Deiss, Ch. Hirlimann, J.L. Loison, M. Robino and G. Versini, "Epitaxial growth of GaN thin films on sapphire (0001) by pulsed laser deposition: influence of surface preparation and nitridation", Materials Science and Engineering B82, 68 (2001)

[41] N.Grandjean, J.Massies and M.Leroux, "Nitridation of sapphire. Effect on the optical properties of GaN epitaxial overlayers", Applied Physics Letters 69, 2071 (1996)

[42] K.Uchida, A . Watanabe, F. Yano, M. Kouguchi, T. Tanaka, and S. Minagawa, "Nitridation process of sapphire subs surface and its effect on the growth of GaN", Journal of Applied Physics 79, 3487 (1996)

[43] P.Merel, M.Chaker, H.Pepin, M.Tabbal. Materials Research Society Symposium Proceedings 572, 401 (1999)

[44] P Merel, M Chaker, M Tabbal, H Pepin, "Structural and electrical characteristics of epitaxial GaN thin films grown using pulsed laser deposition assited by an atomic nitrogen source", Applied Surface Science 177, 165 (2001)

[45] M Niehus P. Sanguino, T. Monteiro, M.J. Soares, E. Pereira, M. Vieira, S. Koynov and R. Schwarz, "Optical properties and transport in PLD-GaN", Solid State Electronics 47, 569 (2003)

[46] T.F. Huang, A. Marshall, S. Spruytte, J.S. Harris Jr., "Optical and structural properties of epitaxial GaN films grown by pulsed laser deposition", Journal of Crystal Growth 200, 362 (1999)

[47] X.J. Chen, V.W. Struzhkin, Z.G. Wu , M. Somayazulu, J. Qia , S. Kung, A.N. Christensen, Y.S. Zhao, R.E. Cohen, H.K. Mao, R.J. Hemley, "Proceedings of the National Academy of Sciences of the United States of America 102 (2005) 3198

[48] S. Granville, B. J. Ruck, F. Budde, A. Koo, D. J. Pringle, F. Kuchler, A. R. H. Preston, D. H. Housden, N. Lund, A. Bittar, G. V. M. Williams, and H. J. Trodahl, "Semiconducting ground state of GdN thin films", Physical Review B 73, 235335 (2006)

[49] A. Delin, O. Eriksson, R. Ahuja, B. Johansson, M.S.S. Brooks, T. Gashe, S. Auluck and J.M. Wills, "Optical properties of the group-IV*B* refractory metal compounds", Physical Review B 54 (1996) 1673

[50] S. H. Jhi, J. Ihm, S.G. Louie and M.L. Cohen, "Electronic mechanism of hardness enhancement in transition-metal carbonitrides", Nature 399 (1999) 132

[51] H.S. Seo, T. Y. Lee, J.G. Wen, I. Petrov, J.E. Greene and D. Gall, "Growth and physical properties of epitaxial HfN layers on MgO(001)", Journal of Applied Physics 96, 878 (2004)

[52] D.I. Bazhavov, A.A. Knizhnik, A.A. Safonov, A.A. Bagatur'yants, M.W. Stoker and A.A. Korkin, "Structure and electronic properties of zirconium and hafnium nitrides and oxynitrides", Journal of Applied Physics 97, 044108 (2005)

[53] Bernard Gil, "Group III Nitride semiconductor compounds", Oxford Science (1998) Chapters 1 and 2.

Chapter 2 PLD GROWTH AND CHARACTERISATION

2.1 Why thin films?

Thin films have been available to mankind as early as 4000 B.C. and were used by the Egyptians to decorate King Tutankhamen's tomb with films as thin as 0.5 μm. Electroplating has been widely used since its invention by Luigi Brugnatelli in 1805 to deposit thin films of metals on conducting surfaces, usually to add a protective layer or improve the aesthetics of a surface. Richard Feynman later made it possible to deposit metals on non-conducting plastic surfaces [1] by pre-treating the plastics with sodium hydroxide and stannous chloride to ensure the metal film sticks to the plastic before placing it in an electroplating bath. The first evaporated thin films were those of Faraday [2], who exploded metal wires in an inert atmosphere in 1857. Depositing thin films by joule heating of platinum wires was discovered by Nahrwold [3] in 1887 and the following year adapted by Kundt [4] to measure the refractive index of metals. For the following couple of decades, interest in thin film deposition remained a rather niche area of academic interest until vacuum technology had developed to make it applicable to industrial applications.

It could be asked why thin films are of interest for scientific and industrial applications. The principal reasons are cost of material, weight of material and the need for low-dimensional structures. In the first case, a good example would be the use of gold as a heat reflector. Gold is the best heat reflector known, but it is an expensive metal so depositing a thin film is often sufficient to take advantage of its reflecting properties while minimising both expense and weight. A familiar example of this is the gold-coated mylar foil on the Apollo lunar module. In the second case, a thin film can be required for its low-dimensionality, e.g. for use as an anti-reflective coating where the film thickness is needed to be a half-integral multiple of the wavelength being suppressed. In this case it stands to reason that only the thinnest film achievable is necessary. Being able to control the film thickness to such a short length scale obviously implies such thin films are achievable. Another example, which takes us more towards the area of this research, is the deposition of thin semiconductor layers to form quantum wells, whose light-emitting

layers differ in emission wavelength from the bulk material by virtue of quantum effects that become appreciable at such a small scale. In the architecture of nanoscale electronics, thin films and other nanosized structures become a natural consequence of the need to miniaturise electronic circuits to allow signal processing and data storage to increase while attempting to maintain device sizes at practical levels. For the purposes of the present research, materials have been grown as thin films simply because the crystal growth process is slow, with typical growth rates of 100 – 200 nm hr^{-1}. Most of the films grown in this research are novel materials, some grown in single crystal form for the first time, and large volumes were not necessary to investigate their properties.

2.2 Why PLD? - Thin Film Growth methods

The thin films researched during the course of this thesis were all grown by PLD. A justification for choosing this growth method is necessary as more established thin film growth methods are available. PLD has a large parameter space which, while flexible, makes for many iterations of film growths in order to establish an optimum growth procedure. The parameters are inter-dependent, which further complicates the growth process. To justify the use of PLD to conduct this research, a brief description of the other major thin film growth methods is necessary in order to appreciate the differences and how they effect the choice of material systems grown.

2.2.1 Molecular Beam Epitaxy (MBE)

MBE is the first of two standard industrial epitaxial growth methods, having established themselves as they lend themselves well to the mass production of large area wafers, typically 6 to 12 inches in diameter. This is in addition to the high purity levels attainable. In MBE, a vacuum chamber is kept at a very low pressure, about 10^{-11} Torr, to eliminate impurities entering the material being grown, and also because it is essential to the nature of the growth process itself, as we shall see. Separate ovens each contain single atomic species which are heated until each species can escape by thermionic emission once the oven shutter is opened. The ultra high vacuum maintained in the chamber allows

the emitted atoms a mean free path long enough to reach the substrate. The substrate itself is heated to quite a high temperature, typically in the range 700 °C to 900 °C, depending on the material system, and this thermal energy gives the impinging atoms enough energy to move to their correct lattice sites for crystal growth to occur. The number of ovens available allows flexibility in growth; for example, the optoelectronic III-V materials such as GaAs can be grown and their bandgaps made wider or narrower with Al or In, respectively. The stoichiometry of the films is controlled by the length of time for which the shutters are opened. Typical deposition rates for MBE are about 1 monolayer per second. This slow growth rate enables rapid changes between growth elements by use of shutters at the oven exits, thus allowing superlattices to be grown with excellent control of heterointerfaces.

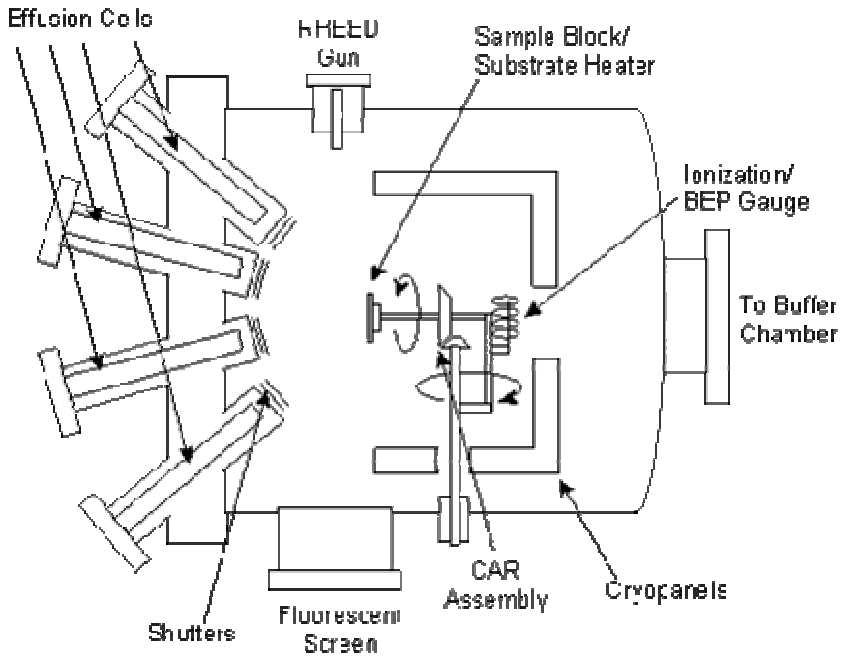

Figure 2.1 Schematic diagram of an MBE growth system. Shuttered effusion cells containing molten growth species are placed opposite a heated substrate.

2.2.2. Metal Organic Chemical Vapour Deposition (MOCVD)

MOCVD, also known as Metal Organic Vapour Phase Epitaxy (MOVPE), is quite a different growth method. The substrate is mounted on a graphite susceptor, which allows for good control of substrate temperature, as well as being resistant to the metal-organic growth species. The substrate is oriented at a shallow angle of about 10° to 30° to the horizontal and is placed in the path of supersonic gasses. Metal-organics, such as Trimethylgallium ($Ga(CH_3)_3$) and arsine (AsH_3), are heated in bubblers or boats, depending on whether they are liquid or solid, until they develop an appreciable vapour pressure, whereupon a carrier gas, usually hydrogen, is passed through or over them to fully saturate the carrier gas with the metalorganic precursors. The carrier gas then sweeps the vapours along which reach the substrate and decompose to allow, in this example, GaAs growth. Similar to MBE, bandgap tuning and doping can be carried out by using other gases such as Trimethylindium (TMI), Trimethylaluminium (TMA) and others.

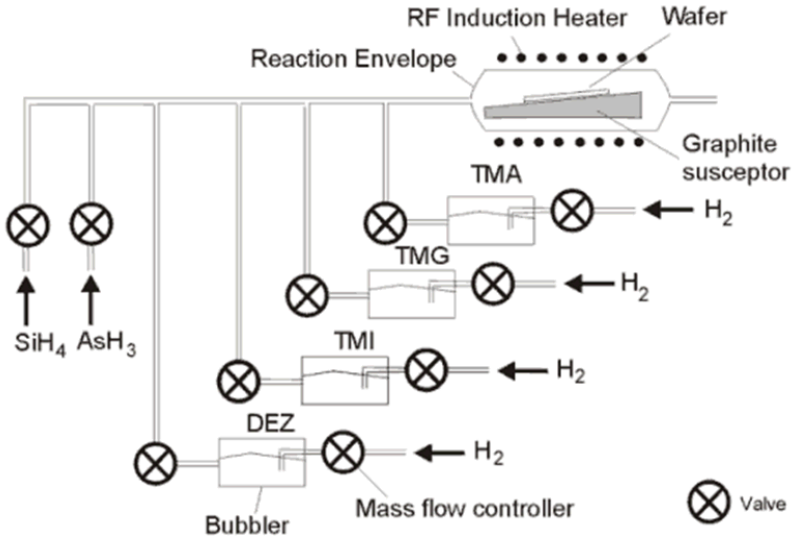

Figure 2.2 Schematic diagram of an MOCVD growth system. Valves control the flow of chemical precursors which react and deposit a film at the heated substrate.

2.2.3 Sputtering

PLD is a essentially a sputtering process carried out using high-intensity laser pulses to remove material from a target source. In conventional sputtering, the target is biased with respect to the substrate. An ionised process gas, usually Argon ions and electrons, bombard the target thereby removing atoms and imparting their energy and charge to them. The ablated target ions are attracted to the substrate where their energy and the energy contributed by the heated substrate allow them to migrate to appropriate lattice sites for crystal growth to occur (Figure 2.3). By placing magnets behind the target to confine the ionising electrons close to the target, the plasma can be intensified. This is known as DC sputtering. Replacing the DC supply with a radio frequency (RF) source allows non-conductive materials to be sputtered in a process known, sensibly enough, as RF sputtering. Finally, to make composite materials, a process gas such as oxygen or nitrogen, can be added to the ionising gas to make oxide and nitride materials.

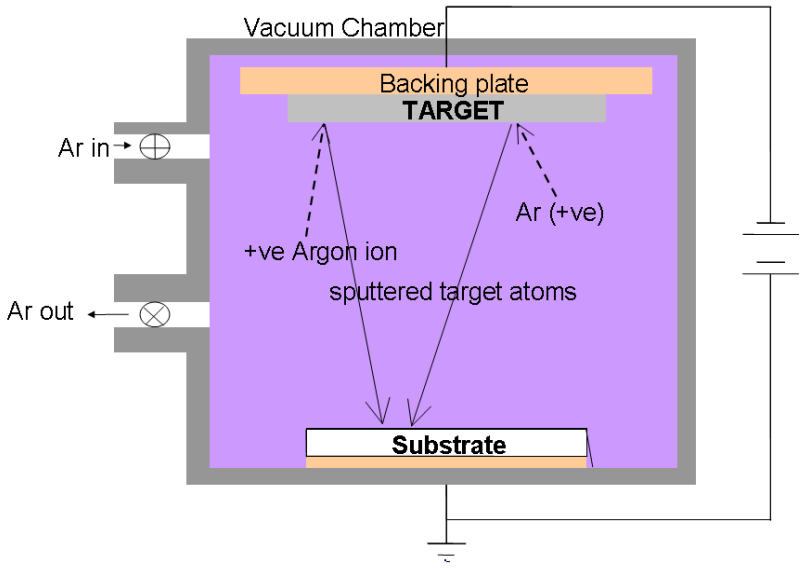

Figure 2.3 Schematic diagram of conventional sputtering process. Energetic argon ions ablate and ionise the target material, which is attracted to a charged heated substrate where film growth occurs.

2.2.4 Pulsed Laser Deposition (PLD)

2.2.4.1 Basic Principle

Pulsed Laser Deposition is effectively a laser-based sputtering technique. Its basic principle is quite simple; a high-power pulsed laser beam is focused onto the surface of an amorphous target where it is absorbed by the surface layers and material is ablated, as shown in Figure 2.4. The ablated species form a plasma plume (Figure 2.5) which is incident on a substrate, typically placed 5 cm to 15 cm away. The highly energetic ablated species (10 – 100 eV) have enough mobility to move to suitable lattice nucleation sites. The stoichiometry of the target is preserved in the growing film, a well-known advantage of PLD, as described in chapter 1. However, some exceptions to this rule were noted during the course of this research, which will be described more fully in later chapters. Specifically, the introduction of nitrogen gas was necessary when growing from ceramic nitride ZrN targets to optimise film properties. The addition of gasses which contribute to growth, usually oxygen or nitrogen, is common in PLD [5,6,7,13,17,18]. As is the case in the present work, these gases, particularly the more inert nitrogen, are activated by an Electron Cyclotron Resonance (ECR) or RF source to maximise their contribution to film growth. This is sometimes referred to as plasma-assisted PLD in the literature [5,6]. Although less frequently used, inert gases not forming part of the film can also be used, for example as a scattering element in eclipse PLD [7]. Eclipse PLD is one of the techniques used to reduce the number of large particulates reaching the substrate. Particulates and attempts to eliminate them will be discussed in later chapters. The fact that the ablating source is a laser means that it is decoupled from the chamber and hence deposition can also be carried out in UHV.

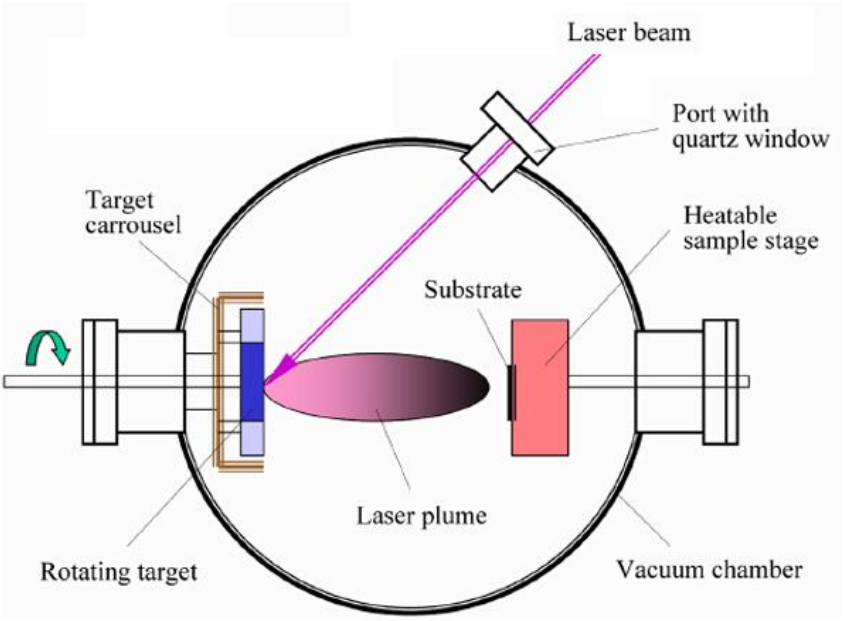

Figure 2.4 Schematic diagram of PLD system. An incoming laser beam ablates a target, creating an energetic plume which forms a film at the substrate, sometimes using a gaseous atmosphere such as nitrogen or oxygen as a film constituent.

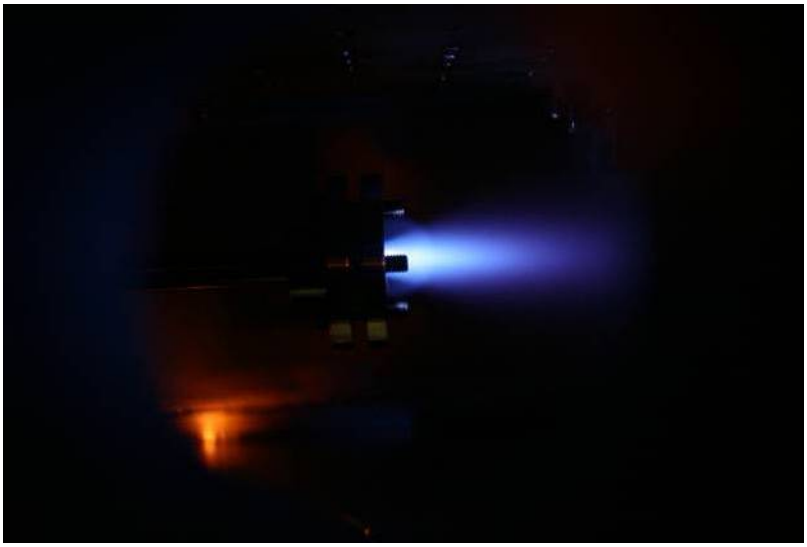

Figure 2.5 Plasma plume from a ceramic ZnO target during laser ablation. The substrate is approximately 4 cm from the target surface on the left of the image.

2.2.4.2 The laser ablation process

The process of pulsed laser ablation works as follows. Each laser pulse has an energy on the order of 100 mJ with a pulse lasting about 10 ns. The beam is focused to a spot of 1 – 2 mm^2 resulting in a power density on the order of 1 GW cm^{-2}. As UV laser wavelengths are often used, the absorption depth of most materials will be shallow, on the order of 10 nm [8]. This produces a sufficiently large electric field that some of the atoms within the absorption depth have their electrons removed by non-linear processes, in particular multiphoton ionisation (MPI). MPI is enhanced by imperfections in the target structure which serve to increase the electric field by a factor of n^4, where n is the refractive index of the target at the laser wavelength [9]. In the case of insulator targets, MPI is also enhanced by self-trapped excitons [10]. As electrons oscillate in the electric field of the laser beam, they collide with and transfer energy to neighbouring atoms, melting and finally vapourising the surface layer (Figure 2.6(a)). This begins the actual ablation as atoms leave the target surface (Figure 2.6(b)). Once a sufficiently high density of free electrons has been created, which typically occurs approximately 7 ns into the laser pulse, inverse Brehmsstrahlung occurs between the laser beam and the ablated species in the plume and the plume strongly absorbs the remainder of the laser pulse to create an intensely hot plasma of 10,000 K upwards [8] (Figure 2.6(c)). After the laser pulse stops, the plume dissipates and the melt front on the target recedes as it re-solidifies (Figure 2.6(d)).

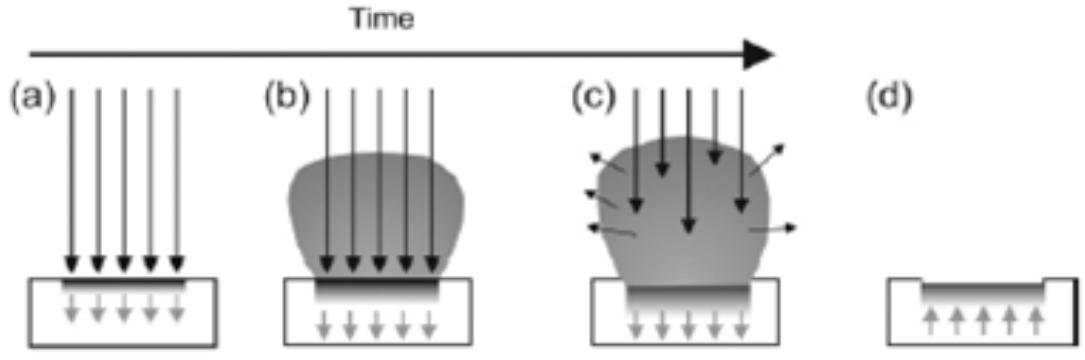

Figure 2.6 Laser – target – plume interaction sequence; (a) initial absorption and melting, (b) onset of vapourisation and melt front propagation into target, (c) absorption

of laser light by plume/plasma, (d) melt front recedes and resolidifies after pulse termination.

2.2.4.2.1 The laser ablation process in metals

When a short intense laser pulse strikes a metal target, the electromagnetic energy is immediately absorbed and converted into electronic excitations of unbound electrons and plasmons. These excitations transfer their energy to the lattice via electron-phonon coupling within a few picoseconds. The type of ablation process is governed by the durations of the laser pulse and the electron-phonon coupling time [11]. When the coupling time is less than the duration of the laser pulse, conventional thermal deposition is limited and other thermophysical effects play a more important role in determining the ablation threshold. When the laser pulse is longer than the coupling time, which it is once in the nanosecond timescale, material ablation occurs via conventional heat deposition. In metals, where the optical absorption depth is smaller than the thermal diffusion depth, the laser energy is first transferred to an absorption layer before being thermally transported to a depth governed by the thermal diffusion length. In both processes, the ablation threshold has been shown to increase with laser pulse duration in metals [12]. Ablation threshold is more commonly defined in terms of energy density rather than power density, as it is quanta of energy that are used to measure the breaking of bonds in target materials.

2.2.4.3 Advantages and disadvantages of PLD

A PLD growth system was chosen to undertake the present research as a consequence of the technique's inherent advantages. Also, the drawbacks of PLD are not of significant detriment to this work.

A principal advantage of PLD is that it allows film growth at lower substrate temperatures than MBE or MOCVD owing to the higher kinetic energy of ablated species (10 - 100 eV). The extra energy of ablated species gives them high surface mobility at the substrate, allowing them to move to suitable sites for bonding rather than relying on

diffusion kinetics supplied by a heated substrate. Lower substrate temps allow for a more varied choice of substrate, such as sapphire or even plastic – the latter would certainly be destroyed by the bombardment of MBE. These substrates would, for example, allow the growth of materials which are transparent to visible light or physically flexible. Growth can be carried out in a vacuum environment or in low pressure, less reactive nitrogen atmospheres as compared to MBE or MOCVD. MOCVD in particular uses gas compounds that can be hazardous and require additional safety procedures in their waste removal and processing. Finally, the PLD technique is very flexible. Virtually all materials can be ablated by UV lasers and as such a wide variety of material types can be grown – magnetic, superconducting, semiconducting, or ferroelectric.

There are two major disadvantages to PLD – poor uniformity and small substrate coverage. The ablation plume is small and highly directional, so it covers only a narrow section of substrate. Within the covered area, there is non-uniformity both in terms of film thickness and also of stoichiometry, factors encountered during this research. The plume is more dense in the centre and, when ablating from a metal target in a nitrogen atmosphere, the metal:nitrogen ratio decreases from the centre of the plume outwards, creating the stoichiometry changes. At a glance, the solution to lack of uniformity seems obvious – locate the plume off the central axis and rotate the substrate, but this can create problems in maintaining uniform substrate temperature. Because of these two disadvantages, PLD does not lend itself well to mass production.

However, PLD systems are designed for research purposes and large coverage areas are not required in this work. Typically, 1 cm × 1cm substrates are used and they provide sufficient sample sizes for analysis. The lack of film uniformity does have to be taken into account in post-growth analyses, but in fact it was even a useful factor in some of the present work, e.g. a HfN sample which showed strong anisotropy had its stoichiometry measured at different locations and the results were correlated with reflectance data from the different areas.

As far as choosing a growth method to investigate refractory metal nitrides, PLD was the best choice. The high melting point of refractory metals mean thermal emission temperatures are in excess of 2000°C, out of the available range of MBE effusion ovens. Also, suitable compounds of refractory metals for MOCVD reactions do not currently

exist. Designing and installing a PLD system was the logical choice to research these and other materials and the flexibility of the system will allow a wide variety of material types to be investigated in the future.

2.3 Assembly and calibration of HV and UHV PLD chambers

2.3.1 Chamber design and system elements

The PLD system used in the course of this research was built and tested as part of the work. Assembly required testing, some minor redesigns and adjustments, and calibration. Two vacuum chambers, custom-built by Thermionics, were assembled at the outset of this work; a high vacuum (HV) chamber and an ultrahigh vacuum (UHV) chamber. The HV chamber has a volume of 250cm^3 and achieves a base pressure of 10^{-6} Torr. Some alterations were made to the chamber design to properly accommodate a substrate holder, heater and a rotating target. Once it was working some ZnO targets were pressed and sintered from powder and ZnO films were grown to test the targets and system elements. The ZnO films grown were found to exhibit photoluminescence, which gave an indication of at least reasonable quality. The HV chamber is used to grow oxide materials and as such further explanation of this work is not of significance to this thesis.

The UHV chamber is a considerably more complex design. To allow for rapid changing of targets and substrates the chamber is load locked and has a six-target carousel, which allows growth of superlattices, capping layers and other types of heterostructures. It is significantly larger (660cm^3) and more complex than the HV chamber. The chamber has an expected base pressure of $<10^{-10}$ Torr but, in order to avoid stresses to the various system elements, it has never been baked out. Justification for this is a result of the pumping arrangement during growth; during growth the chamber is pumped by a turbomolecular pump, which brings the pressure down to the low 10^{-7}/high 10^{-8} Torr range (after outgassing of substrate). When not in use for growth, the chamber pressure is maintained by a Thermionics ion pump which keeps the chamber at $5\times10^{-9} \pm 2\times10^{-9}$ Torr. Thus, the ultimate base pressure is greater than an order of magnitude lower than the base pressure achievable by the Pfeiffer turbopump during growth. Furthermore,

nitride materials are grown in a nitrogen atmosphere of at least 1×10^{-5} Torr, with most growths being at 1×10^{-4} Torr N_2, so the 10^{-9} Torr base pressure is sufficient. Nitrogen used in all film growths (and chamber venting) was 99.9995% pure N_2 with confirmed Argon content of <0.001%. The low Argon content is an important detail as Argon ions created by the plasma source are actually an etchant which can attack chamber seals and the growing film and substrate. The nitrogen input to the plasma source also had Entegris or Aeronex inert gas purity filters fitted just behind the leak valve to reduce O_2, H_2, CO, CO_2 and H_2O to sub-ppb levels and also remove any trace impurities picked up from the stainless steel supply lines. The chamber also has a Stanford Research Systems Residual Gas Analyser (RGA) which can monitor gaseous species of up to 100 a.m.u., so the residual gas content in the chamber is always known before growth starts. This allows outgassing times to be tailored to achieve acceptably low levels of water vapour and also monitor for any residual solvents that may remain after substrate degreasing. The dominant gas species remaining at low pressure is H_2, which is the most difficult gas to eliminate in any UHV system since its tiny molecular diameter allows it to enter the chamber even though Conflat copper O-ring seals.

A diagram and photograph of the UHV PLD system is shown in Figure 2.7. The chamber was assembled in stages, with each system element being checked as it was assembled. First, the RGA, plasma source, vacuum gauges, windows, shutters and blank-offs were put in place and the pumps installed. The chamber was turbopumped down to the mid-10^{-7} Torr range. A small leak in the chamber was found and repaired. The ion pump was started which brought pressure down to the mid-10^{-8} Torr range. This was the base pressure until metals ablated during first growths had a gettering effect on residual gasses and pressure was further reduced to the mid-10^{-9} Torr range. The plasma source was characterised, as outlined in section 2.4. Finally, the chamber was vented to install the RHEED screen and electron gun, which were then aligned, as described in section 2.5. The plasma source is oriented towards the substrate at a 45° angle to ensure effective N_2 plasma delivery. Three other equidistant 4½" ports point toward the substrate around the chamber. These can be fitted with effusion ovens to use the chamber for MBE growth if required. The ovens could be combined with PLD growth to provide low-level doping. Doping in PLD is typically at levels of 1% rather than the ppm doping levels used in

semiconductors. PLD doping is usually from careful mixing of elements in a custom-made target [13] or ablation of a second target as dopant, [14] although low-level doping can be achieved where the dopant is an introduced gas [15, 16] or unintentional background doping can take place [16]. An MBE oven as a dopant source would make this possible.

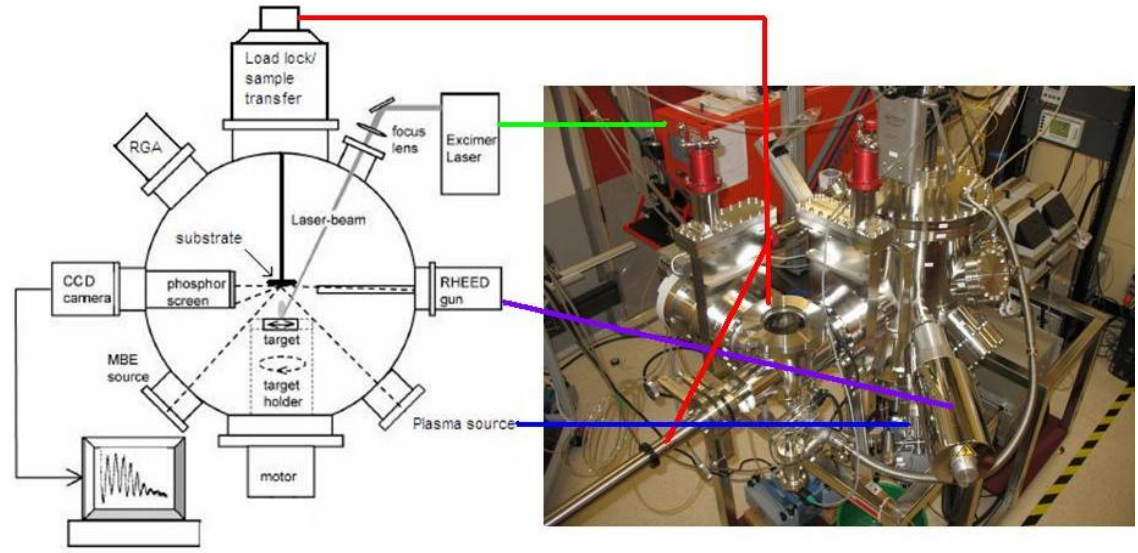

Figure 2.7 Schematic diagram and photograph of the UHV PLD system. Coloured lines are inserted to identify system elements.

2.3.2 The KrF Excimer Laser

The laser chosen for the PLD system is a Lambda Physik Compex 205 KrF excimer laser. It has an emission wavelength that is fixed at 248 nm (5.0 eV), but the gas in the tube can be changed to a different dimer molecule if another wavelength is desired; ArF emits at 193 nm, XeCl at 308 nm and XeF at 351 nm. KrF is the more prudent choice however. Its wavelength is short enough to be readily absorbed in the surface layers of most materials. Absorption by the Schumann-Runge bands of molecular oxygen is minimal at this wavelength so there is little beam attenuation between the laser exit aperture and the chamber laser window. This and the lack of hazardous ozone production mean that the beam path does not have to be enclosed or evacuated, as it does for ArF use. Also, KrF yields the greatest energy per pulse, peaking at 650mJ per pulse when first

operated, but this peak energy has steadily decreased to 450mJ after several years and many millions of pulses later. It is certainly more than sufficient to achieve high enough energy densities to ablate any material without requiring excessively small spot sizes, which can exacerbate particulate generation in the ablation plume. Pulsewidth is fixed at 25 ns and the repetition rate can be varied from 1 Hz to 50 Hz. In the exhaustive array of variable parameters, all of which have an effect on film growth, the rep rate was mostly kept constant at 10 Hz. The laser is delivered to the chamber via a 'periscope' arrangement of mirrors, required to move the beam from horizontal waist-height to a 45° descending beam incident on the target. The beam is enclosed in wide aluminium piping for safety. A single mirror on a magnetic mount alternates the beam between the HV and UHV chambers without effecting other optical elements in the beam path. All optics used are specifically coated for 248 nm UV light.

The laser window periodically becomes coated with ablated material and must be removed for cleaning. To avoid having to vent the chamber to do this, that window has its own gate valve and can be isolated to pump through a bellows attached to the load lock. It was found that the best method of cleaning the laser window was to drip concentrated HCl onto the central area of the window with a glass pipette, using a blunt glass rod to spread a film of HCl around the window, while keeping it away from the edges where it could dissolve the seals. The HCl was left in place for 30 minutes and removed with a pipette. The window was then rinsed multiple times, inspected for cleanliness and the procedure repeated as many times as necessary. Window throughput was measured before and after cleaning, in the former case to estimate any deviation from the expected fluence reaching the target and in the latter case to confirm all deposits had been removed and the window was delivering its factory-specified 90% transmittance.

2.4 Calibrating the plasma source

Growth of nitride thin film materials often requires use of a source of activated nitrogen such as Electron Cyclotron Resonance (ECR) or Radio Frequency (RF) plasma source. The nitrogen molecule is very stable and inert, having a binding energy of about 10eV. It must be activated using a dedicated nitrogen plasma source in order for it to

participate in the growth process. The plasma source gives nitrogen an energy of 10 - 100 eV, placing it on a par with the highly energetic laser-ablated species in PLD, which have an energy of 50 – 1000 eV [17, 18]. This is necessary to provide the energy for crystal growth in PLD, which is derived primarily from the incoming atoms and ions rather than from high substrate temperatures.

Plasma sources create different species of nitrogen, e.g. atomic nitrogen, various species of excited molecular nitrogen and ionic forms of both species. Each of these will have a different effect on the material being grown and hence the composition of the plasma beam must be assessed as a function of pressure and RF power. Plasma sources are not characterised by the manufacturer hence we must do so ourselves to establish which gas flow rates and RF powers to use during PLD growth for optimum conditions [19]. The properties of the material grown are highly dependent on the nitrogen species emitted from plasma, e.g. N, N*, N_2, N_2*, N_2**, N+, N_2+. Which of these species is produced is dependant on RF power and gas pressure and hence the source must be characterised as a function of both.

The results of characterisation of an Oxford Applied Research HD25 RF plasma source (Figure 2.8) are presented here. Characterisation was carried out by analysing the optical emission of the active species while atomic signatures were detected with a Residual Gas Analyser (RGA). The plasma source was subsequently modified with a Pyrolytic Boron Nitride (PBN) insert intended to increase the atomic nitrogen content and characterised again to assess its effectiveness.

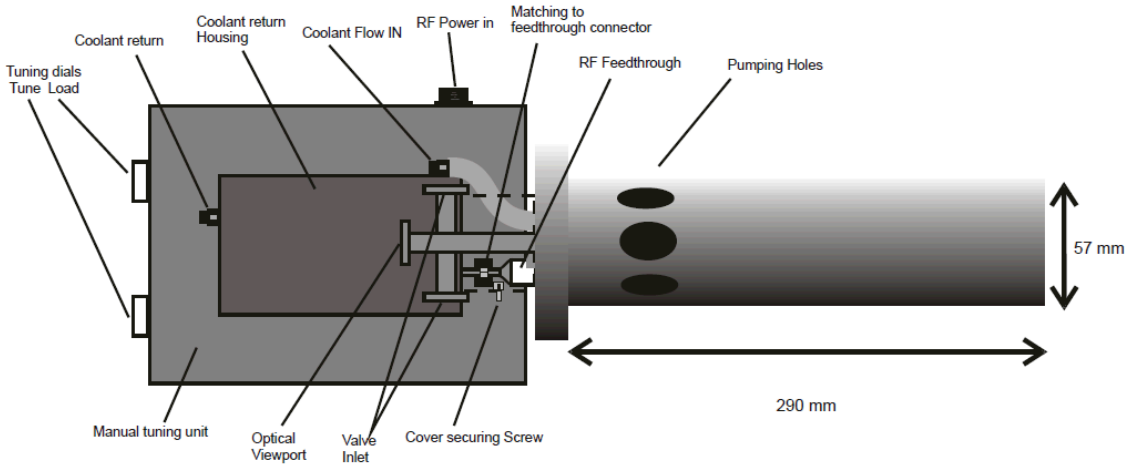

Figure 2.8 Schematic diagram of the Oxford Applied Research HD25 RF plasma source. The right-hand half of the diagram shows the cylindrical discharge chamber which is internal to the vacuum chamber, while the left-hand half shows the external control elements.

In RF atom sources a gas is introduced into an all-ceramic cavity (discharge zone). A plasma is induced in the discharge zone by applying inductively-coupled RF excitation, i.e. there is resonant absorption by nitrogen molecules at the 13.56 MHz supply voltage frequency. The plasma acts to dissociate the molecular species into ions and neutral atoms as well as ionising the molecules. Neutral particles exit from the zone through a series of holes in the source aperture plate and are directed towards the intended site in the vacuum chamber, while charged particles are retained in the plasma.

Figure 2.9 (a) shows the optical spectrum of the nitrogen plasma, measured using a fibre-coupled CCD detector. Spectra were taken through a window on the growth chamber and as such are indicative of the nitrogen in the growth area, rather than in the plasma cavity. A wide spectral range (500 nm) was used to include as much of the spectrum as possible, hence resolution was reduced and the atomic nitrogen peaks are not as sharp as expected, nor is their fine structure resolved. It was found that superposition of atomic and molecular peaks prevent accurate resolving of N and N_2 contributions. Hence spectra yield qualitative information only. The intensities of the separate N : N_2 ratios, shown in Figure 2.9 (b), can be estimated more accurately using the ratio of the

their peak intensities in the RGA scans. The nature of RGA measurement is such that each data point is discrete, being of a particular atomic mass number, so peak ratios suffice and integration of areas is not necessary.

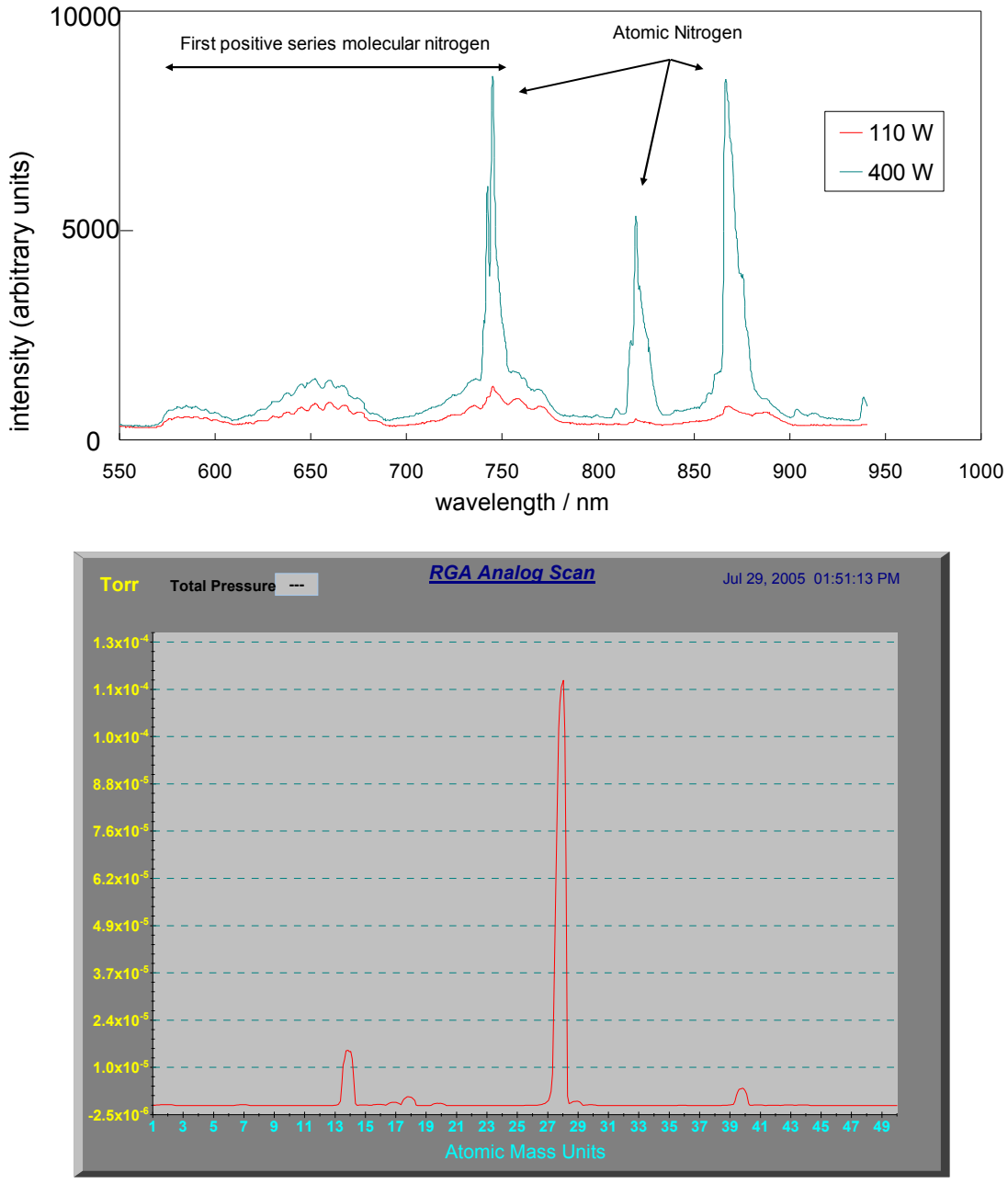

Figure 2.9 Top: Optical spectrum of nitrogen plasma showing the difference in atomic and molecular intensity ratios for high and low applied powers. Bottom: RGA mass spectrometer scan taken at 150 W and 1.2 × 10^{-4} Torr showing N and N_2 peaks at 14 a.m.u. and 28 a.m.u. respectively.

Figure 2.10 shows the partial pressure contribution of excited molecular nitrogen (N_2*) across the RF power range. It does not show any dependence on RF power. The N_2* represents approximately 40% of the overall pressure at each level.

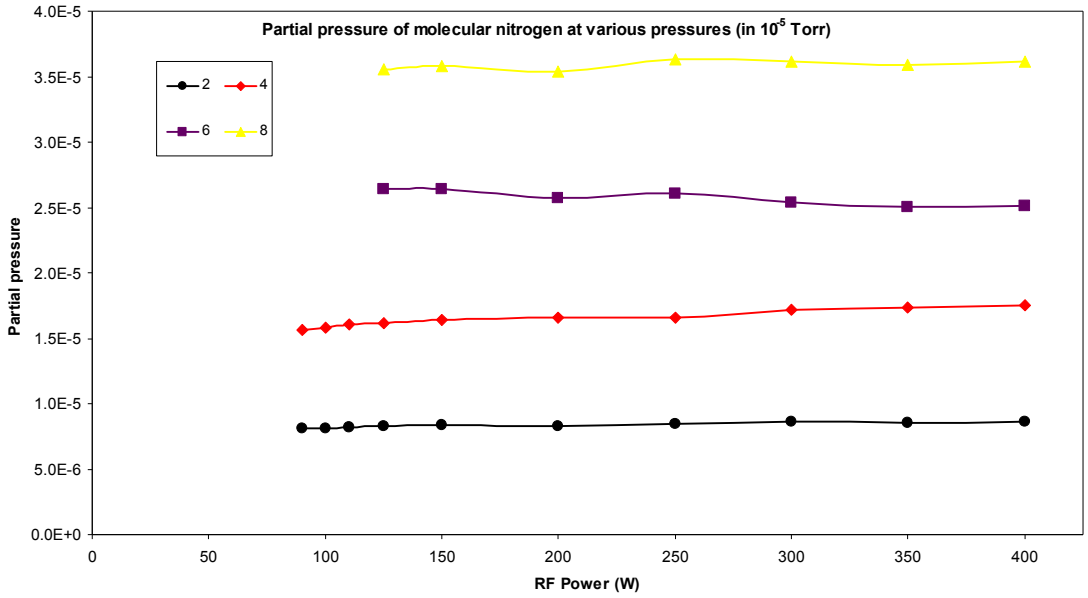

Figure 2.10 Partial pressure of molecular nitrogen as a function of applied RF power. Data is shown for overall chamber pressures of 2 x 10^{-5} Torr (black), 4 x 10^{-5} Torr (red), 6 x 10^{-5} Torr (burgundy) and 8 x 10^{-5} Torr (yellow).

Figure 2.11 shows very different behaviour for excited atomic nitrogen (N*). N* levels increase at higher RF power, a behaviour we expected to observe. However, the increasing slope of the data points as we move to higher overall chamber pressure shows that the rate of N* production increases at higher pressure. Scans taken at 80 µTorr clearly show the elevated levels of atomic N at higher RF power. Thus, by operating at higher chamber pressure we can maximise the amount of N* present.

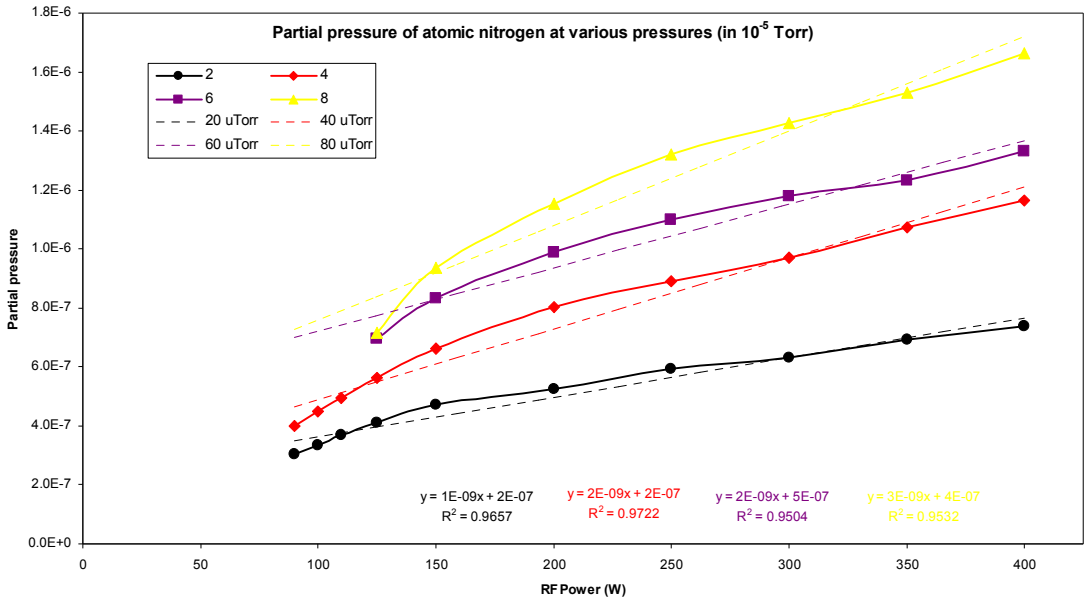

Figure 2.11 Partial pressure of atomic nitrogen as a function of applied RF power. Data is shown for overall chamber pressures of 2 x 10^{-5} Torr (black), 4 x 10^{-5} Torr (red), 6 x 10^{-5} Torr (burgundy) and 8 x 10^{-5} Torr (yellow).

The plasma source is fitted with ion deflection plates to remove ions from the plasma. Ions are detrimental to the formation of good quality crystalline material due to changes in bonding potential. Figure 2.12 shows the variation in ion content of the plasma when the deflection plates are switched off. Ion content is clearly higher at low nitrogen pressures, composing up to 5% of the overall pressure if the deflection plates (E= 150 V cm^{-1}) are left inactive.

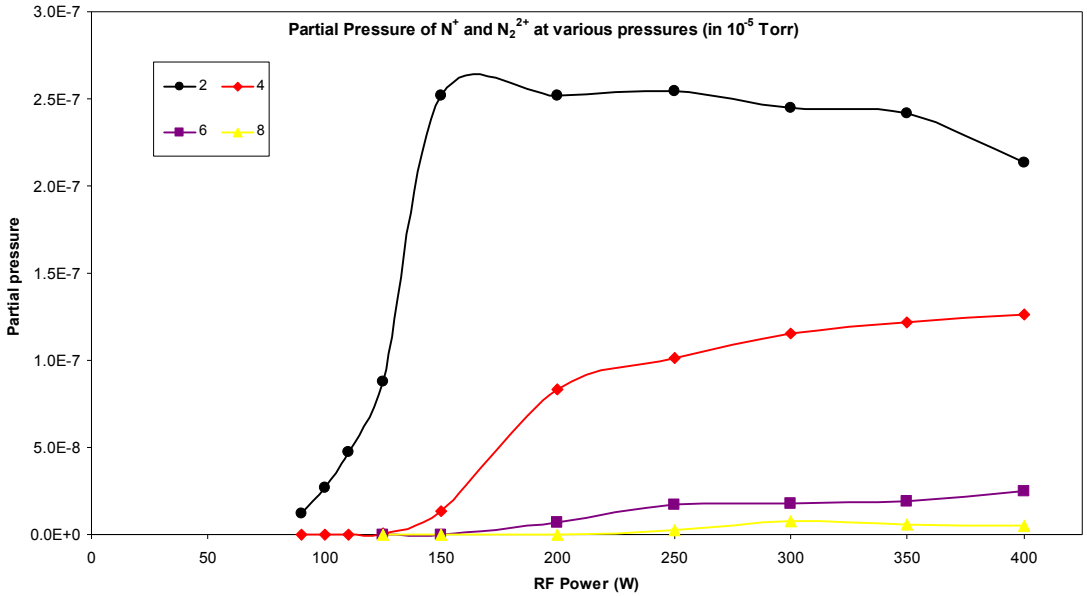

Figure 2.12 Total ion content (both singly and doubly ionised species) of nitrogen plasma when ion deflection plates are not active. Data is shown for overall chamber pressures of 2 x 10^{-5} Torr (black), 4 x 10^{-5} Torr (red), 6 x 10^{-5} Torr (burgundy) and 8 x 10^{-5} Torr (yellow).

2.4.1 Modifications to the plasma source

Attempts were made to improve the N* production by placing a ceramic Pyrolytic Boron Nitride insert into the discharge cavity. This small flat disk was designed to fit snugly in the cavity and had a series of small gaps around its outer edge. It was hoped that this would drive nitrogen to the cavity walls and thus increase coupling of the RF power to the nitrogen. However, it was found that the insert only served to destabilise the plasma. Argon gas was also included in the nitrogen flow, at 5% and 25%, since other researchers have found that this increases N* content [20]. Measurements under otherwise identical conditions to those above were made, but contrary to the other authors' findings, no increase in N* levels was observed.

Thus, the levels of excited monatomic and molecular nitrogen produced by the Oxford Applied Instruments HD25 Nitrogen Plasma Source have been measured as a function of pressure and applied RF power. Attempts to increase the level of excited

atomic nitrogen present in the plasma stream have been made by physically modifying the source and by adding argon, but neither method has shown any improvement. The plasma source is now calibrated and the knowledge of its emitted nitrogen species will prove valuable when nitride materials are grown. The effects of different levels of atomic nitrogen in the plasma will be of interest in growth as they can also prove detrimental to nitride growth in some cases, such as for GaN where the atomic nitrogen is thought to scavenge nitrogen from the growing surface to form N_2 [21].

2.5 Reflection High Energy Electron Diffraction (RHEED)

As thin films reduce in thickness, approaching the fundamental limit of a monatomic layer, the abruptness of interfaces becomes an issue for multilayer and superlattice structures. It is therefore increasingly important to monitor film growth in-situ. Since thin film growth occurs at the surface, it stands to reason that amongst the available in-situ monitoring methods, surface and near-surface analysis is a most important parameter. Sampling methods that use low-energy electrons (100 eV – 2 keV) , such as low energy electron diffraction (LEED), Auger electron spectroscopy or X-ray photoelectron spectroscopy, typically have a penetration depth of 5 – 40 Å in solids, making them very surface specific. However, in this work, nitrides are typically grown in a background of nitrogen pressure up to 10^{-4} Torr and so the higher energy electrons of RHEED (10 – 20 keV) are necessary to overcome gas-scattering and achieve sufficient intensity at the detector (a fluorescent screen / CCD camera combination). Higher energy detection methods, such as Rutherford backscattering spectroscopy which uses ions in the MeV range, are even less subject to gas scattering, but their sampling depth also increases to 0.5 – 2.0 μm, making them less surface-specific [22].

2.6 Reflectivity measurement process

Refractory metal nitride films grown in this work are intended to find applications as buffer layers between silicon and GaN. As such, they must provide suitably low resistivity to be a viable electrical contact while also reflecting an appreciable amount of

light to make any such buffered GaN devices more efficient. An accurate reflectivity spectrum also yields information about the films' electronic structure.

In this work, an Ocean Optics HR4000CG-UV-NIR fibre optic spectrometer has been used to carry out reflectivity measurements. The output of a tungsten halogen white light source is coupled to a spliced fibre which is shone on the film surface at normal incidence. The reflected signal is collected by the same fibre and input to the spectrometer. The light source is allowed to warm for at least 20 minutes before data collection to ensure that its output does not change during measurements. The 3648-element CCD detector is sensitive to light from 200 – 1100 nm and has a resolution of 0.75 nm, although the light source cuts off below 360 nm. The reflectance values are calculated relative to a standard reference as follows;

$$R_\lambda = \frac{S_\lambda - D_\lambda}{Rf_\lambda - D_\lambda}$$

Where R_λ = reflectance at wavelength λ

S_λ = sample intensity at wavelength λ

D_λ = dark intensity at wavelength λ

Rf_λ = reference intensity at wavelength λ

Two mirrors have been used as sources of reference reflectivity; a Newport BD.1 mirror giving an almost flat response of 99.5% over the range 488 – 750 nm and a Thorlabs protected silver mirror which has a flat response in excess of 98% extending further into the infra-red. The switch between reference mirrors is taken at a wavelength at which they have equal reflected intensity (580 nm) and similar shape. Combining these two references ensures an accurate picture of the films' true reflectivity can be built up.

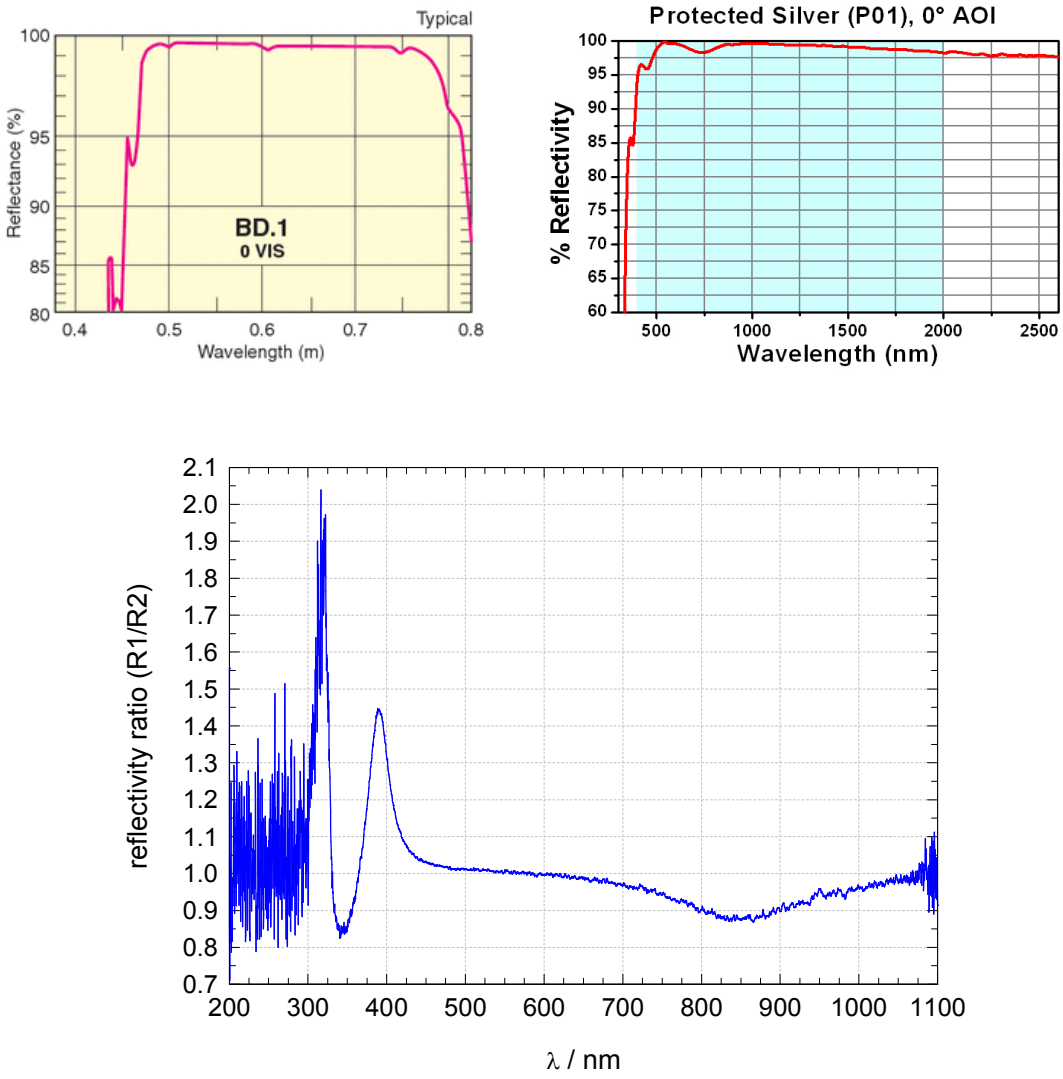

Figure 2.13 Reflectivities of visible-optimised Newport mirror (top left) and Thorlabs IR-optimised mirror (top right) (supplied by manufacturers). Their measured reflectance ratios are shown in the bottom plot.

2.7 Other analysis methods

RHEED and reflectivity measurements have been described in this and the preceding section as these systems were specifically developed as part of the commissioning of the PLD system. However, they are not the only measurement techniques used to analyse thin films grown in this work. Surface morphology of the samples is also very important. Atomic Force Microscopy (AFM) and Scanning Electron Microscopy (SEM) were also regularly used in post-growth analysis. Although AFM can return a value for r.m.s. roughness of the films, SEM was a more practical method of surface investigation, for two reasons. Firstly, the presence of any particulate on the surface, no matter how small, would be several orders of magnitude larger than the roughness of the surface itself. In PLD, surface morphology is most often dominated by the presence of particulates. Secondly, AFM is slow to build up a single image of a very small area. SEM allows the entire surface to be rapidly imaged to show the distribution of particulates across a surface. This gives an indication of the position of the centre of the plume relative to the substrate, as particulate size and density was seen to increase towards the centre of the plume. During some film growth, stoichiometry of the films varied depending on the ratio of metal:nitride arrival at the film surface. This was particularly in evidence in the case of HfN. Correlating the particulate density with localised reflectivity measurements established the degree to which reflectivity was effected by particulates on the surface. These measurements will be outlined in chapter 4.

Raman spectroscopy [23] has been used to investigate the HfN and ZrN materials. In the Raman technique, light is inelastically scattered in a material, creating phonon modes. In this work, the phonon modes measured are verified as agreeing with theoretical calculations and are found to be related to material stoichiometry.

X-Ray Absorption and X-Ray Emission [24] were also employed to describe the bandstructure of HfN and explain the reflectivity observed, while X-Ray Diffraction [25] is used to measure its crystallographic orientation and lattice constant.

2.8 Conclusion

This chapter has outlined the reasons for carrying out this research using the PLD growth method. PLD and other thin film growth methods that could potentially have been used have been described and PLD has been shown to be the best method available to conduct research on refractory metal nitrides, as well as showing the greatest flexibility to switch to different material systems in the future. The design and calibration of the PLD system and its associated elements have been outlined briefly as they formed a significant part of the early work of this PhD. The key analysis techniques, RHEED and reflectivity, have been described in cases where a significant aspect of their set-up was part of this work. Obviously several additional analysis techniques were required for a complete understanding of the films produced, such as SEM, AFM, XRD, RBS and surface profilometry, but these were not implemented by the author and will only be detailed in later materials analysis chapters where appropriate.

References

[1] R. Feynman. “Surely You're Joking, Mr. Feynman!” (1985) Chapter 6

[2] M. Faraday, Philosophical Transactions, 147, 145 (1857)

[3] R. Nahrwold, Ann. Physik, 31 467 (1887)

[4] A. Kundt, Ann. Physik 34, 473 (1888)

[5] Z.B. Dong, Y.F. Lu, K. Gao, L.Q. Shi, J. Sun, N. Xu and J.D. Wu, “Thermal stability of carbon nitride thin films prepared by electron cyclotron resonance plasma assisted pulsed laser deposition” Thin Solid Films 516, 8594 (2008)

[6] I. Marozau, A. Shkabko, G. Dinescu, M. Döbeli, T. Lippert, D. Logvinovich, M. Mallepell, A. Weidenkaff and A. Wokaun “RF-plasma assisted pulsed laser deposition of nitrogen-doped $SrTiO_3$ thin films”, Applied Physics A: Materials Science & Processing 93, 721 (2008)

[7] M. W. Allen, R. J. Mendelsberg, R. J. Reeves,and S. M. Durbin. “Oxidized noble metal Schottky contacts to *n*-type ZnO” Applied Physics Letters 94, 103508 (2009)

[8] P. R. Willmott “Deposition of complex multielemental thin films” Progress in Surface Science 76, 163 (2004)

[9] N. Bloembergen, “Laser-induced electric breakdown in solids”, IEEE Journal of Quantum Electronics QE-10, 375 (1974)

[10] N. Itoh, “Material modification by electronic excitation”, Radiation Effects and Defects in Solids 146,1 (1998)

[11] J. Shen, Z. Gai and J. Kirschner, “Growth and magnetism of metallic thin films and multilayers by pulsed-laser deposition”, Surface Science Reports 52, 163-218 (2004)

[12] P. P. Pronko, S. K. Dutta, D. Du and R. K. Singh, ”Thermophysical effects in laser processing of materials with picosecond and femtosecond pulses”, Journal of Applied Physics 78, 6233 (1995)

[13] Hong Seong Kang, Byung Du Ahn, Jong Hoon Kim, Gun Hee Kim, Sung Hoon Lim, Hyun Woo Chang, and Sang Yeol Lee, “Structural, electrical, and optical

properties of *p*-type ZnO thin films with Ag dopant", Applied Physics Letters 88, 202108 (2006)

[14] M. Okamoto, Y. Khin Yap, M. Yoshimura, Y. Mori and T. Sasaki. "The ohmic character of doped AlN films" Diamond and Related Materials 10, 1322 (2001)

[15] C.M .Rouleau, D.H. Lowndes, J.W. McCamy, J.D. Budai, D. B. Poker, D. B. Geoghan, A. A. Puretxky and S. Zhu, "Growth of highly doped p-type ZnTe films by pulsed laser ablation in molecular nitrogen" Applied Physics Letters 67, 2545 (1995)

[16] M. Cazzanelli, D. Cole, J. Versluijs, J.F. Donegan, J.G. Lunney. "Pulsed laser deposition of GaN thin films" Materials Science and Engineering B59, 98 (1999)

[17] D. B. Chrisey and G. K. Hubler, "Pulsed Laser Deposition of Thin Films", Wiley-Interscience, p.60, p.581 (1994)

[18] H.U. Krebs, M. Weisheit, J. Faupel, E. Süske, T. Scharf, C. Fuhse, M. Störmer, K. Sturml, M. Seibt, H. Kijewski, D. Nelke, E. Panchenk, and M. Buback, "Pulsed Laser Deposition – a versatile thin film technique", Advances in Solid State Physics 43, 505 (2003)

[19] P.A. Anderson, R.J. Kinsey, C.E. Kendrick, I. Farrell, D. Carder, R.J.Reeves and S.M. Durbin, "Influence of Nitrogen Species on InN Grown by PAMBE", Materials Research Society Symposium Proceedings: GaN, AIN, InN and Related Materials, 892, 89 (2006)

[20] J.Liu, F.Sun, H.Yu. "Enhancement of the molecular nitrogen dissociation and ionization levels by argon mixture in flue nitrogen plasma" Current Applied Physics 5, 625 (2005)

[21] A. J. Ptak, M. R. Millecchia, T. H. Myers, K. S. Ziemer and C. D. Stinespring. "The relation of active nitrogen species to high-temperature limitations for $(000\bar{1})$ GaN growth by radio-frequency-plasma-assisted molecular beam epitaxy" Applied Physics Letters 74, 3836 (1999)

[22] O. Auciello and A. R. Krauss. "In-situ real-time characterisation of thin films", Wiley Press (2001)

[23] G. Dent and E. Smith, "Modern Raman spectroscopy: a practical approach", Wiley Press (2005)

[24] J. Nordgren, G. Bray, S. Cramm, R. Nyholm, J.-E. Rubensson, and N. Wassdahl, "Soft x-ray emission spectroscopy using monochromatized synchrotron radiation", Review of Scientific Instruments 60, 1690 (1989)

[25] M. Ladd and R. Palmer, "Structure determination by X-ray crystallography", Kluwer Academic/Plenum Publishers (2003)

Chapter 3 GALLIUM NITRIDE

3.1 Introduction

III-V nitride materials have well-known applications in light emitting and detecting devices due to their direct bandgaps, which can be engineered to tune the bandgaps continuously over the range 0.6 eV to 6 eV. GaN in particular, and the ternary alloys it forms with In and Al, emit light throughout the visible spectrum which has lead to the commercial availability of highly efficient white LEDs. Its resistance to ionising radiation allow it to be used in solar cells on orbiting satellites while its ability to withstand higher temperatures make it attractive for use in power amplifiers. GaN can be deposited in thin film form by several crystal growth methods including MBE [(1)], MOCVD [(2)] and PLD [(3)]. It crystallises in either cubic or hexagonal form, depending principally on the choice of substrate – cubic on SiC and hexagonal on sapphire.

This chapter details attempts to grow good quality GaN on sapphire using a liquid-Ga target and a plasma-activated nitrogen source. GaN was a good choice of material to calibrate growth in the new UHV chamber for a number of reasons. Firstly, there is intense interest in the GaN material system, as evidenced by the number of publications which continue to grow annually. The wealth of literature available is a good guide to producing PLD films. Secondly, GaN lends itself well to being analysed using established techniques: RHEED can be used to monitor the growth process and verify the presence of GaN by calculation of its lattice constant from the patterns. SEM can further verify coverage of the sapphire substrate and help establish optimum fluence conditions; insufficient laser fluence will result in a partially covered or bare substrate which will exhibit charging in the electron beam whereas excessive fluence will result in a film heavily particulated with Ga droplets. Cleaving samples and viewing their edge by SEM should allow their thickness to be estimated and hence extract a growth rate for that sample's particular growth conditions. Photoluminescence, along with RHEED interpretation, will help assess the structural and optical properties of the GaN film. The final reason for choosing GaN in the initial series of growths is that it may be the top layer in multi-layer growths later in this thesis. It can also be used as an encapsulant for

GdN [17]. GdN is a spintronic material also under investigation, but its rapid oxidation upon exposure to atmosphere requires that it be protected before removal from the growth chamber. GaN will also be grown on top of HfN films [18,19], whereupon it is expected to show enhanced PL intensity due to the increased reflectivity of HfN when compared to GaN grown on sapphire or SiC substrates.

Growth from a liquid target is quite common [4-8], sometimes directly onto an untreated sapphire substrate [15]. Many authors have used a nitridation step to pre-treat sapphire surfaces [2,4, 9-14]. One group who studied the nitridation process [11] found an optimum nitridation time of 5 minutes, although they were nitriding under very different conditions (T_{sub}= 1050°C, NH_3 gas stream) compared to the present work (T_{sub} = 200°C, plasma-activated N_2^*), so the two are not directly comparable. They propose that nitriding will improve GaN growth because nitrogen will substitute for oxygen in the top few atomic layers, leading to an amorphous AlN layer. However, in this growth series RHEED patterns did not show any change in the sapphire substrate consistent with AlN formation, such as a change in lattice spacing and/or masking of the sapphire Kikuchi pattern. This result did not change for any of the different nitriding conditions listed in Table 3.1.

3.2 Experimental details

3.2.1 Growth parameters common to the GaN series

A series of films of GaN were grown across a range of growth parameters, listed in Table 3.1. Substrates were 432μm thick, 2" diameter c-axis [0001] sapphire supplied by Honeywell Electronic Materials. Chamber base pressure before introducing nitrogen or beginning ablation was 5×10^{-8} Torr, as growth is carried out under turbopumping. The chamber was periodically checked by a Residual Gas Analyser for the possible presence of impurities, in particular during outgassing for solvent and other residues or after the nitrogen cylinder was replaced. A Lambda Physik Compex 205 KrF excimer laser of wavelength 248nm and pulse length 25ns was used as an ablation source. The laser was mostly operated in constant energy mode to maintain fluence levels. Substrate

heating of up to 1000°C was provided radiatively by a quartz bulb and was monitored by an in-built calibrated thermocouple at the substrate mounting plate. In-situ monitoring of growth was provided by RHEED and subsequent analysis provided by SEM, photoluminescence, RBS and XRD.

A liquid Ga target was prepared by degreasing 99.99999% pure Ga ingots supplied by ESPI. Once inside the vacuum chamber, the ingots were gently melted by bringing the substrate heater close to the target carousel. They remained molten in the vacuum environment. It was found that surface tension caused the liquid to form a reasonably steep radius of curvature which proved problematic in maintaining a known fluence level as the laser spot size was continuously changing on the target. To help overcome this effect two stainless steel target holders were made with shallow conical shapes of differing angles. The more shallow of the two reduced the droplet curvature to some extent, but did not eliminate the problem. It would seem that the solution to the problem of changing incidence angle is simply to shine the laser on a horizontal part of the droplet and not rotate it during growth, yet when this was tried it resulted in no target ablation. This effect is not reported in the literature and a possible reason for this is postulated in section 3.2.3, which concerns precise calculation of laser fluence.

Sample ID#	Target→subs distance	Fluence (Jcm^{-2})	Total no. of pulses	N_2 plasma pressure (Torr)	nitriding	buffer	T_{sub} (°C)	Growth time (min)	notes
#1	7.8cm	0.92	26,000	1×10^{-4}	none	none	750	43	
#2	7.8cm	2.6	600 + 36,000	1×10^{-4}	2hr,200°C	450°C 10min	700	60	
#3	7.8cm	2.5 1 Hz	120 + 3,600	1×10^{-4}	2hr,200°C	450°C 10min	700	60	Mo plate added
#4	7.8cm	2.6	36,000	1×10^{-4}	2hr,200°C	None	700	60	
#5	7.8cm	0.3	36,000	1×10^{-4}	2hr,200°C	None	700	60	(*1)
#6	7.8cm	1.3	36,000	1×10^{-4}	2hr,700°C	None	700	60	(*2)
#7	7.8cm	0.9	36,000	1×10^{-4}	2hr,200°C	None	700	60	
#8	7.8cm	1.2	36,000	1×10^{-4}	2hr,200°C	None	700	60	
#9	7.8cm	1.1	36,000	5×10^{-5}	2hr,200°C	None	700	60	Target not rotated
#10	7.8cm	1.7 broad spot	36,000	1×10^{-4}	2hr,200°C	None	700	60	
#11	7.8cm	1.7	36,000	2×10^{-5}	2hr,200°C	None	700	60	
#12	7.8cm	1.7	36,000	1×10^{-4}	2hr,200°C	None	800	60	
#13	6.0cm	2.4	36,000	1×10^{-4}	2hr,200°C	None	800	60	
#14	6.0cm	2.4	18,000+ 18,000	1×10^{-4}	½hr,200°C	450°C 10min	800	30	
#15	6.0cm	5.1	36,000	1×10^{-4}	2hr,200°C	None	700	60	
#16	6.0cm	5.0	6,000+ 30,000	1×10^{-4}	½hr,900°C	450°C 10min	700	50	
#17	6.0cm	3.4 20Hz	18,000+ 144,000	1×10^{-4}	½hr,900°C	450°C 15min	700	120	

Table 3.1 Growth parameters for GaN on sapphire. All films were grown at a 10Hz laser duty cycle, except where indicated otherwise, and using an applied RF power of 200W for the N_2 plasma. (*1) indicates that for this sample and subsequent growths, the aperture was removed from the laser beam.

(*2) A Ga-deposition test carried out between #5 and #6 indicated Ga was being successfully deposited.

3.2.2 The evolving growth process

Prior to growth, a literature review was carried out to estimate an initial set of growth parameters likely to produce epitaxial GaN on sapphire, which could then be tailored to maximise crystal quality based on analysis of RHEED, SEM and PL. The principal settings to be decided in any growth attempt by PLD are substrate temperature, process gas conditions and laser parameters. There are, of course, individual variations within each parameter set (e.g. setting of applied RF power in addition to gas pressure when using a plasma) and pre-growth treatment of substrate, such as degreasing, outgassing and, in the case of GaN on sapphire, nitriding and buffer layer incorporation.

The first two growth attempts were carried out using a full 2" diameter sapphire wafer held in place at its edges by stainless steel clips, with the heater radiation incident on it directly. RHEED patterns (Figure 3.1) showed the semicircles typical of polycrystalline films. From a visual inspection of these films after growth, it was obvious that appreciable substrate coverage was limited to a central area of about $1cm^2$, hence growing on entire 2" wafers would be wasteful and subsequent wafers were cleaved to a smaller size. Also, it was realised that much of the radiation from the heater will have passed right through the sapphire and hence substrate temperature will have been lower than the desired 700 °C. Samples #3 onwards were bonded to a 2 mm thick Molybdenum plate using the surface tension of a thin InSn liquid layer, thus ensuring a good thermal contact. Sample #3 itself was grown at a reduced laser repetition rate of 1Hz as it was considered possible that the films might have been Ga-rich. The amount of Ga ablated during deposition can easily be significantly higher than the amount of nitrogen available to react and form GaN. Nitrogen pressure cannot be increased above 10^{-4} Torr as this is the maximum operating pressure of the plasma source. Given the large number of parameters that can be changed, nitrogen was kept at 1.0×10^{-4} Torr for all except two growths, with efforts concentrated on changing growth rate by means of laser fluence.

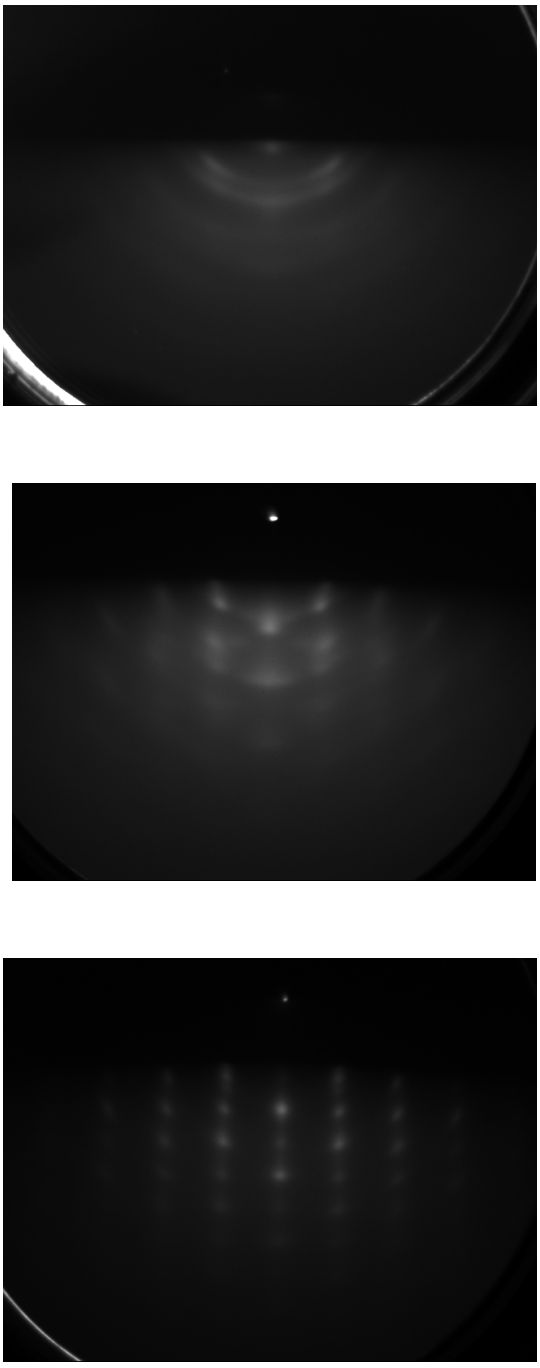

Figure 3.1 RHEED patterns of early samples #1,#2 and #4, showing the transition from polycrystalline films (semicircular patterned) to epitaxial films (streaky patterned) as the growth procedure improves. Sample #3 is too faint to be viewed with the eye and has been omitted.

Nitridation of the sapphire substrate is known to be a necessary step to reduce defect density in GaN [20]. This is most often reported as being carried out at 800 °C – 1050 °C and for a short duration of 30 minutes or less [1,2,10–13]. Most of these nitriding conditions are applied to MBE or MOCVD growth where NH_3 is the nitrogen source. The high substrate temperature is required to dissociate nitrogen atoms from the ammonia molecule. However, since the nitrogen source used in this research is already activated with a plasma source, most nitriding was carried out at a substrate temperature of 200°C and for a duration of 2 hours, similar to the work of Sanguino [21], Deiss [9] and Widmann [22]. Widmann *et al* specifically studied nitridation conditions and found that 200 °C for 90 minutes was optimum to improve the optical and structural properties of GaN epilayers. They concluded that a thin and well ordered AlN layer is formed at the sapphire surface, which can adequately relieve most of the strain in further growth through a well organised edge dislocation network at the interface. By contrast, a high nitridation temperature produced a perturbed interface with cubic crystallites occurring in the AlN layer. Widmann's nitridation study showed a change in the lattice parameter of +1% as the AlN layer forms and relaxes during nitridation. This occurs for all nitridation temperatures studied (200°C, 400°C and 750°C), with corresponding spots from areas of cubic structured GaN present in the pattern at the higher temperatures. By contrast, this work shows no variation of any kind in the RHEED patterns when nitriding at 200°C, as shown in Figure 3.2, implying that the nitridation process used in this research was ineffective in forming the desired AlN buffer on which to nucleate GaN growth. Higher nitridation temperatures of 700°C and 900°C were tried with later samples but were equally ineffective.

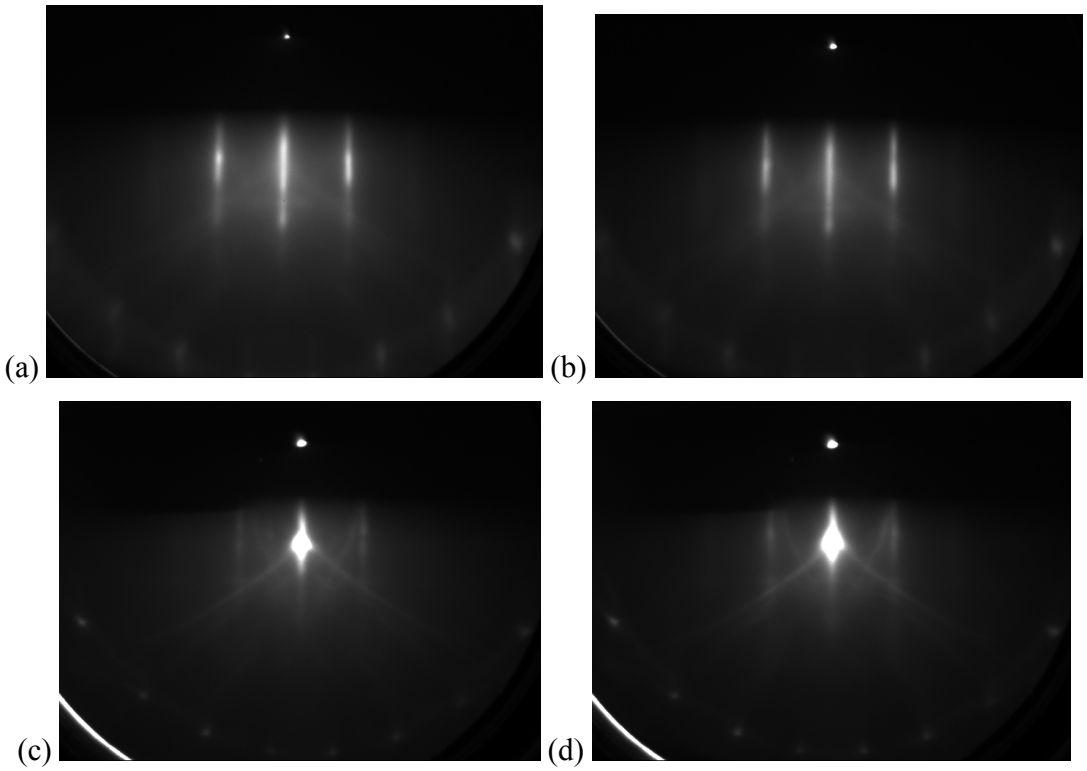

Figure 3.2 RHEED images of sapphire substrate before (a) and after (b) nitriding for 2 hours at 200°C and before (c) and after (d) nitriding for 30 minutes at 900°C. The RHEED images are unchanged, indicating that the nitriding process does not have any effect on the substrates.

After growth, each film was analysed by SEM to examine the surface morphology, particulates and substrate coverage. Many films were cleaved and examined on their edge by SEM to measure the thickness of the film and extract a growth rate. There are other, non-destructive methods available to us that can be used to measure growth rate, such as interferometry and RHEED oscillations. The interferometer, described in section 2.6, is unsuitable for films of dimensions smaller than the wavelength of light used, so its measurements merely indicated that the films were less than 400nm thick. Oscillations in the intensity of the RHEED pattern vary with the same period as a monolayer deposition [23]. In this case, intensity variations due to vibrations from other laboratory equipment were larger than the variations caused by the film and so this method could not be applied to extract a growth rate. No film could be seen from

cross-sectional SEM imaging. Since the insulating sapphire charges strongly in the electron beam, some samples were cleaved and viewed at 45° incidence to help use the conducting GaN surface to obtain a clear image. These images verified that a continuous film was not present. PL spectra taken from samples #5 through #10, which were all particulated, were weak as the only PL was being emitted from very small isolated areas, and varied both in its intensity and energy as the position of the laser spot was moved around the sample. This effect was most striking in sample #8 (Figure 3.3). The variations in energy would be consistent with isolated areas of crystallographic growth rife with dislocation centres where recombination is occurring at below bandgap energies. Only towards the end of this growth series was it realised that the films were not continuous as the complexity of accurately calculating laser fluence was not fully appreciated. This is outlined in section 3.2.3 below.

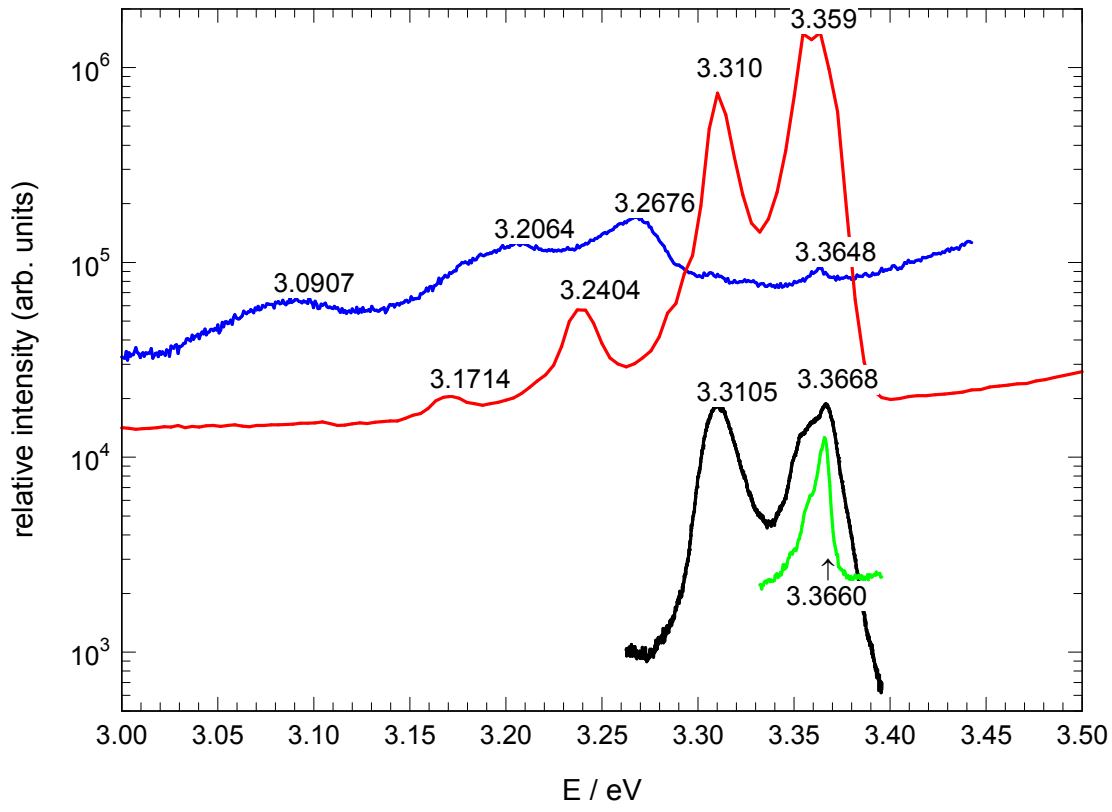

Figure 3.3 Photoluminescence of sample #8 at 3.8K. Each trace is taken from a different portion of the samples surface. The wide variation of below bandgap PL is clearly evident. Shorter traces are taken at higher resolution.

3.2.3 Corrections to fluence calculation

In total, 17 GaN growth runs have been completed to date. Each successive growth tuned a particular parameter to amend the growth process (see "Motivations for Growth" in Appendix A), but the goal was always to achieve complete film coverage of the substrate, rather than the partial coverage observed by SEM in all bar the most recent samples grown (#15 - #17). As it turns out, the fluence had been incorrectly calculated due to five factors, listed in order of their significance, from greatest to least:

(1) as the target is placed closer to the focal distance of the focusing lens, small changes of even 1mm in lens-to-target distance create large changes in fluence. This is difficult to measure with the necessary accuracy.

(2) laser-window-to-target distance had been incorrectly measured in the first instance and re-checks were not fully accurate, so this error compounded with problem (1) above to alter fluence significantly.
(3) the angle of incidence the laser makes at the target changes as the target is raised or lowered in the chamber – it can be varied from 35° to 49° but in practice was confined to the range 40.5° to 37.5°. The resulting change in spot size from angle alone was initially calculated to be negligible, which it would be were it not for the other compounding factors.
(4) the divergence of laser had been accounted for when the laser was passed through a small aperture to improve its profile. With this aperture removed it was assumed that divergence was negligible, but it is not. Although the cavity is long, which should yield a low divergence, the emerging beam has a large area (~12.5 mm × 28 mm) and so has an appreciable divergence (1 mrad × 3 mrad).
(5) combined losses at lenses and mirrors were less than estimates made based on the standard assumption of 90% transmission per optic. Total losses for 3 mirrors and one lens are measured as being 28%, not 35%.

As a final note on fluence calculations, it should be pointed out that the liquid Ga, which initially has a flat top surface, quickly moves into dome shape once the target is rotated due to vibrations from the gearing mechanism. This creates a further uncertainty, both in terms of changing fluence as the angle of incidence with the target is changed and also because the plume leaves the target at normal incidence, hence is not always directed at the substrate. However, the situation has been much improved by making a target holder with a shallow conical dip, which results in a reasonably constant flat surface, particularly at the centre point where the laser strikes. One would think that the obvious solution would have been to simply not rotate the target, but stopping target rotation results in no ablation at all (ablation can be observed as pressure instability registering on the ion vacuum gauge). This was unexpected and the reasons for it remain unclear. The rotation mechanism creates appreciable vibration and it is possible that in the absence of this vibration, the liquid Ga has surface irregularities lower than the wavelength of the impinging beam, resulting in a high degree of specular reflection and hence little beam absorption and ablation. This is backed up to some degree with observations with the eye;

liquid Ga has a very shiny appearance while all solid targets used are rough and do not reflect visible light in a specular manner.

3.2.4 Growth of continuous films

Once the fluence was correctly calculated, it was set to 5 Jcm^{-2}. Films grown thereafter were continuous and of measurable thickness. The films were predominantly particulated in nature, as indicated by the SEM images in Figure 3.6. These images, combined with observations of the chamber pressure, established a low-fluence threshold of 1.0 ± 0.1 Jcm^{-2} for ablation to take place. Although the samples are referred to as "particulated", these particulates may not be unreacted target material condensing on the substrate. Ga particulates were observed in some films – they are very dark, as compared to the brighter GaN areas, which is what would be expected as Ga metal will more easily conduct away the electron beam than less conductive GaN. Furthermore, in SEM observations taken at a 45° angle; the circular "particulates" have a flat profile (Figure 3.4), whereas true Ga droplets have a raised dome shape (Figure 3.5). For this reason, circular areas are more likely to be where growth is seeded. As fluence and hence deposition rate increase, these areas start to merge and a continuous film is formed (Figure 3.6), albeit a very thin one in most of samples #1 through #14.

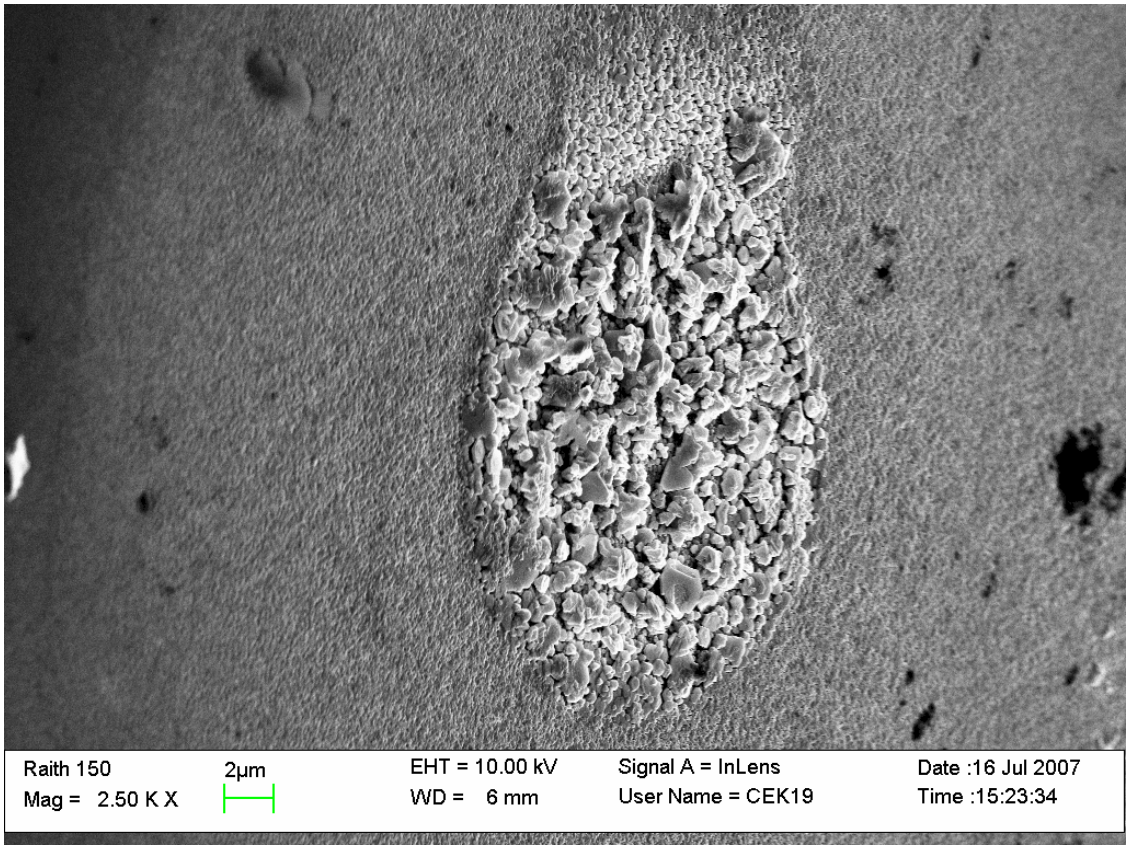

Figure 3.4 SEM image of a GaN sample viewed at 45°. Note the flat structure. Also of interest is the apparent "directional" nature of the deposited area, due either to the direction of the incoming Ga or N_2^*.

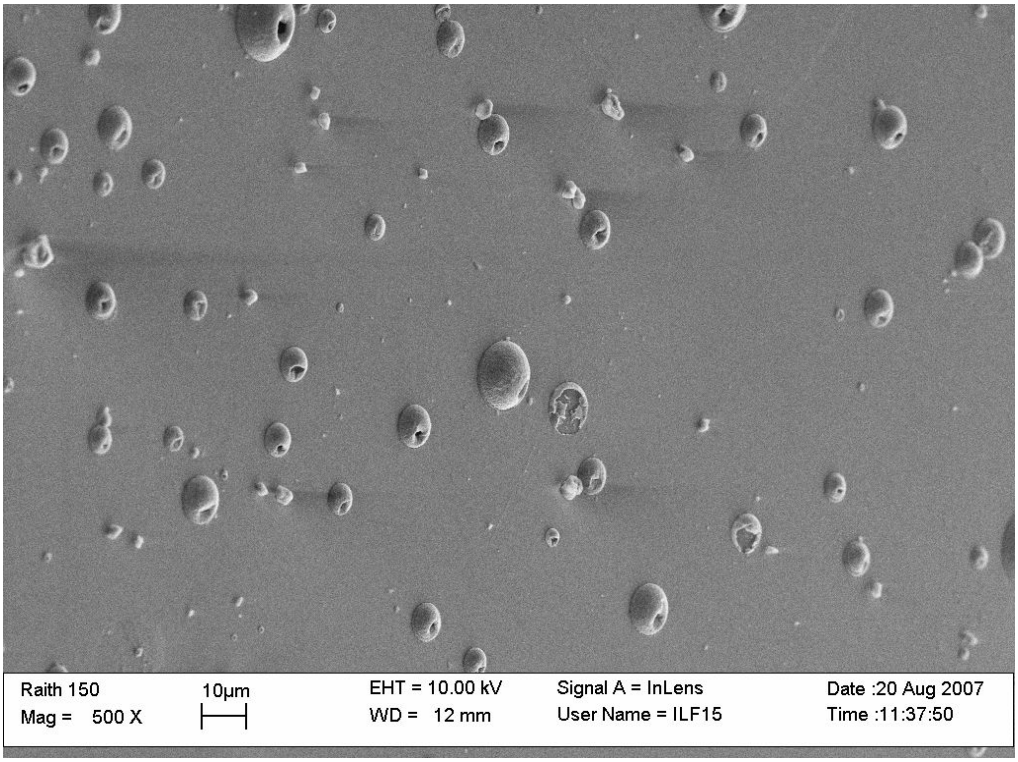

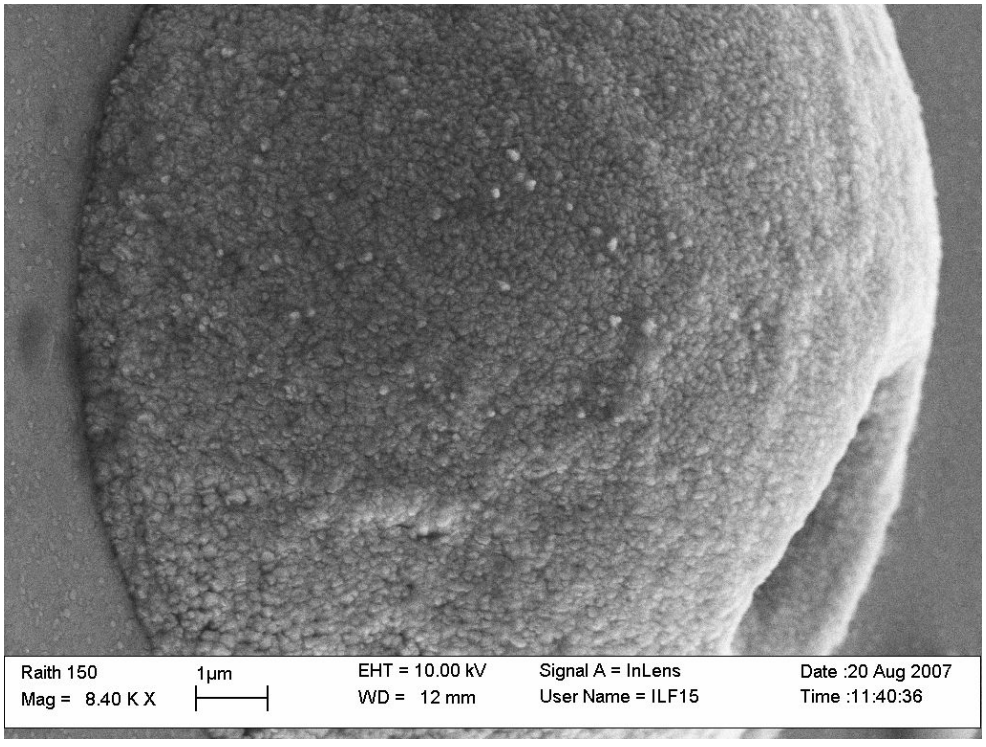

Figure 3.5 SEM images of GaN viewed at 45° showing raised domes of Ga droplets, as compared with the flat images of GaN growth in Figure 3.4. GaN growth on the droplet surface can be seen in the close-up. The directional nature of the opening in the Ga

droplets may be due to the fact that the nitrogen plasma is incident at a 45° angle, whereas the plume is at approximately normal incidence at the sample centre where these images we taken.

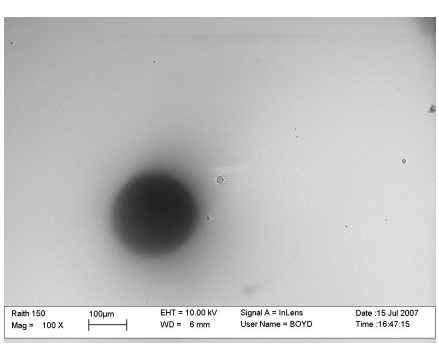

A (#7)

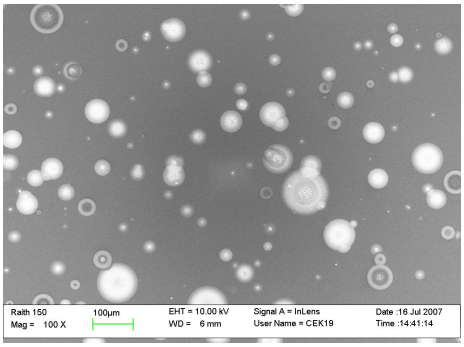

B (#8)

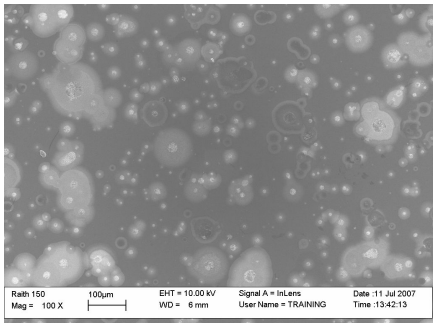

C(#6)

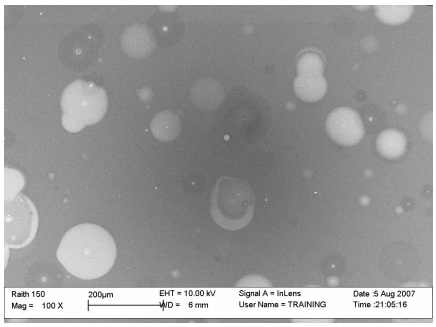

D (#12)

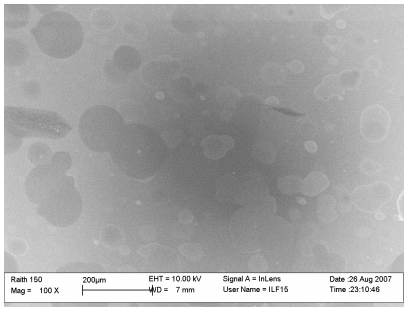

E (#15)

Figure 3.6 Effect of increasing fluence; SEM images of GaN grown at 0.9 J cm^{-2} (A), 1.2 J cm^{-2} (B), 1.3 J cm^{-2} (C), 1.7 J cm^{-2} (D) and 5.1 J cm^{-2} (E). All samples have the same magnification for comparison. All were grown were grown at T_{sub}= 700 °C (except D(#12), grown at 800 °C) and under otherwise identical conditions except E(#15) which had smaller target-to-substrate distance. The large black circle in image A is an artifact of the insulating sapphire substrate charging in the electron beam.

The RHEED images of later films show spotty streaks (Figure 3.7). This indicates three dimensional growth, confirmed by SEM. Since sample #15 is the first continuous film grown, streaky RHEED would not be expected from any earlier samples, hence there is not much to be learned from the diffraction patterns of samples #1 to #14. The RHEED pattern of sample #15, which has shown full substrate coverage, is shown below. It clearly indicates a partially three dimensional surface, something verified by SEM images (Figures 3.6(E) and Figure 3.8).

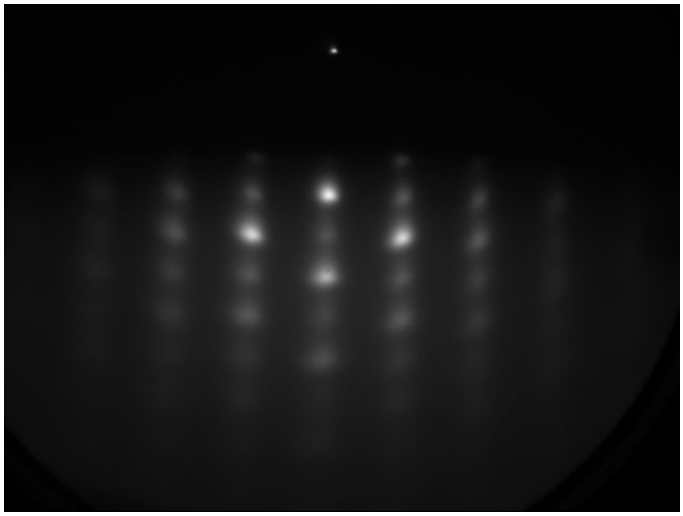

Figure 3.7 RHEED image of sample #15 after growth. This is the only sample (up to this point) that formed a continuous film. Spotty streaks indicate an epitaxial film with growth proceeding in a three dimensional fashion.

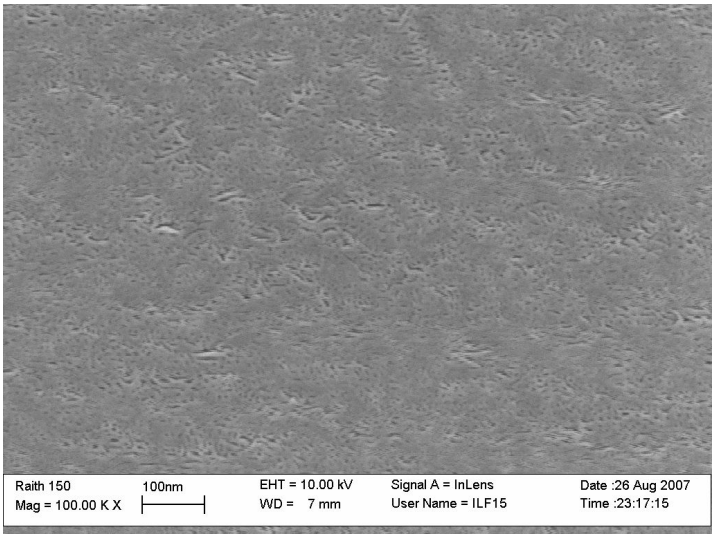

Figure 3.8 High (100k) magnification image of sample #15, showing a relatively smooth surface.

It was expected that a PL signal would be obtained from samples #15, 16 and 17, which were all continuous films grown at a fluence of 5.1 J cm^{-2}, 5.0 J cm^{-2} and 3.4 J cm^{-2}, respectively. However, these samples gave no PL signal at all. This is a disappointing result. Since the only change in growth between this sample and those that gave PL are the fluence and target-to-substrate distance, this could potentially be attributed to poor stoichiometry due to the higher ablation rate yielding a Ga-rich film. RBS measurements were made on later films to see if this was the case, but results indicated a Ga:N ratio of 1.0, shown in Figure 3.9.

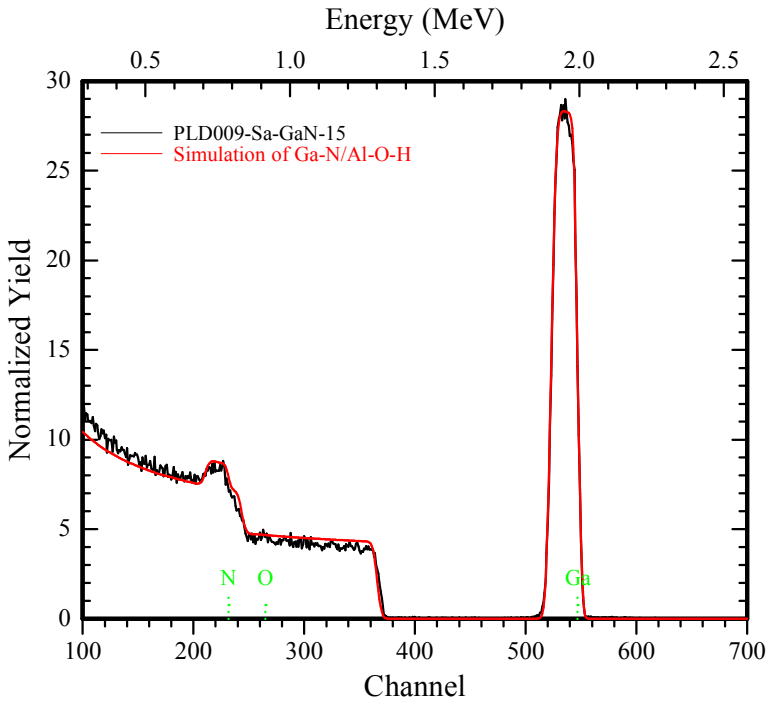

Figure 3.9 RBS data of sample #15, the first continuous film grown. Results indicate stoichiometry of 1.0 and a thickness of 135nm. The observed data for the sample has been accurately fit by the expected shape for GaN on sapphire (AL_2O_3)

To verify the RBS thickness result, an attempt was made to etch the sample in KOH to obtain a thickness profile. However, the KOH would not etch the sample. This makes it likely that that films grown have a +c polar Ga-face, since KOH only etches GaN of N-face (-c) polarity [16]. Since the films could not be selectively etched, a sample was cleaved and coated with a thin layer (~10nm) of gold to view the film. From figure 3.10, a film of thickness 150 ± 20nm was evident.

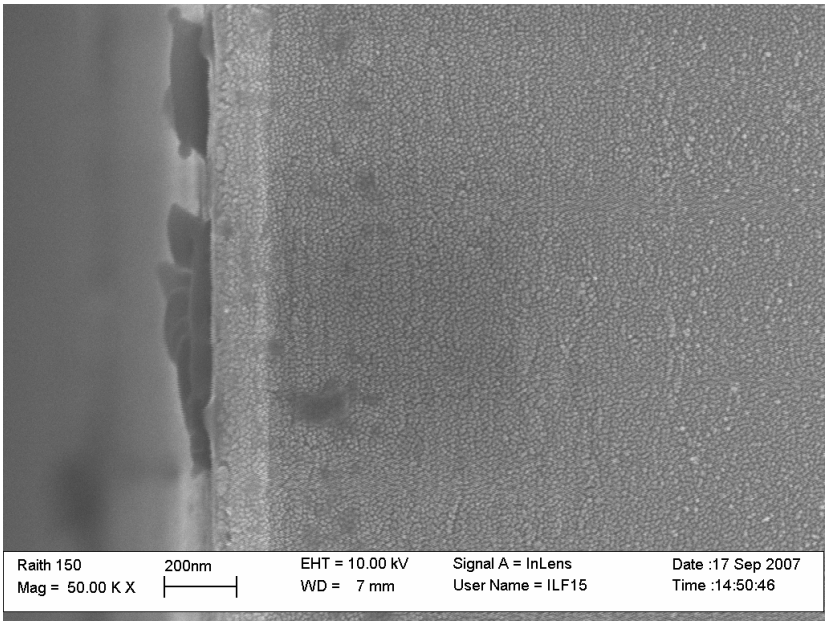

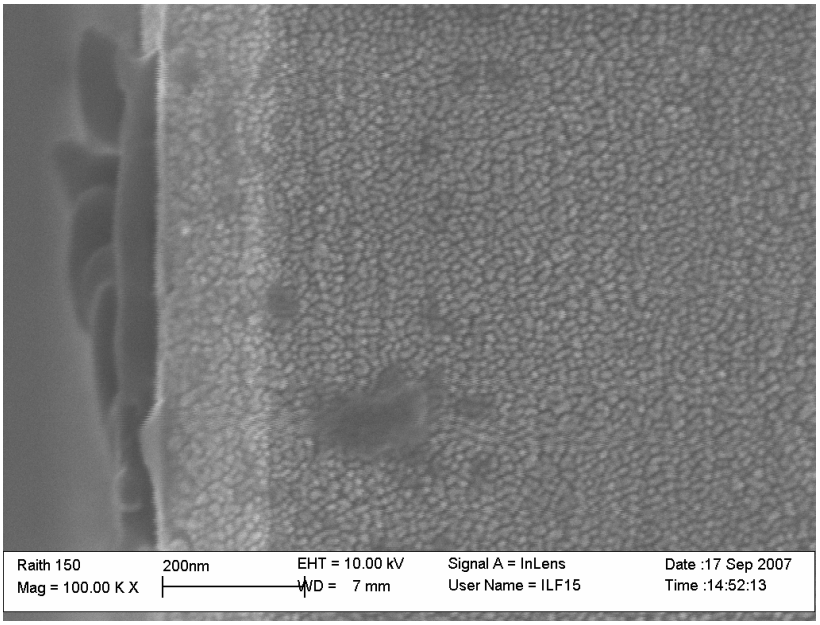

Figure 3.10 SEM images of the cleaved edge of sample #15, gold-coated to prevent charging of sapphire. The GaN film is a bright band left of centre of the images, measured to be 150 ± 20nm thick. The texturing comes from the deposited gold.

3.3 Conclusion

A series of epitaxial GaN growths were undertaken by PLD and the resulting samples have been characterised. Initial growths were unsuccessful since the complexities of laser fluence calculations were not fully appreciated at the time. This has been learned from and will serve as experience gained in later chapters. Similarly, experience has been gained in analysis techniques of RHEED and SEM which will be extensively used throughout this work. A number of technical problems arose and were dealt with in commissioning the UHV chamber, but they fall outside the scope of film growth and analysis and their minutiae have been omitted. The lack of PL signals from the continuous GaN films (samples #15 to #17) is very disappointing as it was intended to compare GaN PL from sapphire and HfN substrates as a gauge of the effectiveness of HfN films in improving PL emission. It might be possible to deposit luminescing GaN on HfN using another growth technique, but it would certainly have been preferable to achieve this *in-situ*. Nonetheless, this work has demonstrated that stoichiometric metal nitride films of appreciable thickness can be grown by PLD and the experience gained will be applied to the production of the more interesting refractory and rare earth metal nitrides.

References

(1) N.Grandjean, J.Massies and M.Leroux, "Nitridation of sapphire. Effect on the optical properties of GaN epitaxial overlayers", Applied Physics Letters 69, 2071 (1996)

(2) S. Keller, B. P. Keller, Y.F. Wu, B. Heying, D. Kapolnek, J. S. Speck, U. K. Mishra and S. P. DenBaars, "Influence of sapphire nitridation on properties of gallium nitride grown by metalorganic chemical vapor deposition", Applied Physics Letters 68, 1525 (1996)

(3) M. Cazzanelli, D. Cole, J. F. Donegan, J. G. Lunney, P. G. Middleton, K. P. O'Donnell, C. Vinegoni and L. Pavesi, "Photoluminescence of localized excitons in pulsed-laser-deposited GaN", Applied Physics Letters 73, 3390 (1998)

(4) R.F.Xiao, H. B. Liao, and N. CueX. W. Sun and H. S. Kwok, "Growth of c-axis oriented gallium nitride thin films on an amorphous substrate by the liquid-target pulsed laser deposition technique" Journal of Applied Physics 80, 4226 (1996)

(5) M. Dinescu, P. Verardi , C. Boulmer-Leborgne, C. Gerardi, L. Mirenghi and V. Sandu, "GaN thin films deposition by laser ablation of liquid Ga target in nitrogen reactive atmosphere", Applied Surface Science 127–129, 559 (1998)

(6) R.F. Xiao, X.W. Sun, H.S. Kwok. "Liquid-target pulsed laser deposition of gallium nitride thin films", Applied Surface Science 127-129, 425 (1998)

(7) P.R. Willmott, F. Antoni and M. Döbeli, "Kinetic, crystallographic, and optical studies of GaN and $Al_xGa_{1-x}N$ thin films grown on Si(111) by pulsed reactive crossed-beam laser ablation using liquid alloys and N_2 or NH_3", Journal of Applied Physics 88, 188 (2000)

(8) K.W. Mah, J.-P. Mosnier, E. McGlynn, M. O. Henry, D. O'Mahony and J. G. Lunney, "Study of photoluminescence at 3.310 and 3.368 eV in GaN/sapphire(0001) and GaN/GaAs(001) grown by liquid-target pulsed-laser deposition", Applied Physics Letters 80, 3301 (2002)

(9) J.L.Deiss, Ch. Hirlimann, J.L. Loison, M. Robino and G. Versini, "Epitaxial growth of GaN thin films on sapphire (0001) by pulsed laser deposition: influence

of surface preparation and nitridation", Materials Science and Engineering B82, 68 (2001)

(10) N.Grandjean, J.Massies and M.Leroux, "Nitridation of sapphire. Effect on the optical properties of GaN epitaxial overlayers", Applied Physics Letters 69, 2071 (1996)

(11) K.Uchida, A . Watanabe, F. Yano, M. Kouguchi, T. Tanaka, and S. Minagawa, "Nitridation process of sapphire subs surface and its effect on the growth of GaN", Journal of Applied Physics 79, 3487 (1996)

(12) P.Merel, M.Chaker, H.Pepin, M.Tabbal. Materials Research Society Symposium Proceedings 572, 401 (1999)

(13) P Merel, M Chaker, M Tabbal, H Pepin, "Structural and electrical characteristics of epitaxial GaN thin films grown using pulsed laser deposition assited by an atomic nitrogen source", Applied Surface Science 177, 165 (2001)

(14) M Niehus P. Sanguino, T. Monteiro, M.J. Soares, E. Pereira, M. Vieira, S. Koynov and R. Schwarz, "Optical properties and transport in PLD-GaN", Solid State Electronics 47, 569 (2003)

(15) T.F. Huang, A. Marshall, S. Spruytte, J.S. Harris Jr., "Optical and structural properties of epitaxial GaN films grown by pulsed laser deposition", Journal of Crystal Growth 200, 362 (1999)

(16) D. Li, M. Sumiya, S. Fuke1, Deren Yang, D. Que, Y. Suzuki and Y. Fukuda, "Selective etching of GaN polar surface in potassium hydroxide solution studied by x-ray photoelectron spectroscopy", Journal of Applied Physics 90, 4219 (2001)

(17) J. Kennedy, S. Granville, A. Markwitz, B. J. Ruck and H. J. Trodahl. "Ion beam analysis of rare earth nitride thin films" Nuclear Instruments and Methods in Physics Research B 266, 1558 (2008)

(18) X. Xu, R. Armitage, S. Shinkai, K.Sasaki, C. Kisielowski and E. R. Weber. "Epitaxial condition and polarity in GaN grown on a HfN-buffered Si(111) wafer" Applied Physics Letters 86, 182104 (2005)

(19) K. Okamoto, S. Inoue, T. Nakano, J. Ohta and H. Fujioka. "Epitaxial growth of GaN on single-crystal Mo substrates using HfN buffer layers" Journal of Crystal Growth 311, 1311 (2009)

(20) L. Liu and J. H. Edgar. “Substrates for gallium nitride epitaxy” Materials Science and Engineering R 37, 61 (2002)

(21) P. Sanguino, M. Niehus, L. Melo, R. Schwarz, A. Fedorov, J. M. G. Martinho, M. J. Soares and T. Monteiro. “Photoluminescence decay in the ps time regime and structural properties of pulsed-laser deposited GaN” Physica B 340, 457 (2003)

(22) F. Widmann, G. Feuillet, B. Daudin) and J. L. Rouvière. “Low temperature sapphire nitridation: A clue to optimize GaN layers grown by molecular beam epitaxy” Journal of Applied Physics 85, 1550 (1999)

(23) D. A. Black, G. J. H. M. Rijnders, G. Koster, H. Rogolla. “In-situ monitoring during pulsed laser deposition using RHEED at high pressure” Applied Surface Science 127, 633 (1998)

Chapter 4 REFRACTORY METAL NITRIDES : HAFNIUM NITRIDE AND ZIRCONIUM NITRIDE

4.1 Introduction

The principal application of refractory metal nitrides are as wear-resistant coatings, but in this research they are being considered as a potential candidate for buffer layers in semiconductor technology. The lattice constant of HfN is 4.524 Å [1] while that of ZrN is 4.584 Å [2], which places them midway between those of Si (5.431 Å) [3] and GaN (3.189 Å) [4]. When stoichiometric and of high-quality, they are highly reflective throughout the visible region and have low electrical resistivities [5]. As such, they may provide a lattice-matched interface between Si and GaN, while also serving as an ohmic contact and optically reflecting layer. Obviously, this has implications for improving the efficiency of GaN-based LEDs and solar cells as well as integrating GaN into Si-based technology.

This chapter will describe the attempts made to grow stoichiometric refractory metal nitrides with a view to establishing a growth procedure which will create films of the highest possible visible reflectivity while simultaneously having minimal resistivity. Both HfN and ZrN films will be grown using Hf, Zr and ZrN targets. Hf and Zr are chemically similar group IV elements and so their nitride films should show similar optical and electrical properties. Their growth parameters should also be similar, hence HfN will be investigated more thoroughly as ZrN might have similar properties.

An anticipated exception to this is in the ablation of each metal; Hf and Zr have vapour pressures and heats of vapourisation within 5% of one another, but their reflectivities at 248 nm (the laser wavelength) are 0.367 and 0.015 respectively [6]. Furthermore, the extinction coefficient, a unitless quantity indicating the strength of absorption of light in a material, in Hf is 1.69 at 248nm, while in Zr it is 0.63 [6]. The variation in reflectivity is far greater so it is likely that Zr will require considerably less laser fluence to ablate the same amount of material.

4.2 Growth optimisation

Growth parameters of the first HfN layer were decided upon by a combination of previous experience in PLD growth of GaN and published experimental procedures carried out by other investigators of HfN who managed to obtain good quality material [3-5, 7-14]. This work is the first growth of HfN by PLD. ZrN growth by PLD has been reported in the literature before [17,18]. A summary of parameter variations are listed in Table 4.1 below.

It was not anticipated that the first growth run (sample HfN1) would produce good material, but visual inspection showed the film had the characteristic golden colour only found in stoichiometric HfN [5,9]. Reflectivity measurements verified that the film has the characteristic spectrum of stoichiometric HfN [16] while SEM images show smooth films with very low particulation density. Reflectivity in particular has proved a useful tool in this growth series as it is simple to use, non-destructive and provides key information pertaining to the ambitions of this work. Its development into a reliable characterisation tool providing absolute, repeatable reflectivity spectra will be described later.

Sample HfN1 had been grown at the lowest available stable N_2 plasma pressure (2×10^{-5} Torr), the intention being to grow across a series of N_2 plasma pressures, keeping all other growth parameters identical. The next sample, HfN2, was grown at the upper limit of plasma pressure (1×10^{-4} Torr) and it too was found to have promising initial results. Its reflectivity spectrum was found to be almost identical to that of HfN1, implying that N_2 pressure was not a critical parameter in growth. Instead, a series of four films (HfN2 through HfN8, excluding HfN6) were grown across a range of substrate temperatures to establish its importance in film quality. The temperature range 350 °C to 600 °C was chosen as it encompassed the range of temperatures found to produce the best material, primarily by DC magnetron sputtering [4,5,7,8,9]. Sample HfN6 was grown at maximum plasma power at the optimum growth temperature (500°C) to gauge the effect of high plasma power on film characteristics.

This optimised HfN temperature, 500 °C, was used in the growth of all ZrN films where a ZrN target was used. Growths from Zr targets were carried out at 450 °C as Lee

et al [24] found a sharp dip in the resistivity of films deposited at this temperature, reducing to 40μΩcm compared to values exceeding 150 μΩcm for films grown at 400 °C and 500 °C. This potentially indicates an acute sensitivity to growth temperature. For growth using a ZrN target, nitrogen pressure variation was the principal parameter investigated. It was not known if stoichiometric ZrN could be grown in vacuum, or if the energy of the ablating laser would be so large as to dissociate the elements in the ZrN molecules, hence requiring added nitrogen to balance the dissociation losses.

N_2 pressure for all HfN samples, apart from HfN1, was kept at the maximum possible, 1×10^{-4} Torr, to grow under nitrogen rich conditions. The reasoning behind this is that laser fluence produces quite a high metal flux which is entirely incident on the substrate, so high N_2 pressure helps to create stoichiometric material. Excess N_2 is simply pumped away. There is also the consideration that hafnium flux varies across the substrate, as determined by the spread of the plume, so stoichiometry could vary across the sample. However, in this case small substrates (1 cm × 1 cm) were used, so thickness and stoichiometry variations were expected to be minor. As will be shown in RBS results, this expectation proved to be incorrect.

4.3 Experimental details

Sample	T_{sub} / °C	N_2 pressure / Torr	Plasma power / W	Laser fluence / J cm^{-2}
HfN1	500	**2×10^{-5}**	200	5
HfN2	500	**1×10^{-4}**	200	5
HfN3	**600**	1×10^{-4}	200	5
HfN4	**550**	1×10^{-4}	200	5
HfN5	**450**	1×10^{-4}	200	5
HfN6	500	1×10^{-4}	**400**	5
HfN7	**350**	1×10^{-4}	200	5
HfN8	**400**	1×10^{-4}	200	5
ZrN2	450	1×10^{-4}	200	**2**
ZrN3	450	1×10^{-4}	200	**5**
ZrN4*	500	**none**	**none**	5
ZrN5*	500	**1×10^{-4}**	200	5
ZrN6*	500	**5×10^{-5}**	200	5
ZrN7*	500	1×10^{-4}	200	**3**

Table 4.1 Summary of variations in growth conditions. Key variations of interest for each growth run are in bold type for clarity. * indicates a nitride target.

The key variations made between each growth are listed in Table 4.1 above and most other parameters were kept constant so that variations could be reliably attributed to the above factors only. An exception to this rule is outgassing temperature and duration. The former was set to at least 100 °C above the growth temperature, or a minimum of 600 °C, whichever was greater. Duration also varied, but this was only to allow chamber pressure to drop to a steady level before introducing N_2.

Growth settings common to all samples are as follows. A KrF laser emitting 25 ns pulses at 248 nm (5.0 eV) with a duty cycle of 10 Hz was focused on a 99.9% Hf target

and a 99.9% Zr target, both supplied by Kurt J. Lesker Company . Fluence on Hf was set to 5.0 ± 0.5 J cm^{-2} and maintained at this level by running the laser in constant energy mode. Fluence on Zr was initially set to 2.0 ± 0.5 J cm^{-2} as it was expected that its reduced reflectivity at 248 nm would require lower fluence to avoid excessive ablation and hence particulated films. Films produced at this fluence were not stoichiometric and had a grey appearance with low visible reflectivity. Fluence was increased to 5.0 ± 0.5 J cm^{-2} which produced films of characteristic golden colour. Some ZrN films were also grown using a ZrN target, also 99.9% and supplied by Kurt J. Lesker Company. Growth from a nitride rather than a metal target is somewhat outside the scope of this thesis, but it is an area of future development worth investigating. It should be noted that the major impurity in the Zr target is Hf, and vice versa, which makes sense as their chemical similarity would make them difficult to separate. These two elements could substitute for one another in a crystal lattice without having very detrimental effects on the film properties since their nitrides have lattice constants which differ by only 1.3% (Table 1.1).

Target to substrate distance was set at 6.0 cm. Nitrogen was activated using an Oxford Applied Research plasma source fitted with ion deflection plates. Growth time was 1 hour for all samples except HfN6, which was stopped 42 minutes into growth as a degrading and disappearing RHEED pattern indicated a N_2 plasma power of 400 W was too aggressive to form a crystalline film. Targets were rotated during growth and the laser moved to a different spot between growths as tracks were etched by the ablation process. This should have avoided changing the metal flux between growths by keeping laser incidence at a more constant angle relative to the target surface, i.e. by eliminating the formation of "valleys" in the target which would scatter ablated species at an angle away from the substrate and back towards the laser window instead.

Since the targets were loaded into the chamber directly from a cleanroom-sealed package, no pre-treatment of the targets was deemed necessary and pre-ablation of the surface prior to growth was limited to 1 or 2 minutes, just to remove any possible settled dust particles picked up during loading or deposits backscattered during previous sample growths. Justification for the short pre-ablation is that the target was exposed to atmosphere for less than one minute, during which time it was inserted into a nitrogen-

flushed load lock. After a further 2 minutes it was pumped down to 1 Torr. This should have prevented a thick oxide layer forming on the target surfaces. Surface oxides formed during the short time exposed to atmosphere would be diffusion-limited to the first few atomic layers and these would be ejected during pre-ablation, which removes material to a depth on the order of a micron.

Polished MgO(100) substrates (MaTeck) with dimensions 1 cm × 1 cm × 0.5 mm were degreased in an ultrasonic bath for 5 minutes each in TCE, Acetone and Methanol, then bonded to a molybdenum plate using an InSn alloy to provide good thermal contact. The substrate was introduced into a load-locked UHV chamber with a base pressure of 5×10^{-9} Torr. Pre-growth/outgassed substrates and film growth were monitored using a RHEED gun operated at 20.0 kV and 1.4 A, although in most cases current was varied slightly when patterns became darker as growth progressed. This is likely due to increased scattering of the electron beam from the growing films, which is not surprising given the tendency of PLD to produce films which are not atomically smooth.

4.4 Results and Analysis

4.4.1 RHEED

RHEED patterns were taken for all samples before and during growth. Observations were made of substrates at room temperature and substrates were rotated to observe different crystal directions. For consistency, a fixed rotation angle was set during outgassing and growth to monitor a single crystal direction. Angles were again varied after growth to look at the different crystal planes.

Some commonalities were observed for growths. Notably, the MgO substrates did not display a streaky pattern, but more of a spotty one, with Kikuchi lines present due to inelastic scattering from the bulk crystal (Figure 4.1). Heating and outgassing introduced a streaky element to the patterns, but often the intensity of the Kikuchi lines decreased at the same time.

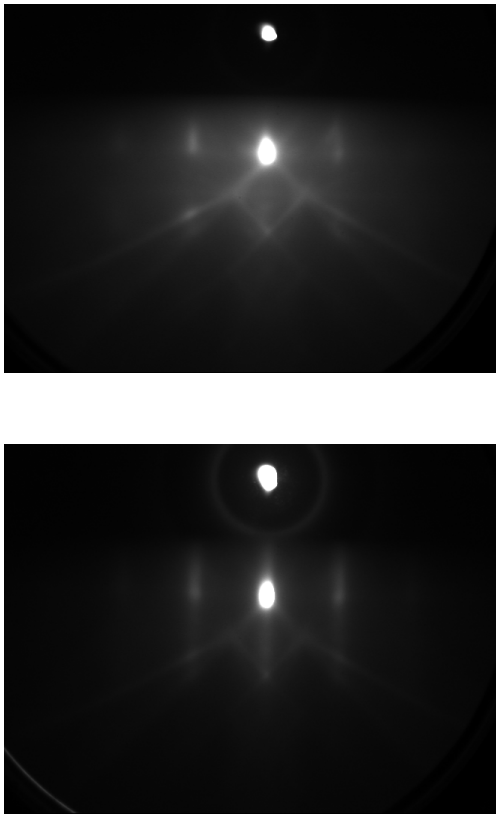

Figure 4.1 RHEED patterns of the (100) planes of MgO(100) substrate before growth (of HfN3) at 26 °C (top) and at 600 °C (bottom), after outgassing at 700 °C for 3 hours. The Kikuchi pattern usually observed for bare substrates is clearly visible. Streaks become clearer during outgassing, implying there is some evaporation of impurities (largely condensed water) from the substrate surface.

Upon commencing growth, substrate patterns quickly disappeared, to be replaced by a broad streaky pattern, with spots superimposed on the streaks (Figure 4.2). This indicates growth is proceeding in a somewhat three-dimensional fashion, but with reasonably epitaxial characteristics overall. This is expected due to the pulsed nature of film growth; a large volume of metal arrives with each laser pulse and migrates to a lattice site while combining with nitrogen. There is clearly more scattering of the electron beam from the nitride films than from the MgO substrate. This is a consequence of their surface being rougher than the highly polished substrates.

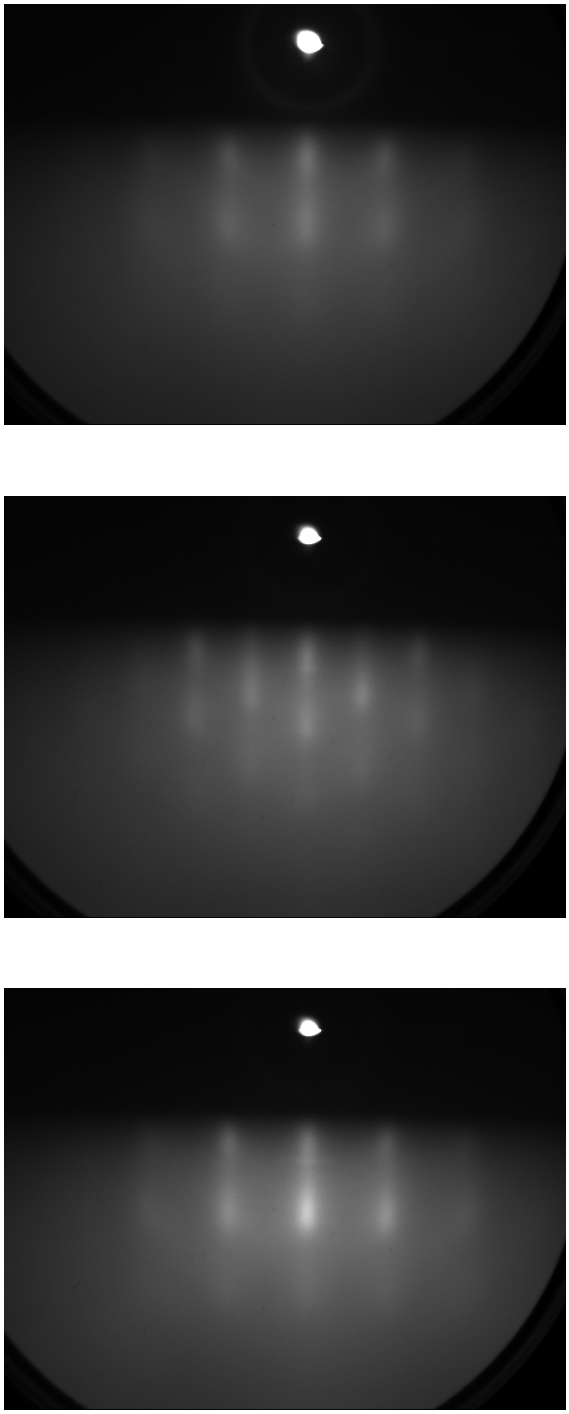

Figure 4.2 Post-growth RHEED patterns of HfN3 taken at room temperature show an epitaxial film. The sample is rotated in-situ to show diffraction patterns from the (100) (top), (220) (middle) and (010) (bottom) crystal planes.

Little variation in the RHEED pattern was observed in most of the HfN films. Compared to the other HfN films, a lattice expansion of 2% was noted for HfN8, grown at 400 °C and exhibiting reduced reflectivity. This is probably not related to stoichiometry since the RHEED electron beam grazes the surface at a glancing angle, so it is sampling the stoichiometry of the entire film, which varies with distance from the centre of the plume. This effect is most pronounced in HfN3, which varied from $Hf_{0.65}N_1$ to Hf_1N_1 within its 1 cm × 1 cm area. What could be observed was the transition from single crystal to polycrystalline growth. This was noted in the sample grown at the lowest growth temperature (350 °C) as a weak semicircular polycrystalline pattern, shown in Figure 4.3.

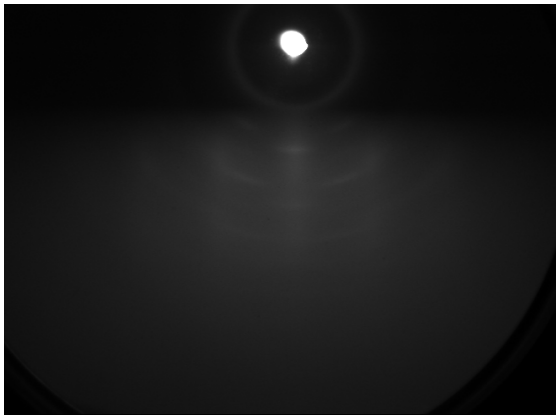

Figure 4.3 RHEED image of HfN grown at 350 °C. Semicircular rings and no streaks indicate a polycrystalline film.

Differences in the nitride target ZrN films could also be observed by RHEED. Among the samples ZrN4, ZrN5 and ZrN6, where only nitrogen plasma pressure was varied, it was obvious that the diffuse pattern of ZrN4 was showing poor surface structure (Figure 4.4). This, along with reflectivity, indicates that nitrogen dissociates from ZrN during ablation and must be compensated for by introducing N_2 to the chamber during growth. Differences in ZrN5 and ZrN6, grown at 1×10^{-4} Torr and 5×10^{-5} Torr respectively, are not so obvious from the RHEED. However, there is a marked difference

in the reflectivity (Figure 4.8), which is clearly much more sensitive to the film surface properties. The lower nitrogen pressure reduces reflectivity by 50 ± 5%.

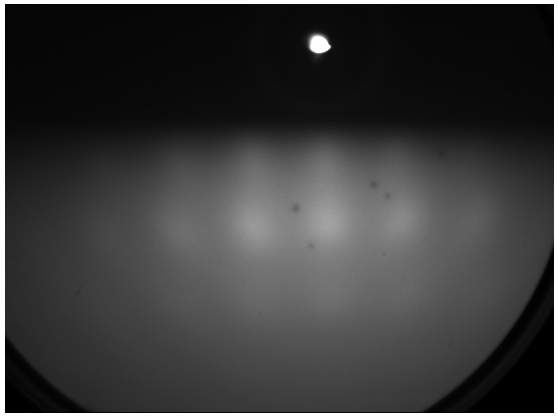

ZrN4, N_2 = 0 Torr

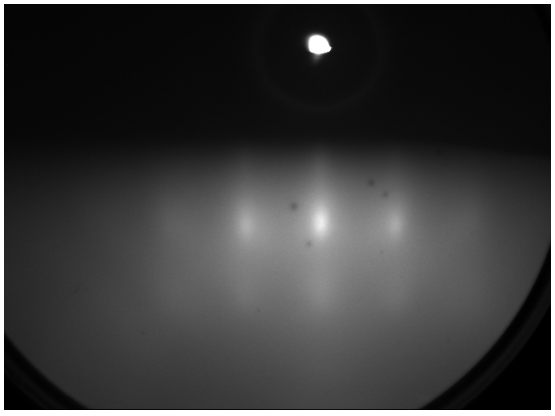

ZrN5, $N_2 = 1 \times 10^{-4}$ Torr

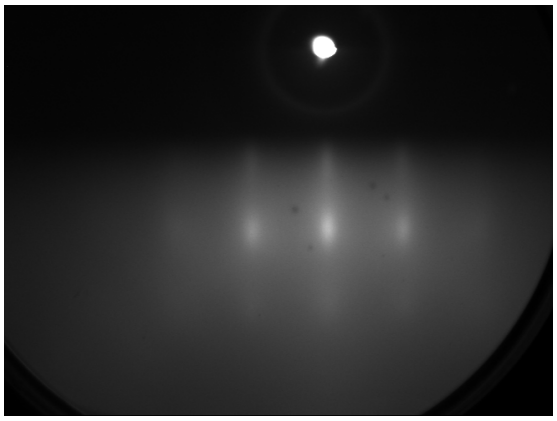

ZrN6, $N_2 = 5 \times 10^{-5}$ Torr

Figure 4.4 RHEED images of ZrN samples grown from ZrN target. Growth parameters vary only in the amount of nitrogen added to the chamber during growth. Broader streaks

from the ZrN film grown without a nitrogen plasma background (top image) demonstrate reduced crystal quality.

In all cases the patterns are quite faint, a common feature observed in PLD growth of nitrides from low vapor pressure metal targets; excess metal at the growing surface is not easily desorbed when the substrate temperature (≤ 600 °C) is much lower than the metal desorption temperatures (> 2000 °C), which weakens and slightly broadens the RHEED streaks.

4.4.2 Reflectivity and RBS

Reflectivity of the HfN films is, along with resistivity, one of the key parameters of interest in this work. The reflectivity measuring process has been refined and improved over the course of this work to enable repeatable measurements to be made, yielding absolute percentage reflectivity values to be obtained. This was made possible by:
(1) averaging 1000 spectra for each measurement to reduce noise
(2) allowing the light source to heat to a stable temperature before conducting measurements – this eliminated any intensity variations in the light source
(3) using a 0.5mm thick metal spacer under the mirror during its reference scan to allow for intensity increase once the 0.5mm thick sample was placed on the mirror.
(4) using high-precision optical mounts
(5) using two high-quality mirrors with known reflectivity spectrum as reference. A Newport BD.1 mirror has an almost flat 99.5% reflectivity spectrum from 488 nm to 740 nm. The spectrum supplied by the manufacturer shows reflectivity decreasing to 80% by 450 nm, and below this wavelength no information on the mirror's reflectivity is know (nor would they supply it when asked). This raises some uncertainty regarding the accuracy of the data below 450 nm. A Thorlabs protected silver mirror is also used which has a known flat response in excess of 98% extending further into the infra-red. Combining data from these reference mirrors with data from the samples enable accurate absolute reflectivities to be calculated.

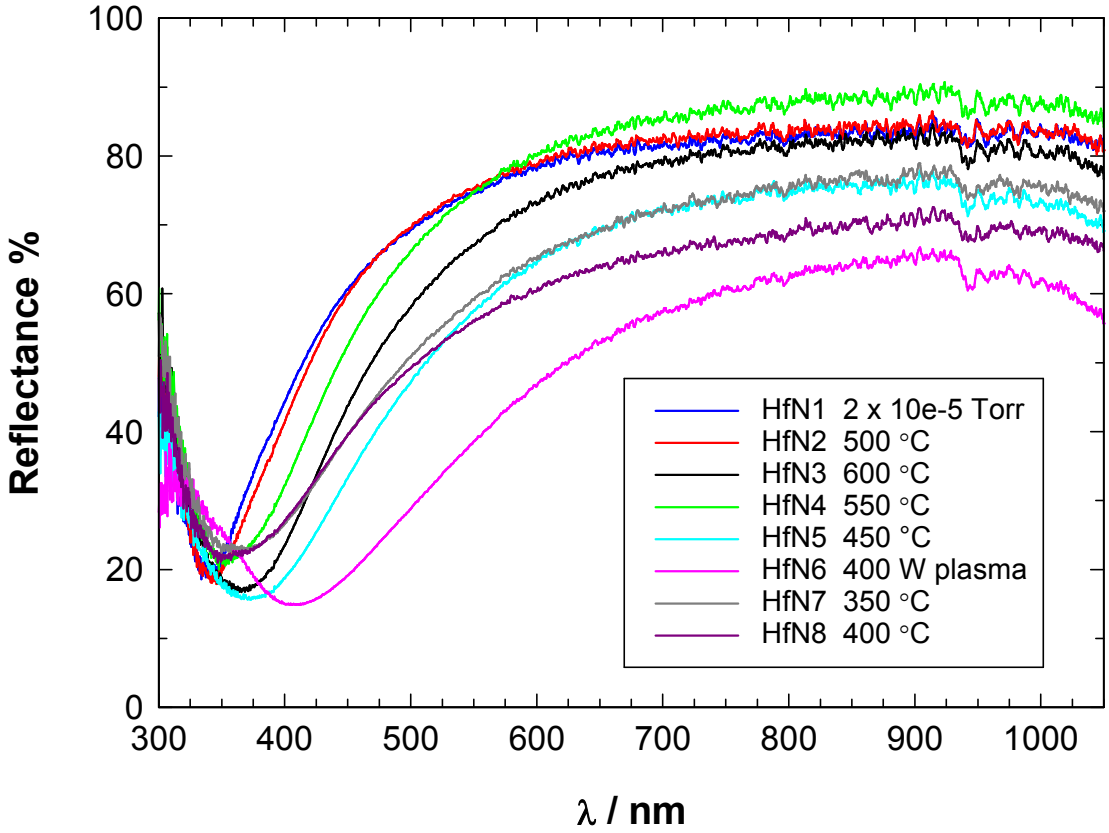

Figure 4.5 Reflectivity spectra of all HfN samples grown under different conditions. Samples grown at mid-range plasma power (200W) at 500 °C have higher reflectivity extending further towards the UV. The dip at 945nm is due to O-H absorption in the optical fibre.

Reflectivity spectra for all samples are shown in Figure 4.5. It should be noted that spectra varied across the sample surface. This could be seen with the eye as slight colour variations, from deeper golden colours to a brighter, slightly more silver-like appearance. The above spectra are from the brightest areas on each sample, apart from HfN2. HfN2 had been contacted for Hall measurements and so was no longer clean enough to compare spectra. This sample has been measured only in the clean central area. For this reason, only HfN1 and HfN2 have had their resistivity measured, since the process of adding indium contacts effectively prevents further accurate comparison of spectra. The instrumentation for reflectivity measurements was being continually improved at the time of sample growth, so keeping film surfaces untainted during this

process was essential to obtain meaningful, accurate reflectivity data. The positions of the reflectivity minima, between 330 nm and 400 nm, vary from sample to sample, but there is uncertainty in this region due to lack of knowledge of the reference mirror reflectivity in this region and also because of weak emission from the light source, as evidenced by the onset of more significant noise. Therefore, it is difficult to gauge whether these minima are accurate.

Obviously, HfN6 is markedly different to the other samples. As mentioned in the growth detail section, its RHEED pattern was found to degrade during growth and growth was stopped at 42 minutes, rather than the full hour allowed for all other samples. HfN6 also displays the broadest FWHM peak in XRD measurements (Table 4.3 and Figure 4.9). In terms of the highest reflectivity in the region of interest for GaN emission, it looks as though samples HfN1 and HfN2 are optimal. HfN4 has the highest reflectivity above 550nm, but this is not the region of key interest. Also, HfN4 has a poor XRD spectrum.

RBS measurements have yielded another interesting dimension to these results. Reflectivity is not uniform across the samples, but varies slightly. Samples HfN2 and HfN3 were selected for RBS measurements; HfN2 because it displayed the best characteristics of all the samples grown, HfN3 because it showed the greatest variation in its reflection spectra across its width (moving diagonally from corner to opposite corner). It was hoped that RBS at different points of this sample would indicate how reflectivity depends on stoichiometry. As mentioned before, HfN2 only had RBS measurements carried out on its clean central area due to deposition of Hall contacts in its corners.

The reflectivity of HfN3, shown in Figure 4.7 below, reveals an interesting anomaly. Contrary to expectations, it is the darker area (more golden in appearance, but with lowest percentage reflectivity) that is stoichiometric. These areas are also smoothest and thinnest. The differences in reflectivity do not correlate with surface roughness and SEM images have also confirmed that there is insignificant difference in Hf particulates on each region. Film thickness differences are also not a factor in this since reflection occurs at the surface. Also, the spectral shapes are different, which is commensurate with changes in stoichiometry. Complete RBS results are shown in Table 4.2. This would imply that stoichiometric material is produced in thinner layers, so future growths with

reduced growth time or lower fluence might have better stoichiometry. However, since stoichiometric material with a smoother surface clearly has reduced reflectivity, this raises some complex issues with subsequent deposition of GaN layers on the HfN.

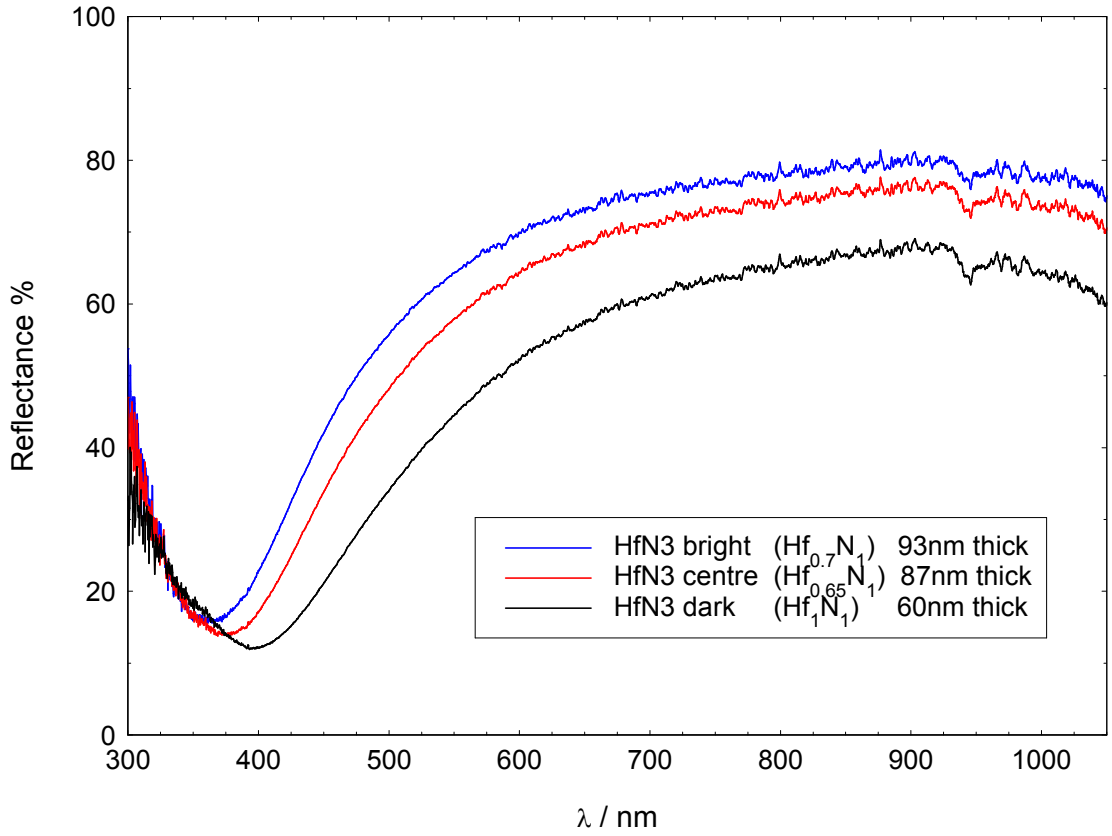

Figure 4.7 Reflectivity variation in HfN3 across its surface. Non-uniform film thickness is inherent to PLD growth and this samples exhibited the effect most strongly. Surprisingly, non-stoichiometric areas have higher reflectivity.

Film	film thickness (nm) *	Hf/N	Impurity concentration (at.%)	uniformity
HfN2	128 ±2	0.86	Nb =1.5%, O at the surface = 2%	rough film
HfN3 bright area	93 ±2	0.7	Nb =1.7%, O at the surface = 1%	rough film
HfN3 central area	87 ±2	0.65	Nb =1.7%, O at the surface = 1%	very rough film
HfN3 dark area	60 ±2	1	Nb =1.5%, O at the surface = 1%	smooth film

Table 4.2 RBS of HfN films obtained using the 2 MeV $^{4}He^{+}$ beam (Statistical and common errors are estimated to 5-10%,). Elemental concentrations are extracted from RBS spectra with RUMP fitting. * Thickness measurements are based on HfN density of 13.8 g cm^{-3}.

Reflectivities have also been measured for ZrN films. ZrN4, grown from a nitride target without any nitrogen in the chamber, does not posses the characteristic spectral shape of refractory metal nitrides and hence is not stoichiometric material. ZrN6, grown with nitrogen pressure reduced to 5×10^{-5} Torr, also has decreased reflectivity. This shows that nitrogen must be introduced into the chamber to grow stoichiometric ZrN from ZrN targets. Compared to the HfN reflectivity plot, there is a clear reduction in reflected intensity. At 500nm, the highest ZrN reflectivity is 54% while for HfN it is 69%. This is not a result of ZrN targets being used, since ZrN3 is grown from a metal target. It appears as though HfN is more highly reflecting, but further growths of ZrN would be necessary to unambiguously state this as fact, especially given the acute growth temperature sensitivity of ZrN reported by Lee *et al*.[24]

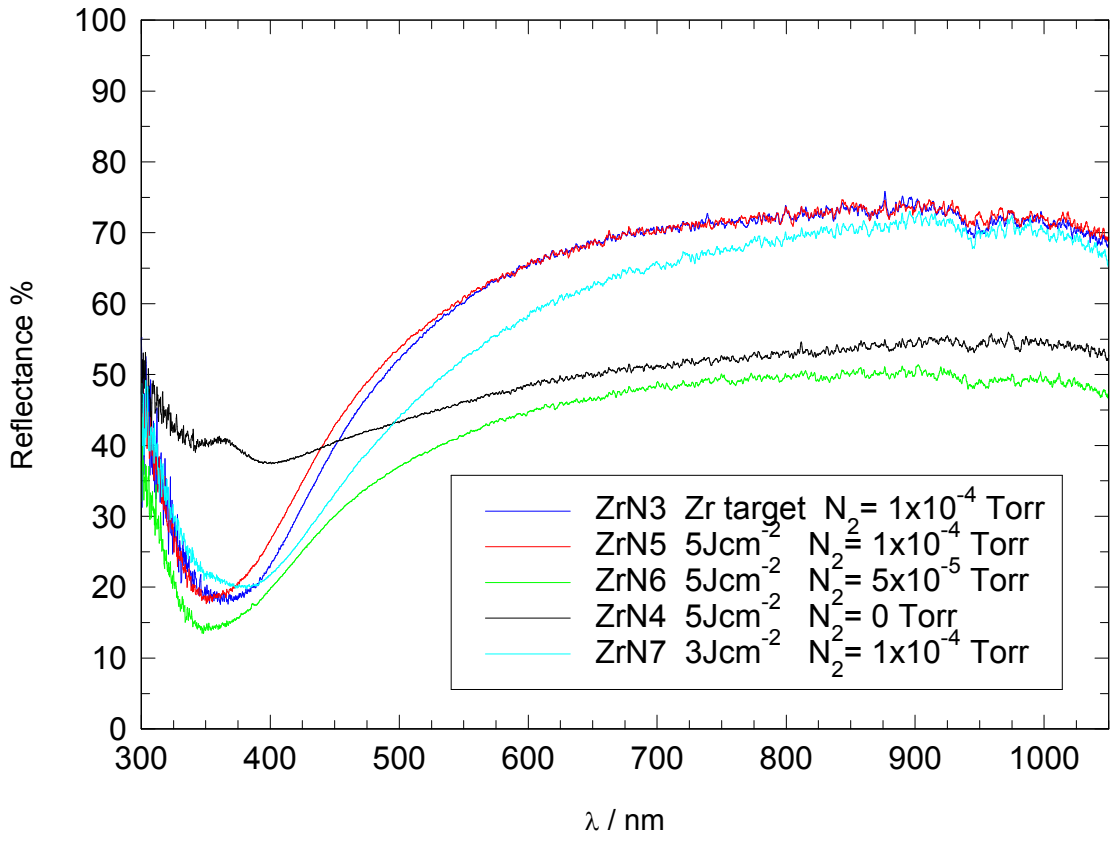

Figure 4.8 Reflectivity spectra of ZrN samples. Films grown from Zr and ZrN targets under similar conditions (ZrN3 and ZrN5 respectively) can have similar reflectivity spectra. A nitrogen background is essential when using ZrN targets to maintain the characteristic ZrN spectral shape.

4.4.3 X-Ray Diffraction

XRD measurements were made on HfN samples, but not ZrN. All samples displayed the HfN(002) peak at 39.9° and in the case of four of the six samples, the MgO(001) peak, in addition to other as yet unidentified peaks. Gueddaoui *et al* [16] identify the peak at 33.5° (33° - 34° in these samples) as HfN(111) as grown on their Si(100) substrates. The existence of the HfN(111) orientation does not correlate with any identifiable growth parameter in this work. The intensity and FWHM of the HfN(002) peak are listed in Table 4.3 below and have been used as an indication of material quality. HfN2 displays the narrowest FWHM, although they are all very broad compared to literature values. HfN5 is the most intense (002) peak, and is slightly wider. Although the intensity values should be directly comparable, FWHM is probably more reliable as an absolute comparison since samples have to be individually mounted and spectra were taken on different days for many of the samples. There is no clear minimum value for FWHM nor maximum for intensity as temperature is varied. XRD measurements place the lattice constant of the better quality samples at around 4.530 Å while for the lower quality samples it is above 4.540 Å.

The sampling volume of the XRD apparatus used is 12 mm across by 5 mm to 20 mm long, the latter range increasing with angle of incidence. This large sampling volume covers the entire width of the samples (1 cm). The broad FWHM, therefore, can be attributed to contributions from areas of varying stoichiometry across each sample and as such do not necessarily indicate poor crystallinity. The XRD system used is designed for powdered samples rather than thin films. It would be interesting to compare the data with that of an XRD system designed specifically for thin films, which would have a typical beam width of 1 mm at the sample surface.

Sample	T_{sub} / °C	N_2 / Torr	Plasma/W	(002) FWHM	(002) intensity	(002) angle
HfN7	**350**	1×10^{-4}	200	1.56°	260	39.76°
HfN8	**400**	1×10^{-4}	200	1.61°	188	39.84°
HfN5	**450**	1×10^{-4}	200	1.12°	860	39.7°
HfN2	**500**	1×10^{-4}	200	0.76°	486	39.8°
HfN4	**550**	1×10^{-4}	200	2.84°	86	39.98°
HfN3	**600**	1×10^{-4}	200	1.14°	317	39.78°
HfN1	500	$\mathbf{2 \times 10^{-5}}$	200	1.86°	282	39.92°
HfN6	500	1×10^{-4}	**400**	2.93°	114	39.88°

Table 4.3 XRD data for HfN. Samples have been arranged in ascending order of substrate temperature in order to reveal possible trends. Key differing growth parameters are in bold text for clarity.

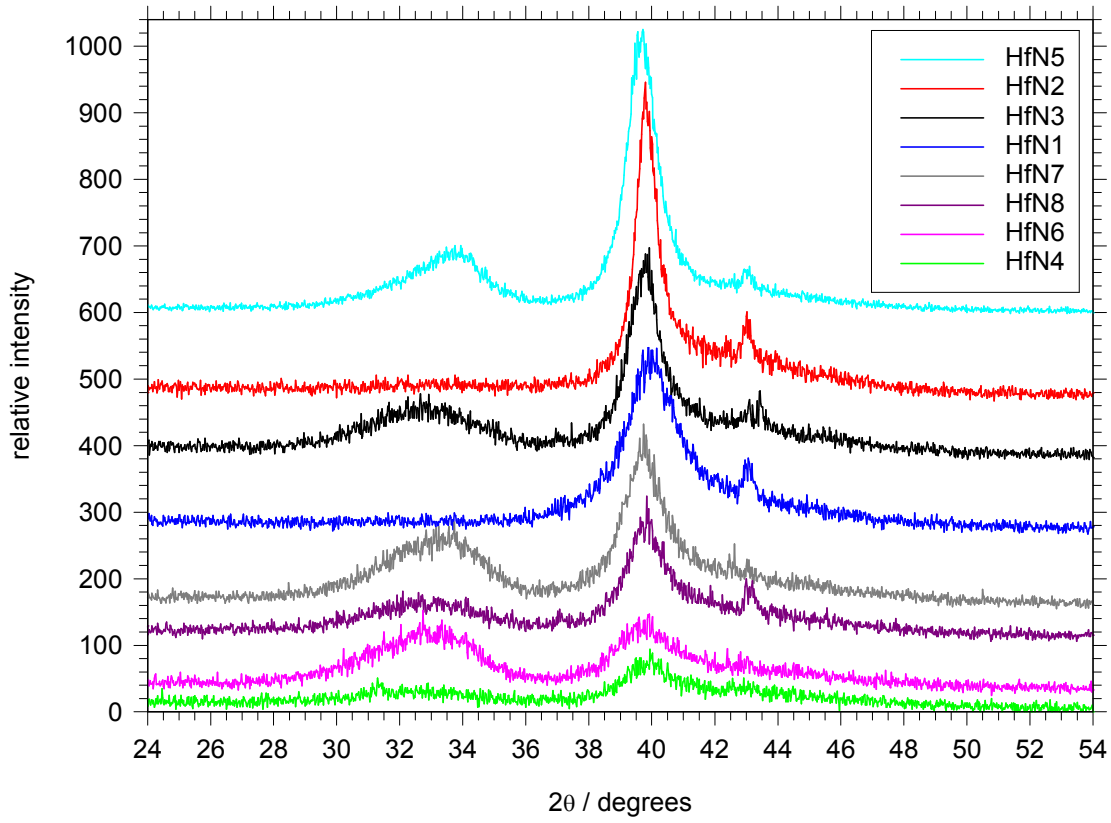

Figure 4.9 XRD spectra of all HfN samples. Spectra are vertically offset and HfN5 has had its intensity halved for clarity. The HfN(002) peak is visible at ~40° in all samples. The relatively large FWHM of the peak is due to the broad beam sampling volume sampling areas of varying stoichiometry.

4.4.4 Resistivity

Samples HfN1 and HfN2 were contacted for Hall measurements. It is worth noting that, in order to avoid effects of a HfN native oxide layer, Seo *et al* [5] contacted their samples by ion-beam milling 4 holes while under vacuum and then filling them with Pt without breaking vacuum. Contacts in the present work were soldered onto the top surface in atmosphere using indium solder. As mentioned previously, the rest of the samples have not been contacted to allow for ongoing reflectivity measurements. Seo *et al* have found that higher reflectivity is commensurate with lower resistivity, so the

measurements made on samples HfN1 and HfN2 should represent the lowest resistivities of any of the films.

It was found that certain parameters varied between successive measurements. In particular, Hall coefficient varied by as much as an order of magnitude in one instance. However, several measurements were made at different currents to eliminate current heating effects. Also, contacts were replaced and improved over time until better consistency was found.

HfN1 was found to have an average sheet resistance of 3.81 Ω cm. HfN2 was found to have an average sheet resistance of 3.45 Ω cm. Since the thickness measured by RBS of HfN2 is 128 nm, this yields $\rho = 44$ μΩ cm. This compares well with literature values, but is still quite a way off the minimum obtained to date by Seo's group (14.2 μΩ cm). As mentioned earlier, their ion-beam milled Pt contacts will have eliminated any additional resistivity from possible oxide formation so HfN2 might have slightly lower resistivity than the value calculated.

Bulk concentration, N_b	-4.93×10^{17} cm^{-2}	Sheet concentration, N_s	-4.93×10^{17} cm^{-2}
Mobility, μ	3.66 cm^2 V^{-1} s^{-1}	Hall coefficient, R_h	-12.65 m^2 C^{-1}
Bulk resistivity, ρ	3.46 Ω cm	Conductivity, σ	0.289 Ω^{-1} cm^{-1}
Magnetoresistance, δR	6.45×10^{-4} Ω	V/H resistance ratio, α	0.984

Figure 4.10 Sample set of results for room temperature Hall measurements on HfN2.

4.4.5 SEM

SEM was carried out on all samples and they were all found to be very smooth and featureless, with low particulate density. To verify that lack of features was not just due to poor set-up of the instrument, small particulates were located and used to focus upon at 50k magnification. Even at this level, there are no features or structure to be found on the sample surfaces. This is somewhat at odds with the RBS data, which claims that HfN2 and HfN3 have some very rough areas. AFM measurements may shed more light on this matter.

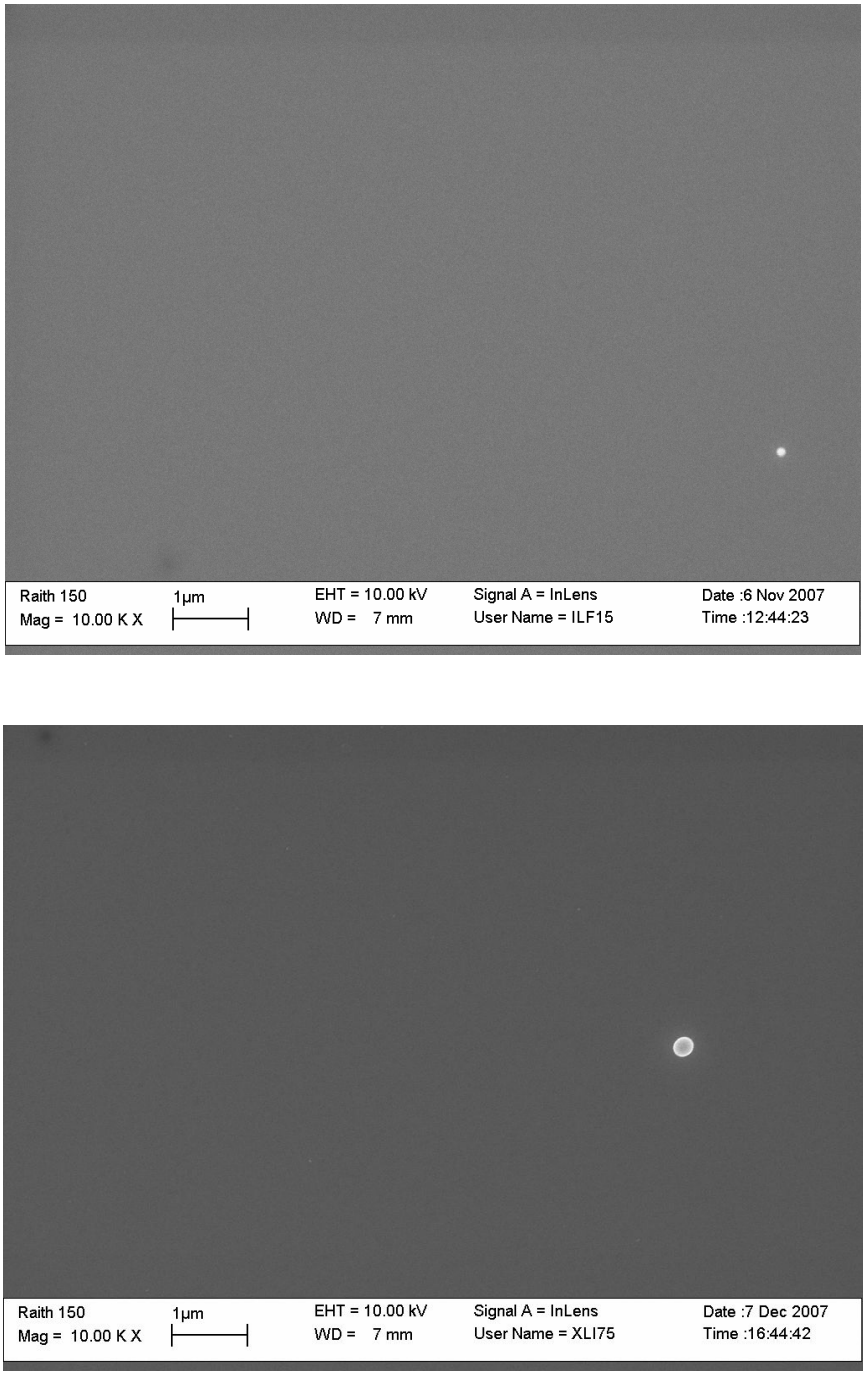

Figure 4.11 SEM image of central areas of HfN1 (top) and HfN3 (bottom). The lack of features indicate very smooth films. Images are from the central of each sample and a particulate has been located to provide some contrast to the smooth film beneath. These are typical images for metal target films.

SEM images of ZrN samples are shown in Figure 4.12. The most heavily particulated areas have been located on each film in this case, which would probably be in the area closest to the centre of the plume. Images are shown of ZrN3, grown from a metal Zr target, and ZrN4, grown from a nitride ZrN target. The different nature of the particulates is evident here; metal targets produce circular molten droplets while nitride targets produce powder-like flakes. It is possible that the molten metal particulates scatter incoming light more effectively and may contribute somewhat to the overall increased reflective intensity (but not the spectral shape) seen from the metal-target film. However, more growths would have to carried out to firmly conclude this.

(A)

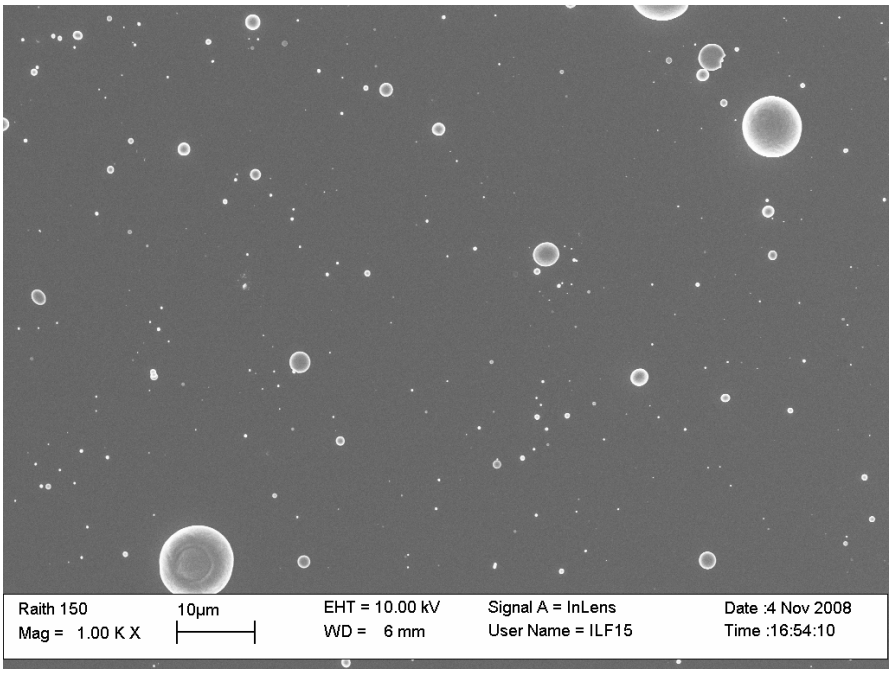

(B)

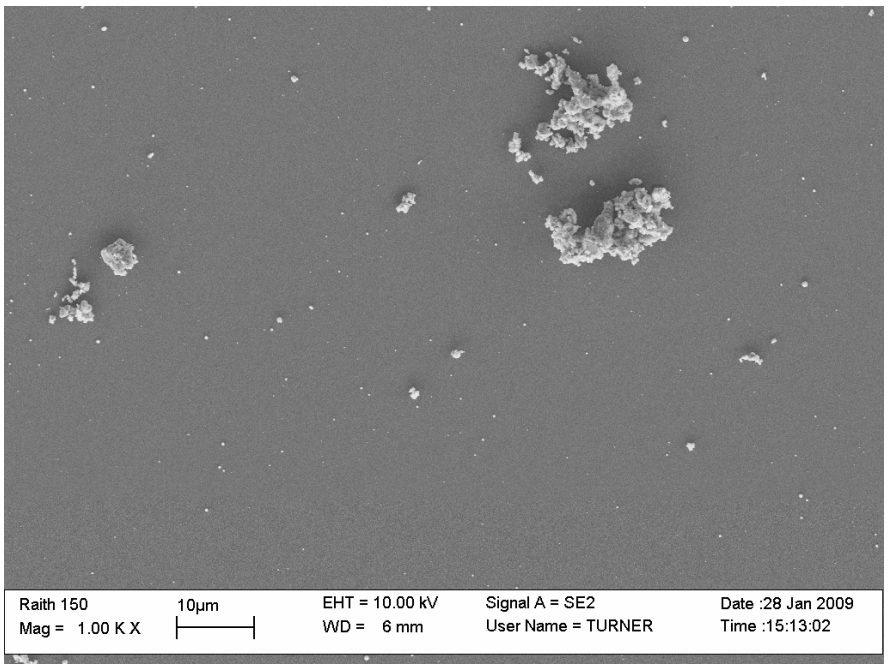

Figure 4.12 SEM images of ZrN films grown from a metal Zr target (A) and a ceramic ZrN target (B). The images show the different nature of particulates ejected from metal and ceramic targets.

4.4.6 Synchrotron measurements

X-ray absorption and emission spectroscopy (XAS and XES) were undertaken at the nitrogen K-edge using the soft x-ray beamline 511 at MAXlab (Lund, Sweden) which is equipped with a spherical grating monochromator that yielded a resolution of 0.2 eV.[25] XES results were recorded using a Nordgen-type grazing incidence spherical grating spectrometer with a resolution of 0.3 eV.[26] Absorption data were recorded in fluorescent yield mode with the sample oriented at 75° to the incident beam.

Figure 4.13 shows the XES (filled black circles) and XAS (open blue circles) data from HfN2 (grown at 500 °C, 200 W plasma power, and 10^{-4} Torr N_2) representing the filled and empty N *p*-projected partial density of states (PDOS), respectively.[20] There is overall similarity between the present data and those obtained for rare-earth nitrides, which have the same physical structure and similar electronic configurations.[22] To compare to experiment a band structure calculation has been performed within the local density approximation to density functional theory using the full-potential linearized muffin-tin orbital method [27,28]. The resulting band structure, also shown in Figure 4.13, is similar to that obtained by Stampfl *et al*.[21] The extracted PDOS (red line in Figure 4.13) is in excellent agreement with the XAS and XES. Particularly striking is the small but significant density of filled states extending from ~395eV to the Fermi level at ~397.5eV. Such a feature does not occur in semiconducting nitrides. An inspection of the full band structure in Figure 4.13 shows that this feature in HfN corresponds to the occupied bands of mostly Hf *d* character that cross the Fermi level (E_F) and give a small density of states with a weak nitrogen *p*-projection. The XAS data appear to overlap slightly with the XES, which is attributed to a small shift of the data due to core-hole effects [22, 23].

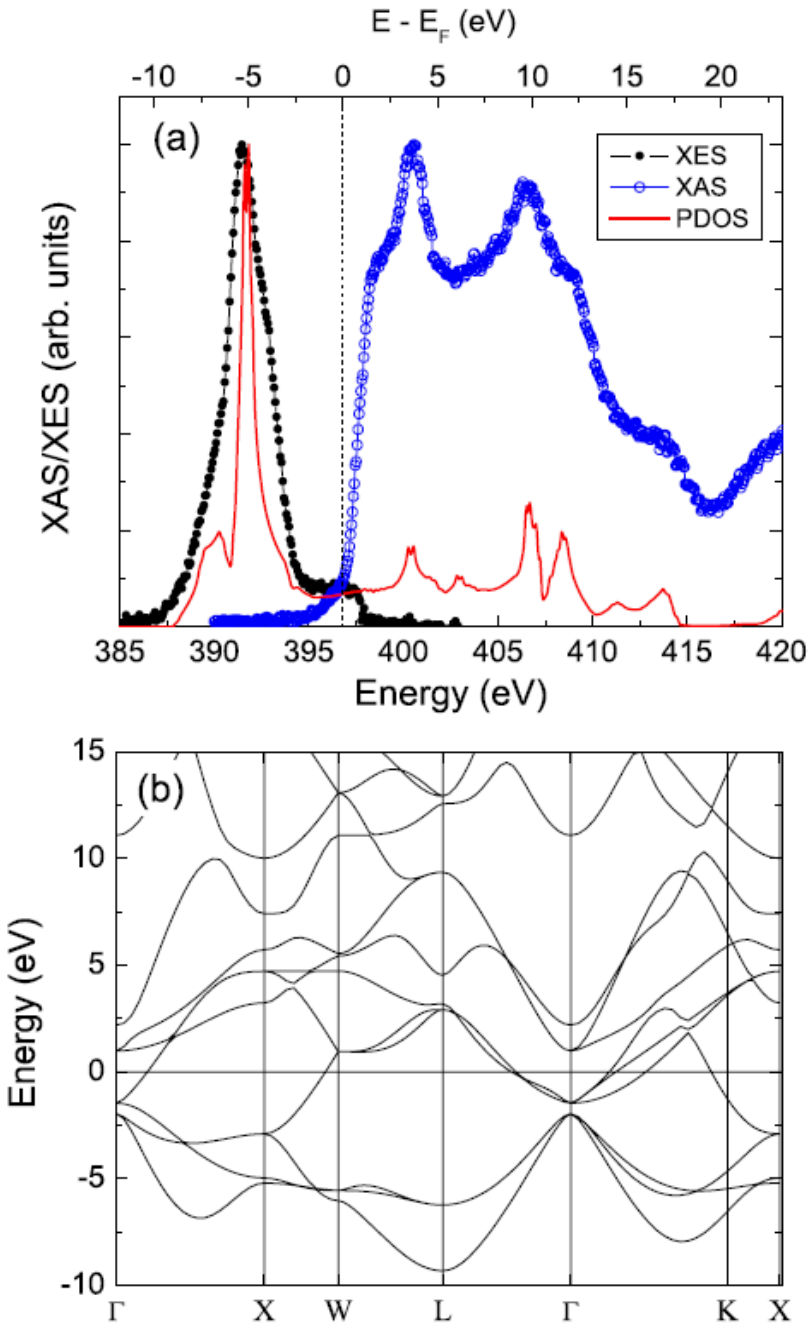

Figure 4.13 Top: X-ray emission (closed circles) and absorption (open circles) which measure, respectively, the filled and empty nitrogen *p*-projected density of states, compared to the calculated PDOS (solid line). The dashed line marks the calculated Fermi level. **Bottom:** Calculated band structure of HfN. The bands crossing the Fermi level (0 eV) originate from Hf *d*-orbitals.

4.4.7 Raman spectroscopy

Phonon frequencies of the HfN and ZrN films have been measured by Raman spectroscopy. Raman spectra were taken with a triple-subtractive Jobin-Yvon T64000 Raman microscope equipped with a liquid nitrogen-cooled Hamamatsu 1024×256 pixel CCD detector. CW excitation wavelengths at 530.9 nm and 568.2 nm were provided by a tunable Ar^+-Kr^+ gas laser and at 830 nm by a MQW InGaAs/AlGaAs diode laser. For all wavelengths, laser power was maintained at 2 mW (measured at the sample). This was focused to a 100 μm diameter spot by the ×100 lens of the Raman microscope. Slits were set to 500 μm. System resolution is 2 – 3 cm^{-1}. The spectrometer was operated in subtractive mode which gives very good stray light rejection, enabling close Raman modes within 10 cm^{-1} of the laser line to be resolved. However, light from the samples exhibited some Rayleigh scattering from particulates and surface roughness, which resulted in a strong tail-off from the laser line. This, coupled with the fact that HfN only produces weak defect-induced Raman scattering in the first order [10], prevented spectral features below about 300 cm^{-1} being resolved. The first-order acoustic phonons could not be resolved and appear in the data only as shoulders in the elastically scattered laser light. Acoustic phonons could only be observed where they interact with the optical phonons.

HfN is a transition metal nitride in which the three second order acoustic lines, 2TA, TA+LA, and 2LA as well as the O-A mode, all of which can be observed, occur within the gap between the first order acoustic and optical bands without overlapping the O-band [10]. The first and second order acoustic modes, measured in HfN samples with stoichiometry ranging from $HfN_{0.85}$ to $HfN_{1.50}$, lie in the range 120 cm^{-1} to 335 cm^{-1}, according to the work of Stoehr *et al* [29]. The Rayleigh scattering of light mentioned earlier prevents these modes being observed except as shoulders in the tail of light scattered from the probe laser. Hence this analysis focuses on the two most clearly resolved Raman peaks observed in these samples; the first-order optical phonon, which varies in frequency from 512 cm^{-1} to 538 cm^{-1}, and the summation of the first-order optical (O) and both the transverse acoustic (TA) and longitudinal acoustic (LA) phonon which is observed over the range 801 cm^{-1} to 811 cm^{-1}.

The sample with greatest variation in stoichiometry has been examined most closely to attempt to correlate changes in the phonon frequencies with variations in the stoichiometry. This was measured by Seo *et al* using stoichiometric HfN and understoichiometric $Hf_{0.94}N$ as well as by Stoeher *et al* with the greater range of stoichiometries mentioned above. Sample HfN3 varies from stoichiometric to $HfN_{1.54}$ and we observe larger phonon shifts as a result, shown in Figure 4.14 with measured optical phonon frequencies listed in Table 4.4. The shifts do not vary linearly with stoichiometry and this includes material with stoichiometries that vary while still retaining the NaCl structure. There is a trend that occurs across the wafer whereby lower phonon frequencies are found to correspond with the area closer to 1:1 stoichiometry. All Raman modes from the work done in reference [29] have been plotted in Figure 4.15 and it is clear from this that there is an overall trend for phonon frequencies to be at a minimum closer to stoichiometry.

The peak at 1087 cm^{-1} is not thought to be due to be coming from the films. Its position is absolutely fixed in all scans taken. It is not from the MgO substrate, whose closest Raman line occurs at 1096 cm^{-1}. Raman frequencies occur for O_2 at 1550 cm^{-1} and for N_2 at 2330 cm^{-1}, so neither of these are candidates for a signal coming from atmosphere [30]. It is also not a plasma line coming from the laser, since different laser sources (gas and semiconductor) were used. The microscope objectives are made of quartz and these do not have a Raman line at 1087 cm^{-1} either.[31] The sharp lines in the spectra are spurious noise, likely created by cosmic rays striking the CCD.

The Raman frequencies measured experimentally by Seo (’99) using Raman spectroscopy and Christensen (’83) by inelastic neutron scattering have been verified theoretically by the ab-initio calculations of Maksimov (’09) and are in agreement with results presented here. This work slightly extends the range of metal:nitride ratios for which Raman frequencies have been measured.

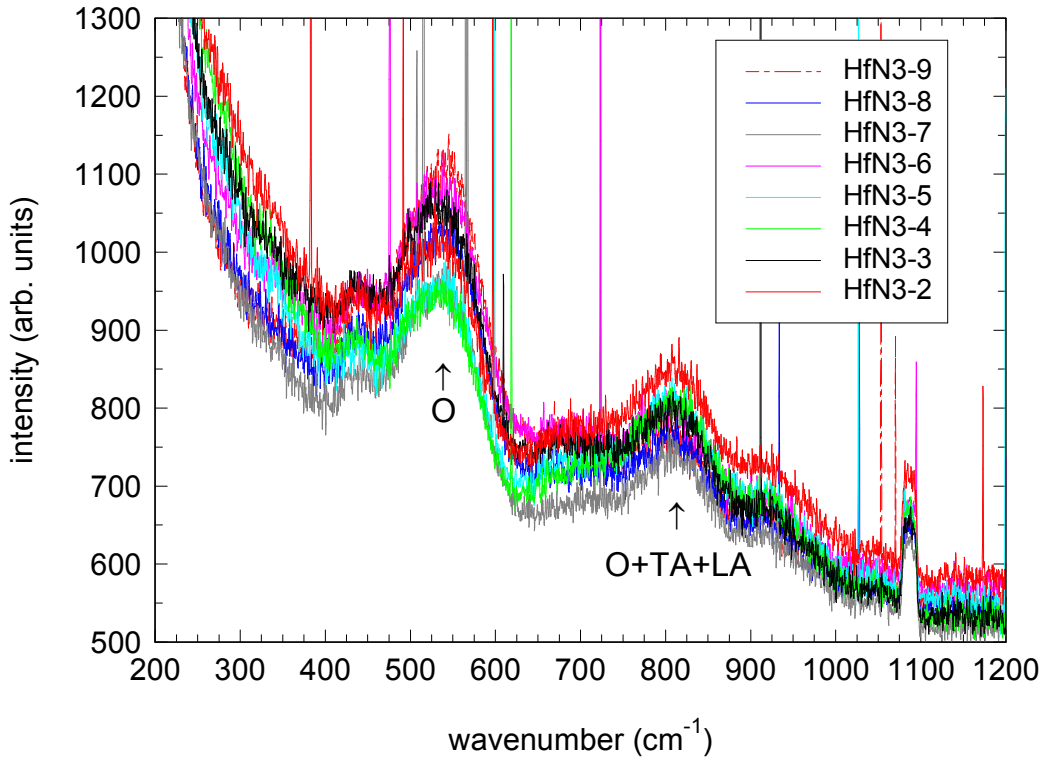

3-1 532 cm^{-1}	3-2 533 cm^{-1}	3-3 531 cm^{-1}
3-4 534 cm^{-1}	3-5 540 cm^{-1}	3-6 538 cm^{-1}
3-7 540 cm^{-1}	3-8 537 cm^{-1}	3-9 542 cm^{-1}

Figure 4.14 Raman spectra taken from nine evenly spaced points across sample HfN3, which showed significant variation in stoichiometry across its surface. The grid below the spectra represents a wafer map of the sample showing the areas from which the spectra are taken. These spectra were taken using a probe laser at 531 nm.

HfN3 sample area #	O (cm^{-1})
1	532
2	533
3	531
4	534
5	540
6	538
7	540
8	537
9	542

Table 4.4 Table of Raman shift measured for the optical phonon in sample HfN3 with an approximate map of sampling positions.

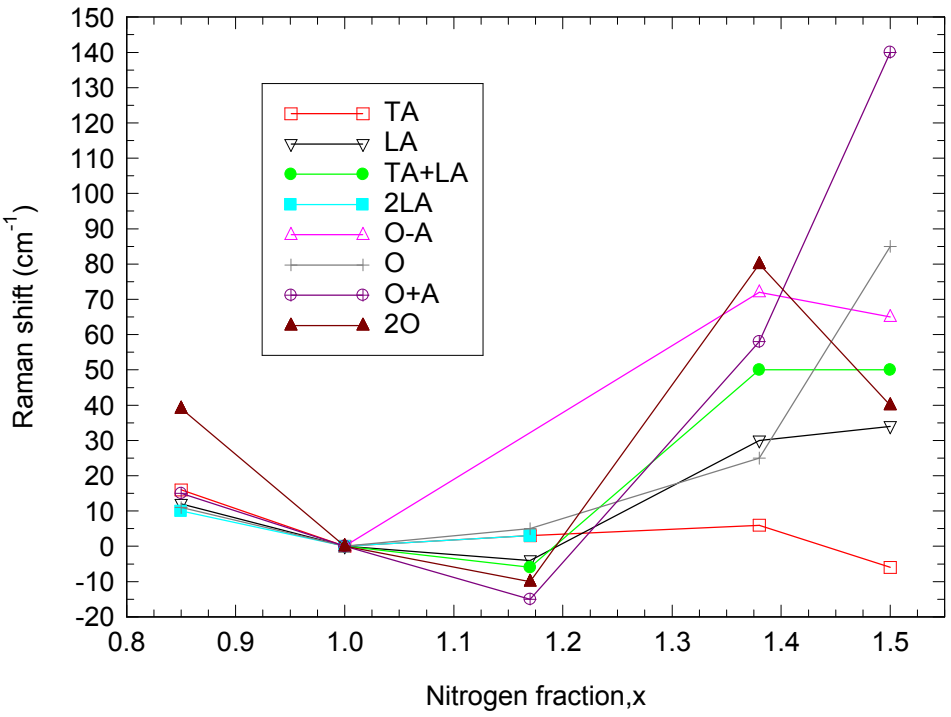

Figure 4.15 Raman modes in HfN_x for $0.85 < x < 1.50$ normalised to the Raman frequency of stoichiometric HfN, taken from the work of Stoehr *et al* [29].

4.5 Conclusion

This work represents the first attempt to grow HfN by PLD. Thin films of HfN have been grown on MgO substrates to assess their potential as buffer layers for GaN on Si growth. Optoelectronic properties of the films have been investigated by resistivity and reflectivity measurements and their bandstructure probed by XES and XAS. Sub-stoichiometric films with rougher surfaces are found to have increased reflectivity which will present challenges for epitaxial overgrowth with GaN. Films grown at temperatures above 500 °C show larger reflectivity which extends further toward the UV, and their electronic structure agrees with the results of a band structure calculation. It has been shown that nitrogen pressure is not a crucial parameter in film quality, although excess plasma energies clearly cause poor growth. An optimum growth temperature of 500 °C has been established for HfN. The fact that the reflectivity of HfN can be tuned by varying growth conditions is relevant for optical device applications, for example to optimize light extraction from GaN-based LEDs grown on silicon using a HfN buffer layer.

ZrN films have also been grown, but have not been as extensively analysed as HfN. Their growth was primarily to instigate the use of nitride targets in the PLD system. Their reflectivity spectra are of similar shape but lower reflected intensity than those of HfN. This may have more to do with the fact that most films were grown from a nitride target rather than being a fundamental property of ZrN itself. Further work on ZrN is required to establish if that is generally true of this material and if they are suitable candidates for GaN-Si integration.

References

[1] H.S. Seo, T. Y. Lee, J.G. Wen, I. Petrov, J.E. Greene and D. Gall, "Growth and physical properties of epitaxial HfN layers on MgO(001)", Journal of Applied Physics 96, 878 (2004)

[2] D.I. Bazhavov, A.A. Knizhnik, A.A. Safonov, A.A. Bagatur'yants, M.W. Stoker and A.A. Korkin, "Structure and electronic properties of zirconium and hafnium nitrides and oxynitrides", Journal of Applied Physics 97, 044108 (2005) and references therein

[3] L. Yuan, G. Fang, C. Li, M. Wang, N. Liu, L. Ai, Y. Cheng, H. Gao and X. Zhao, "Influence of N2 flow on the properties of HfN thin films prepared by DC magnetron sputtering", Applied Surface Science 253, 8538 (2007)

[4] A. Parkhomovsky, B.E. Ishaug, A.M. Dabiran, P.I. Cohen, "Growth of Hf and HfN on GaN by molecular beam epitaxy", Journal of Vacuum Science and Technology A 17, 2162 (1999)

[5] H.S. Seo, T.Y. Lee, I. Petrov, J.E. Greene and D. Gall, "Epitaxial and polycrystalline HfN_x ($0.8 \leq x \leq 1.5$) layers on MgO(100)", Journal of Applied Physics 97, 083521 (2005)

[6] D. R. Lide, "CRC Handbook of Chemistry and Physics' 71st Ed. (1991) p.**12**-87

[7] X. Xu, R. Armitage, S. Shinkai, K.Sasaki, C. Kisielowski and E. R. Weber, "Epitaxial condition and polarity in GaN grown on a HfN-buffered Si(111) wafer", Applied Physics Letters 86, 182104 (2005)

[8] R. Armitage, Qing Yang, H. Feick, J. Gebauer, E. R. Weber, S. Shinkai and K. Sasaki, "Lattice-matched HfN buffer layers for epitaxy of GaN on Si", Applied Physics Letters 81, 1450 (2002)

[9] S Shinkai and K Sasaki, "Influence of Sputtering Parameters on the Formation Process of High-Quality and Low-Resistivity HfN Thin Films", Japanese Journal of Applied Physics 38, 2097 (1999)

[10] M. Stoehr, H. S. Seo, I. Petrov and J. E. Greene "Raman scattering from epitaxial HfN layers grown on MgO (001)", Journal of Applied Physics 99, 043507 (2006)

[11] B. Karlsson, R.P. Shimschock, B.O. Seraphin and J.C. Haygarth, "Optical properties of CVD-coated TiN, ZrN and HfN", Physica Scripta 25, 775 (1982)

[12] M. Stromme, R. Karmhag and C.G. Ribbing, "Optical constants of sputtered hafnium nitride films. Intra- and interband contributions", Optical Materials 4, 629 (1995)

[13] P.R. Aron and A. Grill, "Some properties of r.f.-sputtered hafnium nitride coatings", Thin Solid Films 96, 87 (1982)

[14] R. Nowak and S. Maruno, "Surface deformation and electrical properties of HfN thin films deposited by reactive sputtering", Materials Science and Engineering A 202, 226 (1995)

[15] R.V. Leverenz. "Look at Hafnium nitride coatings", Manufacturing Engineering 79, 38 (1977)

[16] H. Gueddaoui, S. Maabed, G. Schmerber, M. Guemmaz and J. C. Parlebas, **"**Structural and optical properties of vanadium and hafnium nitride nanoscale films: effect of stoichiometry", European Physical Journal B - Condensed Matter and Complex Systems 60, 305 (2007)

[17] Y. Zhu, M. Ikeda, Y. Murakami, A. Tsukazaki, T. Fukumura and M. Kawasaki, "Low-temperature growth of highly crystalline superconducting ZrN thin film on c-GaN layer by pulsed laser deposition", Japanese Journal of Applied Physics Part 2 – Letters and Express Letters 46, L1000 (2007)

[18] H. Spillmann, P.R. Willmott, M. Morstein and P.J. Uggowitzer, "ZrN, Zr_xAl_yN and Zr_xGa_yN thin films - novel materials for hard coatings grown using pulsed laser deposition", Applied Physics A – Materials Science and Processing 73, 441 (2001)

[19] B. J. Ruck, A. Koo, U. D. Lanke, F. Budde, H. J. Trodahl, G. V. M. Williams, A. Bittar, J. B. Metson, E. Nodwell, T. Tiede, A. Zimina, S. Eisebitt, "Filled and empty states of disordered GaN studied by x-ray absorption and emission", Journal of Applied Physics 96, 3571 (2004)

[20] J. Stohr, "NEXAFS Spectroscopy", (Springer, New York, 2003)

[21] C. Stampfl, W. Mannstadt, R. Asahi, and A.J. Freeman, "Electronic structure and physical properties of early transition metal mononitrides: Density-functional theory LDA, GGA, and screened-exchange LDA FLAPW calculations", Physical Review B 63, 155106 (2001).

[22] A. R. H. Preston, S. Granville, D. H. Housden, B. Ludbrook, B. J. Ruck, H. J. Trodahl, A. Bittar, G. V. M. Williams, J. E. Downes, A. DeMasi, Y. Zhang, K. E. Smith and W. R. L. Lambrecht, "Comparison between experiment and calculated band structures for DyN and SmN", Physical Review B 76, 245120 (2007)

[23] U. von Barth and G. Grossmann, "Dynamical effects in x-ray spectra and the final-state rule", Physical Review B 25, 5150 (1982)

[24] M.B. Lee, M. Kawasaki, M. Yoshimoto, M. Kumagai and H. Koinuma, "Epitaxial growth of highly crystalline and conductive nitride films by PLD", Japanese Journal of Applied Physics 33, 6306 (1994)

[25] R. Denecke, P. Vaterlein, M. Bassler, N. Wassdahl, S. Butorin, A. Nilsson, J.-E. Rubensson, J. Nordgren, N. Martensson, and R. Nyholm, "Beamline I511 at MAX II, capabilities and performance", Journal of Electron Spectroscopy and Related Phenomena 101-103, 971 (1999)

[26] J. Nordgren, G. Bray, S. Cramm, R. Nyholm, J.-E. Rubensson, and N. Wassdahl, "Soft x-ray emission spectroscopy using monochromatized synchrotron radiation", Review of Scientific Instruments 60, 1690 (1989)

[27] P. Larson, W.R.L. Lambrecht, A. Chantis, and M. van Schilfgaarde, "Electronic structure of rare-earth nitrides using the LSDA plus U approach: Importance of allowing 4f orbitals to break the cubic crystal symmetry", Physical Review B 75, 045114 (2007)

[28] H.J. Trodahl, A.R.H. Preston, J. Zhong, B.J. Ruck, N.M. Strickland, C. Mitra, and W.R.L. Lambrecht, "Ferromagnetic redshift of the optical gap in GdN", Physical Review B 76, 085211 (2007)

[29] M. Stoehr, H. S. Seo, I. Petrov and J. E. Greene, "Effect of off stoichiometry on Raman scattering from epitaxial and polycrystalline $HfN_x(0.85 \leq x \leq 1.50)$ grown on MgO(001)", Journal of Applied Physics 104, 033507 (2008)

[30] G. Herzberg, “Molecular Spectra & Molecular Structure” (Princeton, New Jersey: D. Van Nostrand Co., Inc.,1950), p.62

[31] D.Krishnamurti, “The Raman spectrum of quartz and its interpretation”, Proc. Ind. Acad. Sci. A, Vol XLVII, Pl. XVI

Chapter 5 RARE-EARTH NITRIDES : GADOLINIUM NITRIDE AND SAMARIUM NITRIDE

5.1 Introduction

The rare earth nitrides (REN) have recently gained attention, with significant advances in treating the theoretical problem of their electronic and magnetic properties [1,2]. Those computations have suggested properties that might be exploited in optoelectronic and/or spintronic applications. However, the experimental situation is still far from clear; extensive studies forty years ago were plagued by the instability of these materials in air, along with the difficulty of growing well-ordered materials with stoichiometric RE:N ratios and low levels of oxygen. Thus, until recently, there were disagreements about such fundamental questions as to whether they are metals or insulators. Their magnetic behaviour is characterised more reliably, at least for the few that have been carefully studied. They are thought to show magnetic order at low temperature, although in many cases even the form of that order, ferro- or antiferro-magnetic, remains uncertain. Much of this uncertainty arises from a lack of epitaxial single-crystal materials from which to deduce properties.

Of the RE nitrides, the most studied to date is GdN [3] Uniquely among the RE elements, Gd has both partially filled 4*f* and 5*d* orbitals [4]. While the magnetic coupling strength of the *f* orbitals are much weaker than those of the *d* orbitals due to the stronger localisation of the *f* electrons, taken together these orbitals can take part in a new coupling mechanism proceeding via intra-ion 4*f*-5*d* exchange interaction followed by inter-ion 5*d*-5*d* coupling mediated by charge carriers. As the active dopant in GaN:Gd materials, Gd has been found to have an unprecedented magnetic moment of 4000 μ_B per atom [5] with a Curie temperature of 400 K [6] in GaN. Samarium has two less electrons in the 4*f* shell, but the same number of valence electrons and its total magnetic moment is zero. Nanocrystalline SmN has been produced by thermal evaporation [7], but single-crystal material production under ultra-high vacuum conditions is desirable if decomposition by oxygen contamination is to be prevented. Stoichiometric single-crystal

material might also prove to be a deterrent to the SmN degradation mechanism first identified by Eick [8]:

$$SmN + 3H_2O \rightarrow Sm(OH)_3 + NH_3$$

Recent developments have begun to point the way toward the growth of stoichiometric films and effective capping procedures for passivating REN films against oxidation. Most of that work has been on nanocrystalline films prepared by reactive ion-beam sputtering [9,10]. . Molecular beam epitaxy (MBE) was shown to be capable of growing epitaxial GdN thin films [11]. The growth in that study was on MgO substrates, for which the very large lattice mismatch led to strongly disordered films on which XRD showed crystallite diameters on the order of 10 nm. In order to advance to a full understanding of their properties and device exploitation it is essential to grow strongly textured or single-crystal epitaxial films with well-characterised physical properties. This chapter reports epitaxial growth and passivation of GdN and SmN films on yttria-stabilised zirconia (YSZ) by PLD. YSZ provides a reasonable lattice match to both materials resulting in large crystallite diameters, and passivation has allowed studies of the magnetic and electronic film properties to be carried out. In the case of SmN, it is the first reported growth of epitaxial single-crystal material.

The work was carried out with collaborators from the MacDiarmid Institute for Advanced Materials and Nanotechnology at Victoria University, Wellington, New Zealand. This author's role in the project was to use skills developed in metal-nitride PLD growth to produce single-crystal material of the highest possible quality so that the fundamental properties of GdN and SmN could be established. Aside from optical transmission and SEM, all other characterisation was carried out by collaborators at Victoria University.

5.2 Experimental procedure

GdN and SmN thin films were grown on double-side polished YSZ(100) and YSZ(111) substrates measuring 1 cm × 1 cm × 0.5 mm. Substrates were subject to a

standard ultrasonic degreasing procedure of 5 mins immersion in each of trichloroethylene-acetone-methanol before being blow-dried in a nitrogen stream and bonded to a molybdenum plate using an InSb liquid alloy. Substrates were then transferred via load lock to the UHV chamber and outgassed at 800°C for a minimum of 1 hour. During outgassing, chamber pressure was monitored with an ion gauge to assess outgas progress and partial pressures of gasses were monitored using a Residual Gas Analyser to look for the presence of any impurities. Base pressure of the vacuum system prior to growth was kept in the high-10^{-8} Torr range using a turbopump (before introducing nitrogen), although base pressure is maintained in mid-10^{-9} Torr range by an ion pump when not growing.

A Lambda Physik Compex 205 KrF excimer laser of wavelength 248 nm and pulse length 25 ns was normally operated at a repetition rate of 10Hz in constant energy mode to maintain fluence levels to within ±12% of desired levels. Fluence was varied from 2 J cm^{-2} to 5 J cm^{-2}. Most targets were 1" × 0.25" discs supplied by Kurt J. Lesker, including 99.9% Sm, 99.95% Cr and 99.8% AlN. The Gd target was a 99.9% 1" × 0.125" disc supplied by ESPI and a diced YSZ substrate was used as a target for film capping. 99.9995% nitrogen gas, with less than 0.001 % Argon content, was passed through an Aeronex purity filter to an Oxford Applied Research RF plasma source operated at powers ranging from 100 W to 400 W and pressures ranging from 2.5×10^{-5} Torr to 1.2×10^{-4} Torr. Target-to-substrate distance was between 6.0 cm and 6.3 cm for all growths. Film thicknesses are on the order of 100 nm to 200 nm, depending on fluence and growth time.

Growth was monitored *in-situ* with a RHEED system comprising a Staib electron gun operated at 20.0kV and approximately 1.4A and a KSA imaging camera with associated analysis software. Optical/IR absorption measurements were carried out on a Cary spectrometer. The InSb bonding alloy was removed from the back of the substrate with fine (2000 - 4000) grit SiC sandpaper. It was found from testing on bare polished YSZ substrates coated with InSb, that the fine sandpaper could remove the metal alloy without unduly roughening the polished surface. A piece of bare double-side polished YSZ(100) was used as a reference sample to ensure final transmission data came from the nitride films only.

5.3 Results and Discussion

5.3.1 Film growth monitored by RHEED

SmN thin films were grown at substrate temperatures varying from 350 °C to 800 °C in steps of 50 °C. Analysis of the lattice constant via RHEED streak spacing (Figure 5.1) indicated that all films were found to relax except the film grown at the upper extreme of 800°C which was strained. RHEED patterns in the temperature range 450 °C to 700 °C were found to be streaky indicating single-crystal epitaxial growth. The FWHM of the n=0 diffracted line gives a qualitative indication of crystal quality as a function of growth temperature (Figure 5.2) and the shorter relaxation times in the 450 °C to 700 °C range correlate with this data. The film grown at 350 °C had a short relaxation time, but its RHEED pattern showed semicircles indicative of polycrystalline material superimposed on broad streaks (Figure 5.3).

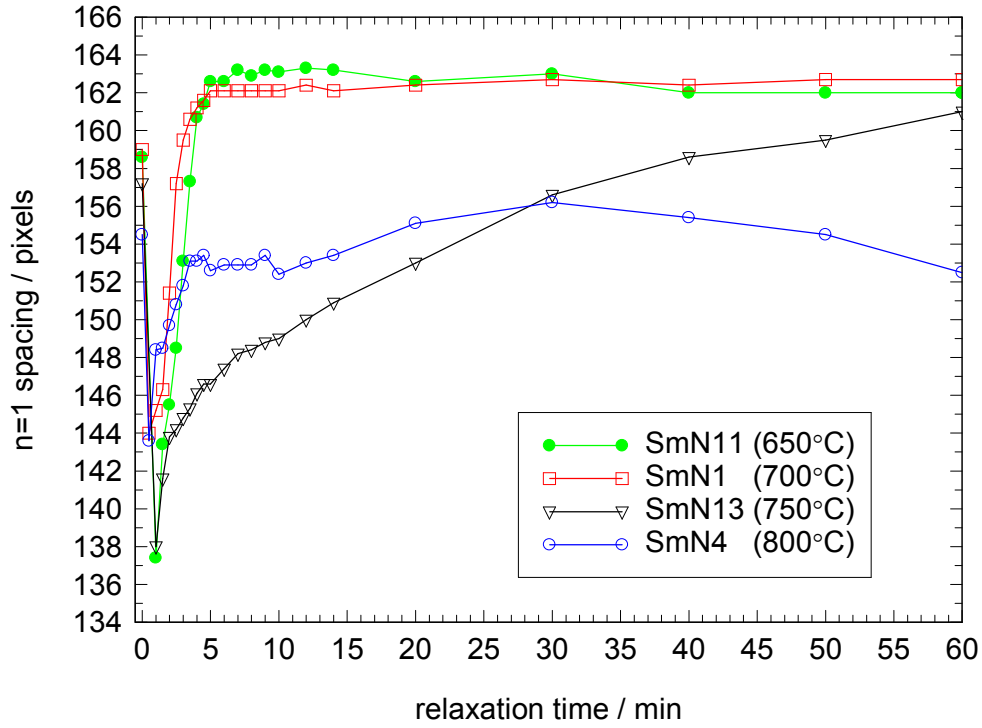

Figure 5.1 Relaxation times of SmN films during growth. Plots are only shown from optimum growth (650 °C) to strained (800°C) to illustrate the trend clearly. Film relaxation occurs more quickly at growth temperatures closer to 650 °C.

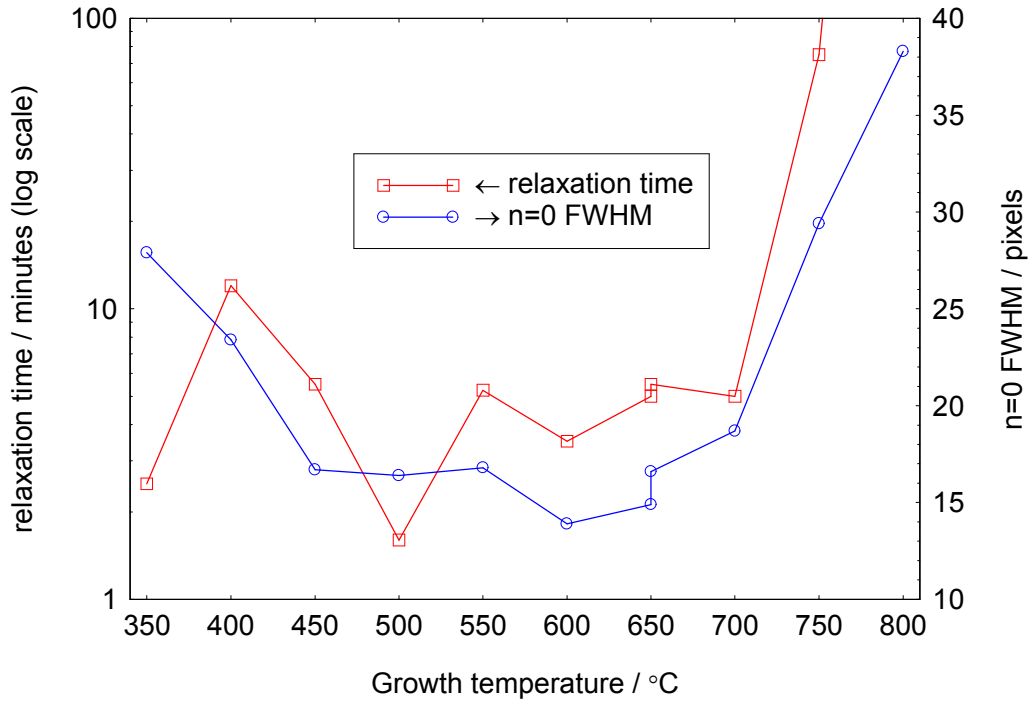

Figure 5.2 Variation of relaxation time (left axis) and FWHM of n=0 diffracted line (right axis) with growth temperature. The film grown at 800 °C remained strained, hence no relaxation data point exists. Note how two growths at 650°C show good repeatability between separate growth runs under near-identical conditions.

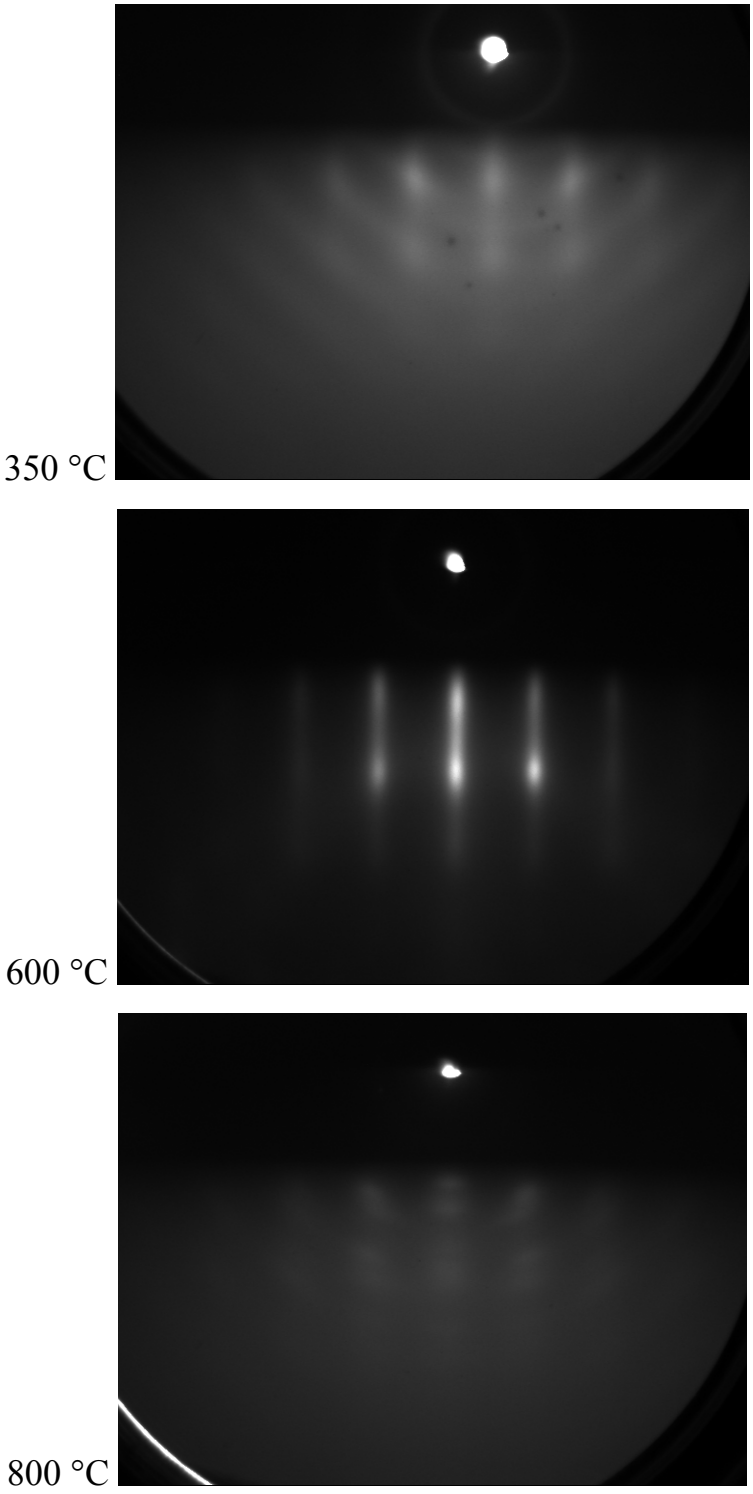

Figure 5.3 RHEED patterns after 60 mins of growth for SmN grown at 350 °C (top), 600 °C (middle) and 800 °C (bottom). In all cases, RHEED is monitored along the (100) direction. There is an obvious strong dependence on growth temperature for SmN, with

optimum crystal quality occuring at 600 °C, as evidenced by narrow streaks in the diffraction pattern.

Films could also be assessed qualitatively by the intensity of the RHEED patterns relative to the background and their shape. Figure 5.3 shows how patterns easily indicate the nature of the growth; at 350 °C polycrystalline material is grown, growing at 600°C produces an intense streaky single-crystal pattern while growth at 800°C produces a weak spotty pattern. The FWHM were measured after 60 minutes of growth as some films were grown for 2 hours to produce a thicker film for subsequent magnetic or X-Ray Magnetic Circular Dichroism (XMCD) measurements by collaborators. The clarity of some of the streaks in the SmN films grown between 450 °C to 700 °C is quite striking when compared to patterns of other nitrides studied in this research. This is due to the growth temperature producing appreciable desorption of unreacted Sm from the film surface during growth. For other metals it is significantly higher (Table 5.1). Excess Sm at the surface is boiled off leaving a clear surface from which the electron beam diffracts.

Metal	temperature producing 1 Pa vapour pressure	temperature producing 100 kPa vapour pressure
Ga	1037 °C	2245 °C
Gd	1563 °C	3262 °C
Hf	2416 °C	4603 °C
Sm	728 °C	1788 °C
Zr	2366 °C	4405 °C

Table 5.1 Vapour pressures (v.p.) of metals at atmospheric and low pressures [12]. Both are shown to give an idea of how much they change, since growth pressure is on the order of 0.01 Pa.

In contrast to SmN growth, the growth of GdN does not show such a large dependence on substrate temperature (Figure 5.4). Before beginning this growth series optimum growth temperatures were known from literature values [11] and from

discussions with collaborators, who have produced GdN by sputtering, so the range 700 °C to 800 °C proved to be suitable. The films grown at 850 °C were slow to relax so this temperature was taken as an upper limit for good quality growth. Fast relaxation times are generally understood to indicate atoms moving quickly to their lattice sites, resulting in a crystal with a lower level of strain and dislocation-inducing defects. The purpose of GdN growth from the perspective of this thesis was to produce good quality single-crystal material and this was achieved within the first few GdN samples from prior experience gained during GaN, HfN and ZrN growths. Experimentation with nitrogen plasma pressures has shown what has become a fairly predictable result; films grown at 1.0×10^{-4} Torr are of better quality. In Figure 5.5 below, this is evident from the faster relaxation time of GdN grown at this pressure.

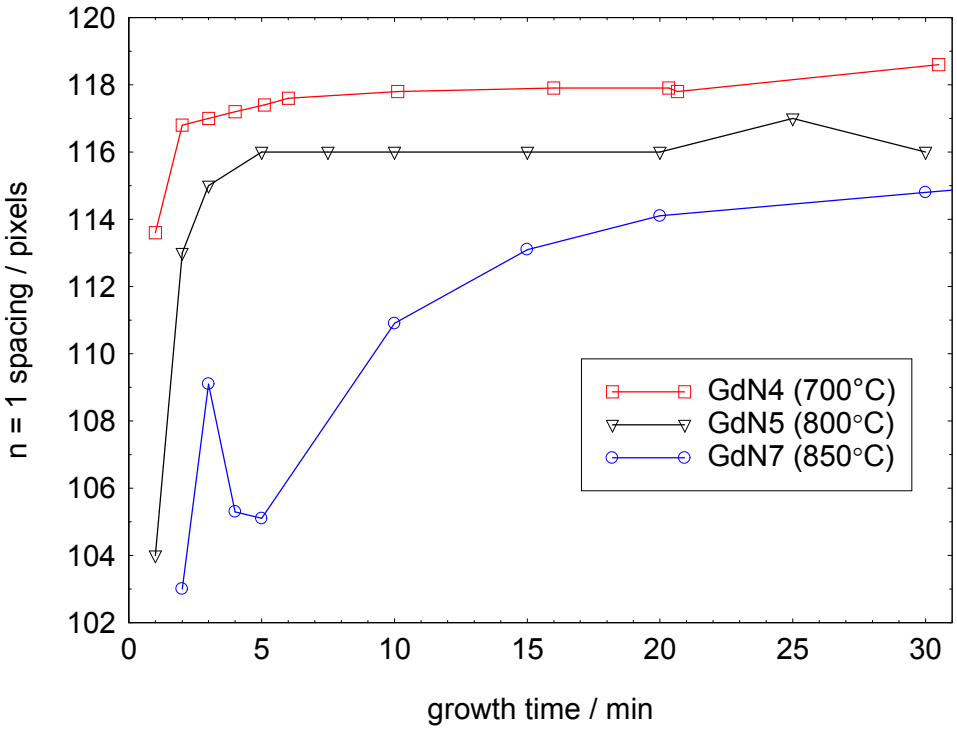

Figure 5.4 GdN film growth at different substrate temperatures. In a similar fashion to SmN, films are quicker to relax at lower growth temperatures, in this case closer to 700 °C.

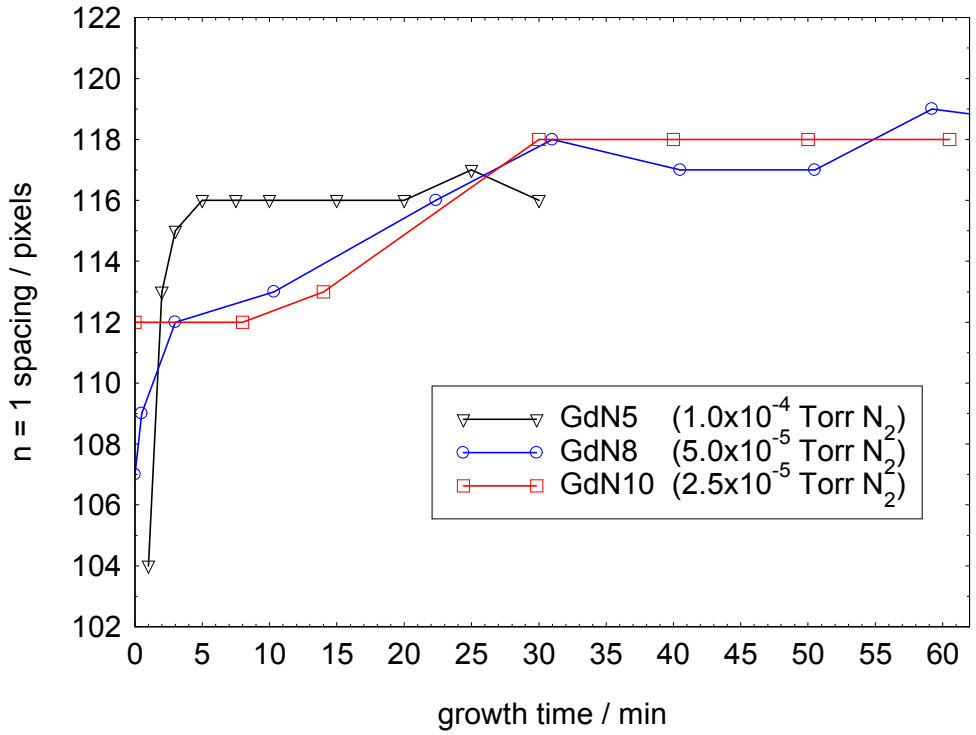

Figure 5.5 GdN film growth at different nitrogen pressures. The highest available nitrogen plasma pressure is favourable to forming a quickly relaxing GdN film.

In addition to varying growth temperature, the effects of Sm-flux were investigated by varying the laser fluence at the target. During the substrate temperature analysis series, fluence was maintained at 3 J cm^{-2}, although this will have varied by as much as 20% due to ablation deposits building up on the laser window during each growth run. Films were grown at fluences of 3, 4 and 5 J cm^{-2}, all at the established optimum growth temperature of 600 °C. Film quality deteriorated with increasing fluence; the lowest value selected (3 J cm^{-2}) yielded the best films. Similarly for GdN growth, low fluence of 3 J cm^{-2} led to the best film growth due to reduced particulation.

Variation of nitrogen plasma power showed no obvious trends for either GdN or SmN, although deleterious effects were noticed at extreme values of either, noted by subtle changes in RHEED patterns and regrettably causing more rapid degradation and delamination of films once removed from the growth chamber. The requirement for moderate plasma power has been a typical feature of metal nitride PLD growth – 200W forms the best quality films, while those at 400W or 100W are always of lesser quality.

Also, growing in a nitrogen ambient without striking a plasma has proved to be unsuccessful. This is due to the necessity to activate the stable nitrogen molecule to enable it to engage in the growth process.

Prior to capping, additional experiments were carried out on some the films. One of the SmN samples was cooled to room temperature to look for evidence of surface reconstruction in the RHEED, but none was observed. The only change was in the n=1 streak spacing, which occurs with change in temperature. The spacing reverted to the initial high temperature level when reheated for capping. For one growth run, RHEED was monitored in the (110) direction but nothing new was observed. The poor-quality sample grown at 400 °C was heated to 700 °C in steps of 50 °C to test whether annealing improvements could be made on the films, but there was no indication in the RHEED of any improvement. 700 °C was chosen as a suitable anneal temperature since it seems to be the upper temperature limit at which high-quality SmN can be grown and also because the AlN caps are grown at 700 °C. The consensus on optimum growth temperature for AlN as reported in the literature seems to be 750 °C, but we chose the lower value of 700 °C to ensure the underlying SmN films were not degraded during capping. It was also considered prudent to stay above the Al melting temperature of 660 °C to help alleviate any clustering of dissociated Al on the surface during the capping process. It is worth pointing out that the nitrogen plasma source and gas flow were turned off during cap growth as AlN is also reported to grow better under UHV conditions rather than a background of N_2.

Regarding capping, we have tried using caps composed of AlN, YSZ and Cr. Caps were grown for 15 minutes in earlier growth runs, but this was increased to 30 minutes when early samples degraded after some time (days to weeks) outside the vacuum chamber. To date, no effective long-term capping solution has been found to prevent the degradation of the SmN in atmosphere. The Cr-capped samples are more recent and are the only caps which display a streaky RHEED pattern. However, the cap is not well-bonded to the SmN, as evidenced by a rapid transition from the lattice constant of SmN to that of Cr in only 10s of Cr-growth. This is too fast for epitaxial layers to relax if they are properly bonded. AlN and YSZ caps were mostly polycrystalline or amorphous in nature and did not have strong RHEED patterns. To test the viability of

GdN surviving unprotected in atmosphere, a sample grown under optimum conditions was removed without capping. The film degraded within minutes, proving that the capping procedure remains essential despite the advances we have made in epitaxial growth of these materials. A similar experiment was performed on SmN by removing an uncapped sample from the chamber. Emboldened by the high degree of film quality displayed in RHEED patterns, we hoped stronger Sm-N bonding might prevail against the onslaught of atmospheric water vapour. The film turned from the characteristic golden brown colour to cloudy white within approximately 5 seconds and then delaminated.

5.3.2 Optical Transmission

Optical transmission spectra for samples grown under optimum conditions are shown in Figure 5.6. The GdN sample was capped with YSZ, so a YSZ cap was grown on YSZ substrate was used as a reference to ensure the response of the GdN alone was being accounted for. The SmN sample was capped with AlN, which has a bandgap of 6eV and so does not effect the region of interest. The transmission curves show an absorption onset of 1.3 eV for GdN and 1.0 eV for SmN, indicating that they are semiconductors.

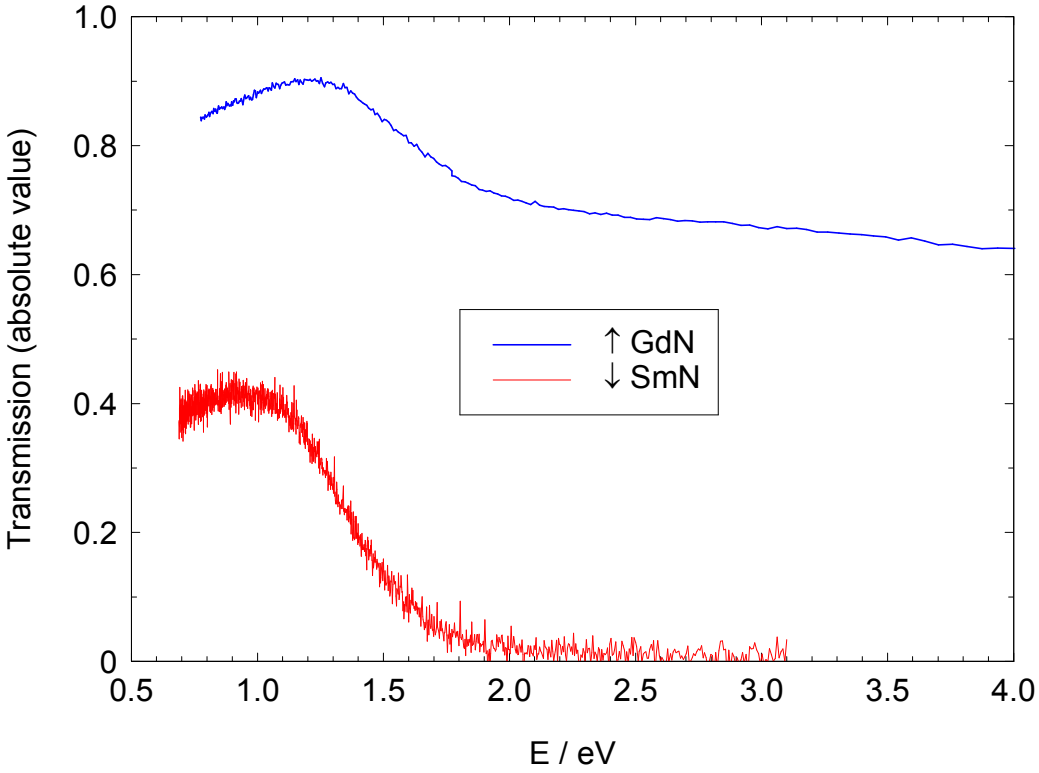

Figure 5.6 Optical transmission spectrum of GdN (top) and SmN (bottom) showing an absorption onset of 1.3 eV for GdN and 1.0 eV for SmN.

5.4 Conclusion

Thin films of single-crystal GdN and SmN have been epitaxially grown on YSZ(100) and YSZ(111) substrates by plasma-assisted PLD using elemental metal targets. Optimum growth conditions have been established by interpretation of RHEED patterns of growing films. The effects of laser fluence, substrate temperature, nitrogen pressure and plasma power on the films have been investigated. Efforts have been made to find a cap which will provide long-term protection of the films from atmospheric water, although success to date has been limited to a few weeks' protection. This work is ongoing. Samples are transported and stored under vacuum for further characterisation by collaborators. The bandgaps for GdN and SmN have been measured by optical transmission to be 1.3 eV and 1.0 eV respectively.

References

[1] C. M. Aerts, P. Strange, M. Horne, W. M. Temmerman, Z. Szotek and A. Svane, "Half-metallic to insulating behavior of rare-earth nitrides", Physical Review B 69, 045115 (2004)

[2] P. Larson, W.R.L. Lambrecht, A. Chantis, and M. van Schilfgaarde, "Electronic structure of rare-earth nitrides using the LSDA plus U approach: Importance of allowing 4f orbitals to break the cubic crystal symmetry", Physical Review B 75, 045114 (2007)

[3] S. Granville, B. J. Ruck, F. Budde, A. Koo, D. J. Pringle, F. Kuchler, A. R. H. Preston, D. H. Housden, N. Lund, A. Bittar, G. V. M. Williams, and H. J. Trodahl, "Semiconducting ground state of GdN thin films", Physical Review B 73, 235335 (2006)

[4] S. Dhar, L. Perez, O. Brandt, A. Trampert, K.H. Ploog, J. Keller and B. Beschoten, "Gd-doped GaN: A very dilute ferromagnetic semiconductor with a Curie temperature above 300K", Physical Review B 72, 245203 (2005)

[5] S. Dhar, O. Brandt, M. Ramsteiner, V.F. Sapega and K.H. Ploog, "Colossal magnetic moment of Gd in GaN.", Physical Review Letters 94, 037205 (2005)

[6] N. Teraguchi, A. Suzuki, Y. Nanishi, Y.K. Zhou, M. Hashimoto and H. Asahi, "Room temperature observation of ferromagnetism in diluted magnetic semiconductor GaGdN grown by RF-molecular beam epitaxy.", Solid State Communications 122, 651 (2002)

[7] J. Kennedy, S. Granville, A. Markwitz, B.J. Ruck and H.J. Trodahl, "Ion Beam analysis of rare earth nitride thin films.", Nuclear Instruments and Methods in Physics Research B 266, 1558 (2008)

[8] H.A. Eick, N.C. Baenziger and L.Eyring, "The prepartion, crystal structure and some properties of SmN, EuN, and YbN." Journal of the American Chemical Society 78, 5987 (1956)

[9] F. Leuenberger, A. Parge,W. Felsch, K. Fauth and M.Hessler ,"GdN thin films: Bulk and local electronic and magnetic properties", Physical Review B 72, 014427 (2005)

[10] H.J. Trodahl, A.R.H. Preston, J. Zhong, B.J. Ruck, N.M. Strickland, C. Mitra, and W.R.L. Lambrecht, "Ferromagnetic redshift of the optical gap in GdN", Physical Review B 76, 085211 (2007)

[11] J.W. Gerlach, J. Mennig and B. Rauschenbach, "Epitaxial gadolinium nitride thin films", Applied Physics Letters 90, 061919 (2007)

[12] CRC Handbook of Chemistry and Physics, 88th edition (2008), CRC Press.

Chapter 6 CONCLUSIONS

6.1 Summary of results

Epitaxial thin films of metal nitrides have been grown by Pulsed Laser Deposition. Elemental metal targets have been used as ablation sources in conjunction with an active nitrogen source to grow the films. The majority of literature data on PLD growth reports on growth from multi-element and composite targets, so this thesis has contributed to the field of single-element sources.

Prior to beginning thin-film growth, the UHV PLD system was installed and its constituent elements were calibrated and characterised. In particular, a knowledge of the nitrogen species produced by the plasma source across the available range of nitrogen pressures and applied plasma powers was carried out. This was essential to give an indication of how nitrogen interacts with metals in the growth process. In all materials studied, it was found that operating the plasma source at high plasma power resulted in films displaying less than optimal qualities. These quality reductions manifested themselves as broadening and weakening of RHEED streaks, at times even resulting in polycrystalline rather than single crystal growth. In the case of HfN, the reflectivity was also significantly reduced. Since the characterisation results showed higher levels of atomic nitrogen being produced at higher plasma powers, it can be concluded that excited atomic nitrogen is detrimental to the epitaxial growth of metal nitride films.

The refractory metal nitrides HfN and ZrN were grown to assess their suitability as buffer layers that could potentially integrate GaN and Si technologies. Their lattice constants and cubic crystal structure are known to be appropriate to this task. These are the first reported films of HfN grown by PLD. Reflectivity of the films was shown to be sufficiently high in the visible region to form a back contact for GaN LEDs and resistivity of one of the most highly reflecting films was measured to be 44 μΩ cm, which is low enough to enable current injection without undue resistive losses.

Tuning of the film properties by suitable selection of growth conditions has also been carried out. Nitrogen pressure was shown to have little effect on HfN reflectivity across the range available for plasma source operation (1.0×10^{-5} Torr to 1.0×10^{-4} Torr).

Substrate temperature was shown to affect film properties and films grown ≥ 500 °C have higher overall reflectivity extending further towards the UV. Closer examination reveals that a 500 °C growth temperature is optimum for this material. XRD measurements place the lattice constants of the growth series between 4.530 Å and 4.540 Å.

X-ray absorption and emission spectra of the HfN films have been measured and the results found to be in agreement with the calculated bandstructure. The high reflectivity in the red and infrared is consistent with the metallic nature of HfN. The reflectivity then begins to decrease with the onset of direct band-to-band transitions and as the plasma frequency ω_p is approached. The band transition are most likely to be from the N *p*-band 2 eV below the E_F to the unoccupied Hf *d*-bands 1eV above E_F.

ZrN thin films have also been epitaxially grown, 3 from metal targets and 4 from nitride targets. Although the number of metal-target films is limited, it would seem from SEM images that Zr is more prone to particulate production at equal fluence levels to similar films produced with Hf. This is not surprising given the higher absorption of Zr at 248 nm. Reducing fluence from 5 J cm^{-2} to 2 J cm^{-2} resulted in non-stoichiometric ZrN, as evidenced by the lack of the characteristic reflectivity spectrum. The rest of the ZrN films were grown at 5 J cm^{-2} identical to HfN fluence levels. They best ZrN films produced had reflectivity 50 % ± 5 % lower than the best HfN film, but there is insufficient ZrN material available to conclude this as being generally true. What is certain, however, is that particulate density on ZrN film surfaces grown from a metal target far exceed those on a HfN grown under the same conditions.

GdN and SmN thin films have been grown by PLD and RHEED patterns have shown them to be consistently single crystal. This represents an improvement for GdN growth, as epitaxial films are largely reported to be polycrystalline. In the case of SmN, this work is the first recorded epitaxial growth of any kind.

RHEED has been the predominant factor in analysing these films. Relaxation times of each film have been calculated by measuring the rate of change in the lattice spacing, as evidenced by changes in the first order diffraction lines. Films that are quicker to relax to their own lattice constant are of higher quality. Furthermore, qualitative assessment of the films can be gauged by the visual appearance of the RHEED streaks.

Some quantitative measure of this has been developed by comparing the FWHM of the zeroth order line in the diffraction images.

The relaxation time and n=0 FWHM have both been shown to be indications of crystal quality, and plots of these have been used to establish the temperature range necessary for epitaxial growth of SmN. This material grows best between 450 °C and 700 °C. The clarity of the streaks in SmN in this range are particularly clear, indicating the growth is two dimensional, unlike those of other metal nitrides studied. This has been attributed to the vapour pressure of Sm. At the growth temperature, excess Sm is evaporated from the surface resulting in very clear and streaky RHEED without the usual diffuse streaks observed in the growth of other metal nitrides.

Relaxation times obtained from RHEED streak spacing have also been used to tailor the growth parameters of GdN to improve its crystallinity. Growth temperatures of 700 °C to 800 °C and the highest available nitrogen pressures of 1×10^{-4} Torr have been found to improve the films. In later work, laser fluence was changed by broadening the spot and increasing the beam energy proportionately while keeping the fluence value constant at 4.0 ± 0.4 J cm^{-2}. This was found to decrease the level of metal particulates occurring the samples without reducing the growth rate. This technique has been applied to other materials in more recent work by the author and other researchers as a means of particulate reduction.

GdN and SmN films are very susceptible to rapid decomposition when exposed to atmospheric water vapour and this has been shown to remain the case even when they are grown in single crystal form. The films must be capped if they are to survive in air and capping materials and growth conditions have been monitored and altered to increase the longevity of samples outside the chamber. There have been some successes in this regard, with material lifetimes having been extended by a few days in the case of SmN or weeks in the case of GdN. That said, the films do eventually degrade regardless of cap quality and they are transported under vacuum before being analysed off-site by collaborators.

6.2 Future work

The growth of ZrN from both metal and nitride targets needs to be investigated further. A series of ZrN films should be grown from metal targets, first by varying laser fluence to obtain particulate densities on a par with HfN. Then, presumably, some tailoring of other growth parameters like nitrogen plasma pressure and substrate temperature would be necessary to maximise reflectivity and minimise resistivity. Once this is achieved something more concrete could be said about the comparison of the fundamental properties of these two materials and which might be better suited to GaN-Si integration.

Metal-nitride and other composite targets are also worth investigating. Some initial work on how choosing between metal target or nitride target PLD growth affects fundamental film properties should be carried out, and the existing data on ZrN provides and avenue into completing this research.

Regarding capping of GdN and SmN, RHEED images of caps have shown that the caps themselves are not of good crystalline quality. YSZ caps are completely amorphous. Cr and AlN caps show a hint of streaks in the RHEED, but these are very faint and usually dissipate after 5 minutes of growth. In the rare cases where streaks persist long enough for relaxation times to be measured, it was obvious that the diffraction pattern from the underlying thin film was immediately masked by a streaky pattern with a lattice constant of the cap material. The time interval of this is too fast for relaxation to be occurring, so the caps are clearly loosely bonded to the films underneath. Further study of this could be warranted as lattice-matched caps are essentially heterostructures and heterostructure growth by PLD should be achievable. It must also be cautioned that water vapour can also enter the films from the film edges, regardless of how effective the cap growth is.

One heterostructure that has been successfully grown by PLD at the very end of this research is GaN on HfN (on an MgO substrate). The HfN was grown at established optimised settings of 500 °C and 1.0×10^{-4} Torr nitrogen and GaN was grown at the same settings as the best film produced to date. RHEED patterns indicated both HfN and GaN were single crystal, but the diffraction pattern of GaN was considerably more spotty than

those of the sample grown on sapphire. AFM of the GaN gave an r.m.s. roughness of 3.61 nm. The sample has not had any other tests performed on it yet. It is possible that the parameters for growing GaN on HfN will be different to those for GaN on sapphire. It is also possible that altering substrate temperature has deleterious effects on the HfN film, such as increasing the growth temperature from 500 °C (HfN optimum) to 700 °C (GaN optimum), although no changes were observed in the HfN RHEED at 700 °C. This is worthy of further investigation if GaN-on-HfN devices are to be fabricated.

Appendix A : Motivations for growth runs in GaN-on-sapphire series

PLD009_SA_GN_1 : to grow GaN film as an encapsulant for GdN or NbN. Also, since growth of NbN was unsuccessful to date, the aim is to grow a thin film of a material that is better known (to us) than NbN and hence characterise its quality more easily. This is the overall aim of this series. In each growth, principal analysis was RHEED and SEM. RHEED gave an idea of crystal quality during growth. SEM revealed morphology and coverage of substrate. Each time I have been trying to achieve full coverage of the substrate, and also measure film thickness by cleaving samples and looking at it side-on with the SEM.

PLD009_SA_GN_2 : growing at higher fluence, lower subs temp, using buffer layer and nitridation.

PLD009_SA_GN_3 : subs bonded to Mo-plate since sapphire would not have been absorbing all the radiated heat from the heater, so previous growth temps were probably lower than the value indicated by the temp controller. I also reduced pulse rate from 10Hz to 1Hz, having considered that perhaps I was saturating the surface with Ga and it might need more time for N to bond with it. Nitrogen plasma pressure is already at the upper limit (1×10^{-4}Torr).

PLD009_SA_GN_4 : growing without buffer layer, since the buffer layer seems to have had a negative effect. Back to 10Hz growth.

PLD009_SA_GN_5 : Aperture on laser removed. Fluence intended to be same as sample #4, but was miscalculated.

PLD009_SA_GN_6 : Grew at higher fluence. Heavily particulated films, of particulate size $\leq$40μm. Hexagonal and other GaN crystallites, $\leq$800nm observed growing on the particulates. Smaller, non-hexagonal crystals grow in the area around the particulate.

Edge-on SEM shows no film. 45° SEM shows the particulates to be reasonably flat and not dome shaped, as I suspected they might be from their circular shape.

PLD009_SA_GN_7 : Growing at reduced fluence to reduce particulation. Very little coverage of substrate.

PLD009_SA_GN_8 : growing at fluence between that of samples #6 and #7. #6 was heavily particulated and #7 had hardly any coverage, so this sample is intended to find an optimum interim fluence value.

PLD009_SA_GN_9 : target not rotated during growth. laser lined up part of liquid target . the constant angle the beam makes at the surface should result in more uniform particulate size. Plasma pressure also reduced (halved) as recoil pressure from ambient gas against the expanding plume is also know to cause particulates.

PLD009_SA_GN_10 : Ammending laser spot to give desired fluence with largest possible spot (limited by laser energy), as broader spots create less particulates. Reverting to usual fluence (1×10^{-4}Torr) and rotating target again.

PLD009_SA_GN_11 : previous film particulated. Reducing N_2 pressure by factor of 5, but unlike sample #9, target will be rotated.

PLD009_SA_GN_12 : growing at higher subs temp, as this is also reported to cause less particulation. GaN is still often grown at 800°C with good quality (although 700°C is the consensus for best quality).

PLD009_SA_GN_13 : reducing target→subs distance to allow particulates to merge to form a continuous film. Also keeping T_s=800°C as the crystal structures are quite interesting, quite different to samples grown at 700°C. Also, particulates on this film seem to merge better, rather than simply overlap and not interact with their neighbours, as

is the case for 700°C growth. possible 30μm film thickness seen in edge-SEM, but it is difficult to interpret.

PLD009_SA_GN_14 : making 3 major changes to growth in the hope of making a significant difference to results. These are;
(1) reducing nitridation time. No consensus in papers, so will reduce from 2 hours to ½hour.
(2) growing buffer layer
(3) main layer growth reduced from 1 hour to ½ hour

PLD009_SA_GN_15 : the fluence levels for all previous samples were carefully reviewed and recalculated. This sample was grown at a genuine fluence of 5Jcm^{-2}.

PLD009_SA_GaN_16 : nitridation at 30mins 900°C, 10min 450°C buffer, 50min 700°C, ion delfection plates repaired before this growth.

PLD009_SA_GaN_17 : "films" grown at low fluence were actually patchy coverage of sapphire subs, but some did emit light, e.g. samples 5,6,8,9. Trying a long growth time at low fluence and higher rep rate will hopefully give a continuous film which emits light. Also, new Ga-target prepared.

Sample ID#	Target	substrate	Target→ subs distance	Out-gassing	Total no. of pulses (film + cap)	N_2 pressure (Torr) + pwr (W)	T_{sub} (°C)	Growth time of Film/cap (min)	Laser fluence J cm^{-2}	RHEED n=0 FWHM at 30min (pix)±1.5pixels	
GdN_1	Gd/YSZ	YSZ (100) ssp	6.3 cm	1 hr 800 °C	18000+ 9000	1.2×10^{-4} no plasma	700°C	30 / 15	5	**(see *4)** n/a	
GdN_2	Gd/YSZ	YSZ (100) ssp	6.3 cm	1¼ hr 800 °C	18000+ 9000	1.0×10^{-4} 200W	700°C	30 / 15	5	18	
GdN_3	Gd/YSZ	YSZ (100) ssp	6.3 cm	40 min 800 °C	18,000+ 9000	1.0×10^{-4} **(see *1)**	700°C	30 / 15	5	23	
GdN_4	Gd/YSZ	YSZ (100) ssp	6.0 cm	40 min 800 °C	18,000+ 9000	1.0×10^{-4} 200W	700°C	30 / 15	5	16	
GdN_5	Gd/YSZ	YSZ (100) ssp	6.0 cm	1 hr 900 °C	18,000+ 9000	1.0×10^{-4} 200W	800°C	30 / 15	5	19	
GdN_6	Gd/YSZ	YSZ (100) dsp	6.0 cm	1 hr 950 °C	18,000+ 9000	1.0×10^{-4} 200W	850°C	30 / 15	5	n/a	
GdN_7	Gd/YSZ	YSZ (100) ssp	6.3 cm	1 hr 950 °C	36,000+ 9000	1.0×10^{-4} 200W	850°C	60 / 15	5	25	
GdN_8	Gd/YSZ	YSZ (100) dsp	6.0cm **(see *2)**	40 min 900°C	36,000 + 4800	5.0×10^{-5} 200W	800°C	60 / 8	5	24	
GdN_9	Gd/YSZ	YSZ (111) dsp	6.0cm **(see *2)**	40 min 900°C	36,000 + 4800	5.0×10^{-5} 200W	800°C	60 / 8	5	n/a	
GdN_10	Gd	YSZ (100) dsp	6.0cm **(see *3)**	40 min 900°C	36,000 No cap	2.5×10^{-5} 200W	800°C	60	5	24	
GdN_11	Gd	YSZ (111) dsp	6.0cm **(see *3)**	40 min 900°C	36,000 No cap	2.5×10^{-5} 200W	800°C	60	5	n/a	
GdN_12	Gd/YSZ	YSZ (100) dsp	6.0cm	1hr 900°C	18,000 + 4800	2.5×10^{-5} 200W	800°C	30 / 8	5	n/a	
GdN_13	Gd/YSZ	YSZ (111) dsp	6.0cm	1hr 900°C	18,000 + 4800	2.5×10^{-5} 200W	800°C	30 / 8	5	37	
GdN_14	Gd/YSZ	YSZ (100) ssp	6.0 cm	1 hr 900 °C	36,000 + 9000	1.0×10^{-4} 200W	800°C	60 / 15	**7.5**	19	
GdN_15	Gd/YSZ	YSZ (100) ssp	6.0 cm	1 hr 900 °C	36,000 + 9000	1.0×10^{-4} **400W**	800°C	60 / 15	7.5	28	
GdN_16	Gd/YSZ	YSZ (100) dsp	6.3 cm	1 hr 900 °C	30,000 + 18000	1.0×10^{-4} **120W**	800°C	50 / 30	7.5	28	

Sample ID#	Target	substrate	Target→ subs distance	Out-gassing	Total no. of pulses (film + cap)	N_2 pressure (Torr) + pwr (W)	T_{sub} (°C)	Growth time of Film/cap (min)	Laser fluence J cm^{-2}	RHEED n=0 FWHM at 30min (pix)±1.5pixels
GdN_17	Gd / **Cr**	YSZ (100) dsp	6.3cm	1 hr 850 °C	72,000 + 18,000	1.0×10^{-4} 200W	750 °C	120 / 30	**3.0**	17
GdN_18 +19	Gd/YSZ	YSZ (100) + (111)dsp	6.3cm	45min 850 °C	**6,000+ 72,000 + 18,000**	1.0×10^{-4} 200W	**200 °C** 750 °C	**10**/120/30	**2 / 2 / 5**	31
GdN_20	Gd/YSZ	YSZ (100) dsp	6.3cm	4hr 600° 1hr 800°	18,000 + 9,000	1.0×10^{-4} **no plasma**	700°C	30 / 15	5	32
GdN_21	Gd/YSZ	YSZ (100) dsp	6.3cm	1½ hr 800°C	18,000 + 9,000	1.0×10^{-4} no plasma	**21°C**	30 / 15	5	34
GdN_22	Gd/YSZ	YSZ (100) dsp	6.3cm	2½ hr 800°C	18,000 + 9,000	1.0×10^{-4} 200W	700°C	30 / 15	5	22
GdN_23	Gd/YSZ	YSZ (100) dsp	6.3cm	1½ hr 800°C	18,000 + 9,000	1.0×10^{-4} 200W	16°C	30 / 15	5	poly
GdN_24	Gd/YSZ	YSZ (100) dsp	6.0cm	4 hr 800°C	18,000 + 9,000	1.0×10^{-4} 200W	700°C	30 / 15	5 **triple energy**	17
GdN_25	Gd/YSZ	**YSZ (111) dsp**	6.0cm	1 hr 800°C	18,000 + 9,000	1.0×10^{-4} 200W	700°C	30 / 15	4.3	poly
GdN_26	Gd/YSZ	YSZ (100) dsp	6.0cm	1 hr 800°C	18,000 + 9,000	**5.2×10^{-5}** 200W	700°C	30 / 15	3.8	16
GdN_27	Gd/YSZ	YSZ (100) dsp	6.0cm	1½ hr 800°C	18,000 + 9,000	5.0×10^{-5} 200W	700°C	30 / 15	3.0	16
GdN_28	Gd/YSZ	YSZ (100) dsp	6.0cm	1 hr 800°C	18,000 + **4,500**	**2.5×10^{-5}** 200W	700°C	30 / 15	3.0	15.5

Table 1. Growth parameters individual to particular GdN films. Parameters listed in the table are those which changed between growths. Other cor
Note *1 – N_2 plasma mistakenly left on during YSZ cap growth for sample PLD015_YSZ_GdN_3.
Note *2 – started rotating target at max. speed for this and all subsequent growths
Note *3 – neglected to rotate target until 9 min into growth
Note *4 – underlined FWHM are from the more narrowly spaced planes, at 45° to the edge of YSZ(100) substrates
Common growth parameters:
Rep rate = 10 Hz Spot size = 1.4 × 1 mm (except GdN_17) f = 50 cm plano-convex lens RHEED images taken at 20.0 kV (constant), 1.4 A (

Sample ID#	Target	substrate	Out-gassing	Fluence J cm^{-2}	No. of pulses (film+cap)	T_{sub} (°C)	Growth time (min) Film/cap	N_2 plasma pressure	FWHM at 30min ±1.5pix	FW at 60 ±2
SmN_1 2=(111),3=small	Sm/YSZ	YSZ (100) dsp 1×1cm	1 hr 800 °C	~3 ± 1	54000+ 9000	**700°C**	90 / 15	1.0×10^{-4}	19.3 **(see *1)**	
SmN_4 5=(100)small	Sm/YSZ	YSZ (100) dsp 1×1cm	1 hr 900 °C	~3 ± 1	36000+ 9000	**800°C**	60 / 15	1.0×10^{-4}	34.9	
SmN_6 7=small,8=(111)	Sm/YSZ	YSZ (100) dsp 1×1cm	1 hr 800 °C	~3 ± 1	36000+ 9000	**600°C**	60 / 15 **(see *2)**	1.0×10^{-4}	14.2 **(see *2)**	
SmN_9 10=(100)small	Sm/YSZ	YSZ (100) dsp 1×1cm	½ hr 800 °C	~3 ± 1	36000+ 9000	**500°C**	60 / 15 **(see *3)**	1.0×10^{-4}	16.3 **(see *3)**	
SmN_11	Sm/**AlN**	YSZ (100) dsp 1×1cm	1 hr 800 °C	~3 ± 1	72000+ 9000	**650°C**	**120** / 15	1.0×10^{-4}	15.9	
SmN_12	Sm/**YSZ**	YSZ (100) dsp 1×1cm	1 hr 800 °C	~3 ± 1	72000+ 18000	**650°C**	**120** / **30**	1.0×10^{-4}	17.3	
SmN_13 14=(111)	Sm/AlN	YSZ (100) dsp 1×1cm	1¼ hr 800 °C	~3 ± 1	48000+ 18000	**750°C**	**80** / 30	1.0×10^{-4}	28.4 **(see *4)**	
SmN_15	Sm/AlN	YSZ (100) dsp 1×1cm	1¼ hr 800°C	~3 ± 1	48000+ 18000	**550°C** SmN 700°C AlN	80 / 30	1.0×10^{-4}	18.2 **(see *4)**	
SmN_16	Sm/AlN	YSZ (100) dsp 1×1cm	1¼hr 800°C	~3 ± 1	72000+ 18000	**400°C** SmN 700°C AlN	120 / 30	1.0×10^{-4}	26.2 **(see *4)**	
SmN_17	Sm/AlN	YSZ (100) dsp 1×1cm	3½hr 800°C	**5 J cm^{-2}**	36000+ 18000	**600°C** SmN 700°C AlN	60 / 30	1.0×10^{-4}	17.3	
SmN_18	Sm/AlN	YSZ (100) dsp 1×1cm	2 hr 800°C	**3 J cm^{-2}**	54000+ 18000	**600°C** SmN 700°C AlN	90 / 30	1.0×10^{-4}	17.9	
SmN_19	Sm / **Cr**	YSZ (100) dsp 1×1cm	1½ hr 800°C	**4 J cm^{-2}**	72000+ 18000	**600°C**	120 / 30	1.0×10^{-4}	16.6	

Sample ID#	Target	substrate	Out-gassing	Fluence J cm^{-2}	No. of pulses (film+cap)	T_{sub} (°C)	Growth time (min) Film/cap	N_2 plasma pressure	FWHM at 30min ±1.5pix	FV at 60 ±2
SmN_20	Sm/YSZ	YSZ (100) dsp 1×1cm	1½ hr 800°C	4.2Jcm^{-2} **broadspot**	18,000+ 9,000	600°C	30 / 15	**1.0 × 10^{-4}**	15.5	
SmN_21	Sm/YSZ	YSZ (100) dsp 1×1cm	2 hr 800°C	4.0Jcm^{-2} broadspot	18,000+ 9,000	600°C	30 / 15	**5.0 × 10^{-5}**	polyxtal	po
SmN_22	Sm/YSZ	YSZ (100) dsp 1×1cm	1½ hr 800°C	3.7Jcm^{-2} broadspot	18,000+ 9,000	600°C	30 / 15	**7.5 × 10^{-5}**	17.1	
SmN_23	Sm/YSZ	YSZ (100) dsp 1×1cm	1 hr 800°C	3.5Jcm^{-2} broadspot	18,000+ 9,000	600°C	30 / 15	**2.6 × 10^{-5}**	15.2	
SmN_24	Sm/YSZ	YSZ (100) dsp 1×1cm	1½ hr 800°C	4.2Jcm^{-2} **broadspot**	18,000+ 9,000	600°C	30 / 15	1.0 × 10^{-4}	16.7	
SmN_25	Sm/YSZ	YSZ (100) dsp 1×1cm	1½ hr 800°C	**4.0/2.0 Jcm^{-2} broadspot**	**18,000+ (1800×2)+ 9,000**	600°C **700+800°C anneals**	**30/3/3/15**	1.0 × 10^{-4}	16.7	
SmN_26	Sm/YSZ	YSZ (100) dsp 1×1cm	1½ hr 800°C	3 Jcm^{-2}	36,000+ 9,000	**450°C**	60 / 15	1.0 × 10^{-4}	17.0	
SmN_27	Sm/YSZ	YSZ (100) dsp 1×1cm	1½ hr 800°C	3 Jcm^{-2}	36,000+ 9,000	**350°C film** 700°C cap	60 / 15	1.0 × 10^{-4}	30.3	

Table 1. Growth parameters individual to particular SmN films. Alternating colour indicate samples grown simultaneously. Para between growths. Other common parameters are listed below/overleaf.

Common growth parameters:

Rep rate = 10 Hz; Spot size = 1.4 × 1 mm; Laser fluence = 5 Jcm^{-2} ; f = 50 cm plano-convex lens; N_2 Plasma = 1.0 ×10^{-4} To RHEED images taken at 20.0 kV (constant), 1.4 A (varied slightly to optimise brightness)

Note *1 – FWHM are from the (100) direction, parallel to the edge of YSZ(100) substrates

Note *2 – cap growth: laser was hitting s.s. target holder intermittently for 1st 43s of cap growth

Note *3 – new YSZ capping target loaded **Note *4** – N_2 off during AlN cap growth